LATITUDINAL (APEX-HEIGHT) VARIATIONS OF ION DRIFTS IN THE IONOSPHERE AT LOW- AND MID- LATITUDES

by

Edgardo Enrique Pacheco Josán

APPROVED BY SUPERVISORY COMMITTEE:

_____

Roderick A. Heelis, Chair

_____

Phillip C. Anderson

_____

William R. Coley

_____

Gregory D. Earle

_____

Xinchou Lou

_____

Brian A. Tinsley

To my family

A mis padres y mis hermanas

# LATITUDINAL (APEX-HEIGHT) VARIATIONS OF ION DRIFTS IN THE IONOSPHERE AT LOW- AND MID- LATITUDES

By

EDGARDO ENRIQUE PACHECO JOSAN, B.S., M.S.

DISSERTATION

Presented to the Faculty of

The University of Texas at Dallas

in Partial Fulfillment

of the Requirements

for the Degree of

DOCTOR OF PHILOSOPHY IN PHYSICS

THE UNIVERSITY OF TEXAS AT DALLAS

December, 2009

ACKNOWLEDGEMENTS

Some of the most memorable moments of my childhood, and one of the first things I remember watching on TV, were the images of space mission rocket launches leaving earth to explore the space that surrounds us. So it amazes me now, that I actually have had the opportunity to pursue the path that allows me to investigate this environment and to continue to develop that singular interest in space discoveries and exploration. The passion for science and exploration is something that was always present and continues to be with me.

This moment it would not be possible if I had not received the help, support and guidance of many other people. Their wisdom, encouragement and enthusiasm motivated me to give my best of myself and to keep pursuing my goals.

I feel much honored to have had Dr. Rod Heelis as my advisor. His support and guidance have been vital in the success of this research work. I learned a lot not only from his excellent guidance and his vast scientific knowledge, but also from his personal qualities such as his enormous enthusiasm, patience and excitement to learn more. His professional skills motivate everyone that works with him to develop high standards for quality. I am grateful for his mentoring, the time we spent discussing my work and his willingness to explain the intricate processes of space physics in a very didactic manner.

Also I want to thank all the members of my committee; Dr. Gregory Earle, Dr. Phillip Anderson, Dr. Brian Tinsley, Dr. Robin Coley and Dr. Xinchou Lou for their support, suggestions and feedback. I was able to finish my work because they generously shared their time and knowledge about space physics, and data processing with me.

Thanks to the William B. Hanson Center for Space Science and the UTD Physics Department staff and faculty members for their help and assistance. Special thanks to Margie Renfrow, Cindy Long, Brenda Walston, Becky Kester, Keith Swaim, Robert Power and Sarita Venkatraman. My special gratitude also to Marc Hairston for his reviews and feedback of my writing. He is always willing to provide students with good advice.

I am grateful to all my friends and fellow students for sharing this special time as a graduate student with me, and for their support, help and encouragement particularly during the hard times. Thanks to all those I met when I started on this path and to those who are on the path to become Doctors soon. Matt Hei, Erick Johnson, Patrick Roddy, Drew Hartman, Tony Musumba, Kelly Ann Drake, Jeff Klenzing, Bob Johnston, Sasmita Mohapatra, Russel Stoneback, Preeti Bhaneja, Bob Haaser, Ryan Davidson, Angeline Burrel, Rob McIntosh and Jake Hebert. Special thanks to Bob Johnston for his feedback about my writing and also to Kelly Ann Drake for her help, suggestions on my writing and her valuable friendship.

I want to thank my father Delfin, my mother Leny and my sisters Silvia and Nancy for being the best example of strength, optimism and wisdom. They were my first teachers, and taught me the fundamental principles to succeed in life. The close ties between us have helped me to overcome difficulties and keep trying to do my best in all aspects of my life, particularly during this period of becoming a scientist researcher and completing this dissertation work.

I will always be thankful to all my friends and colleagues at the Jicamarca Radio Observatory where I met Dr. Cesar Valladares, Dr. Jorge Chau and Dr. Woodman who gave me the opportunity to start a career in the field of ionospheric research. This was my first real contact with ionospheric studies using radars instruments, and this allowed me develop the necessary background and knowledge of the importance of atmospheric investigations. I want to thank

Fernando Villanueva for being an excellent supervisor and an excellent friend. He is always prompt to help his colleagues, is a good example of professionalism and is inspiring for his ability to always find a solution for problems. I am also grateful to all my friends at Jicamarca with whom I shared good fellowship times. We shared times of fellowship and played soccer and ping pong tournaments, and they also helped me anytime I asked for their support.

I am grateful also to my friends outside of the UTD Physics Department who also give me encouragement and the motivation to do my best. John and Mary Anderson, and Cynthia Manning have been very supportive during throughout these years, and I appreciate their friendship.

We gratefully acknowledge our data providers for this work: the National Central University of Taiwan for the ROCSAT-1 data, NASA Space Physics Data Facility (SPDF \ OMNIWeb database)/Goddard Space Flight Center for the Kp index and for the 4D orbit viewer application, NASA National Space Science Data Center/Goddard Space Flight Center for the Corrected Geomagnetic Coordinates and IGRF/DGRF Model Parameters, the International Association of Geomagnetism and Aeronomy (IAGA) and Susan Macmillan for the IGRF model, and the World Data Center for Geomagnetism, Kyoto for the Dst index. This research has been supported by NASA grants NNX07AF36G and NNX07AT82G.

November, 2009

LATITUDINAL (APEX-HEIGHT) VARIATIONS OF ION DRIFTS IN THE IONOSPHERE AT LOW- AND MID- LATITUDES

Publication No. _____

Edgardo Enrique Pacheco Josán, Ph.D.
The University of Texas at Dallas, 2009

Supervising Professor: Roderick A. Heelis

In this study we focus on the dynamics of the ion drift velocities at low and middle latitudes. We describe how these ion drifts vary in latitude for different longitudes, seasons and specific local times during quiet times.

During quiet times we use data from the ROCSAT-1 satellite to describe the latitude dependence of three main features of the meridional ion drifts; the large-scale upward drifts during daytime, a so-called prereversal enhancement near dusk, and a downward sunrise enhancement. The longitude, latitude and seasonal dependences in these features are influenced by the alignment of the terminators with the magnetic meridian, the flux tube integrated conductivities and the action of diurnal and semidiurnal tides in the lower ionosphere.

We also obtained a description of the zonal ion drifts during quiet times. These drifts show latitude, longitude and seasonal variations, driven by the combined effects of the E-region and F-region winds. Changes in the wind and the F-region Pedersen conductance are responsible for latitude, longitude and seasonal changes in the net superrotation of the ionosphere.

Additionally, we describe storm time perturbations in the ion drifts at the magnetic equator. These perturbations are mainly produced by undershielding and overshielding of the magnetospheric electric field during times when the Interplanetary Magnetic Field is changing. The role of the disturbance dynamo can also be seen in the perturbation drifts at the equator.

Using measurements from the DMSP-F13, F-15 and ROCSAT-1 satellites we are able to describe for the first time, storm-time drift perturbations at the equator observed simultaneously at different local times.

TABLE OF CONTENTS

ACKNOWLEDGEMENTS……v

ABSTRACT ……viii

LIST OF FIGURES……xii

LIST OF TABLES…..xviii

ABBREVIATIONS……xix

CHAPTER 1 ..... 1

INTRODUCTION AND BACKGROUND ..... 1

1.1 INTRODUCTION ..... 1
1.2 BACKGROUND ..... 3
1.2.1 The Ionosphere ..... 3
1.2.2 Ion drifts in the ionosphere ..... 5
1.2.3 Latitude, Altitude and Longitude variations in the ionospheric density ..... 13
1.2.4 Ion drift latitude variations ..... 15
1.2.5 Ion drift longitude variations ..... 18
1.2.6. Ion drift altitude variations ..... 21
1.2.7. Ion drift storm time perturbations ..... 22
1.3 Objectives ..... 24

CHAPTER 2 ..... 25

APPROACH ..... 25

2.1 DATA SELECTION ..... 25
2.1.1 DMSP data ..... 26
2.1.2 ROCSAT data ..... 26
2.1.3 Additional data ..... 27
2.2 INSTRUMENTATION ..... 27
2.2.1 Defense Meteorological Satellite Program (DMSP) ..... 27
2.2.2 ROCSAT ..... 28
2.2.3 Instruments ..... 30
2.2.4 Jicamarca and Arecibo radars ..... 33
2.3 Data Analysis ..... 35
2.3.1 Storm-time drift perturbations ..... 37
2.3.2 Latitude variations during quiet times ..... 38
2.3.3 Derivation of the horizontal ion drift biases ..... 46

2.3.4 Conversion of ion drift vectors from spacecraft reference frame to geomagnetic reference frame....51

CHAPTER 3 RESULTS....57

3.1 Storm Time Vertical Drift Perturbations....57
3.2 Observations....58
3.3 Discussion and Conclusions....68

CHAPTER 4....74

Quiet time meridional ion drifts....74

4.1 Introduction....74
4.2 Methodology....75
4.3 Observations....81
4.3.1 PRE features....83
4.3.2 Daytime upward-downward drifts features....85
4.3.3 Downward enahancement near sunrise....87
4.3.4 Ion density features....89
4.3.5 Apex Height ion drift variability....92
4.4 Discussion and Summary....99
4.5 Conclusions....109

CHAPTER 5....112

Quiet time zonal ion drifts....112

5.1 Introduction....112
5.2 Observations....112
5.3 Discussion....120
5.4 Conclusions....123

CHAPTER 6....125

CONCLUSIONS AND FUTURE WORK....125

6.1. Conclusions....125
6.2. Future Work....127

BIBLIOGRAPHY....128

VITA

LIST OF FIGURES

Figure 1.1. Typical density profile of the ionosphere derived from the International Reference Ionosphere (IRI) model. Regions D, E and F during the day (blue curves) and night (black curves) for high (solid curves) and low solar activity conditions (dashed curves)……..…….....4

Figure 1.2. Values of the ratio of the gyrofrequency to the collision frequency with respect to altitude, for ions ($K_i$) and electrons ($K_e$). (From *Kelley*, 1989. Copyright 1989 Elsevier. Reproduced with permission of Elsevier.)……7

Figure 1.3. Representation of the altitude variation of the conductivities. The heavy curves indicate daytime values while the lighter curves indicate nighttime values. The direct conductivity is represented by the curve sigO, the Pedersen current corresponds to the dotted line sigP, and the Hall current is the dashed line sigh. (From *Heelis*, 2004. Copyright 2004 Elsevier. Reproduced with permission of Elsevier.)…….....9

Figure 1.4. Local time distribution of the equatorial vertical and zonal plasma drifts observations from Jicamarca (solid line) and a numerical simulation model by *Crain et al*., 1993a. The measurements correspond to equinox solar maximum conditions. (From *Fejer*, 1997. Copyright 1997 Elsevier. Reproduced with permission of Elsevier.)……..……13

Figure 1.5. Height/Latitude structure of plasma density using the Coupled thermosphere ionsophere plasmasphere electrodynamic model (CTIPe). Altitude coverage is from 200 to 800 km, through the 20 LT sector at 14 UT. This corresponds to quiet conditions and moderately high solar activity conditions with 10.7 cm solar flux of 160 units. (From *Fuller-Rowell et a*l., 2002. Copyright 2002 Elsevier. Reproduced with permission of Elsevier.)…….14

Figure 1.6. IMAGE-FUV observations of nighttime ionospheric emissions at 2000 LT. The longitudinal variability of the equatorial ionospheric anomaly can be noticed. The southern anomaly is represented with a mirror image of the northern anomaly due to a poor sampling of the southern observations. The amplitude of the diurnal temperature variation at 115 km is represented in white dashed contour lines. (From *Immel et al*. 2006. Copyright 2006 American Geophysical Union. Reproduced by permission of American Geophysical Union.)……..15

Figure 1.7. Ion density maps at 1000-1200 LT (top) and 2100-2300 LT (bottom). The averaged density in each bin of 10° longitude by 2° latitude is calculated from ROCSAT-1 data during March 1999 to June 2004. (From *Kil et al*. 2007. Copyright 2007 American Geophysical Union. Reproduced by permission of American Geophysical Union.)……...…….16

Figure 1.8. (a) Vertical ion drift at Jicamarca for different seasons and solar flux conditions during quiet time (from *Fejer et* al., 1991b, copyright 1991 American Geophysical Union, reproduced by permission of American Geophysical Union); (b) Perpendicular/north F-region plasma drifts over Arecibo for different seasons during quiet times (Kp≤3). The averaged 10.7 cm solar flux values (Sa) are also shown. (From *Fejer*, 1993. Copyright 1993 American Geophysical Union. Reproduced by permission of American Geophysical Union.)…….....17

Figure 1.9. (a) Zonal plasma drifts observed by the Jicamarca radar for different solar flux conditions and seasons (from *Fejer et al*., 1991b, copyright 1991 American Geophysical Union, reproduced by permission of American Geophysical Union); (b) Zonal plasma drifts over Arecibo for the same conditions as in Figure 1.8(b). (From *Fejer*, 1993. Copyright 1993 American Geophysical Union. Reproduced by permission of American Geophysical Union.)…….....19

Figure 1.10. Vertical drifts measured by AE-E satellite near the magnetic equator in different longitude sectors after sunset. (From *Fejer et al*., 1995. Copyright 1995 American Geophysical Union. Reproduced by permission of American Geophysical Union.)…….....20

Figure 1.11. Monthly vertical ion drift versus longitude. Measurements obtained from DMSP F15 near 0930 LT for the year 2002 corresponding to the month period from June to December. The solid line represents the fitting of the distribution using the first five elements of the Fourier series. (From *Hartman and Heelis*, 2007. Copyright 2007 American Geophysical Union. Reproduced by permission of American Geophysical Union.)……..21

Figure 1.12. Altitudinal profile of the zonal plasma drifts over Jicamarca with an integration time of about 5 minutes during daytime. The average profile (AVG) is obtained with integration time of 20-30 minutes. (From *Fejer*, 1985. Copyright 1985 American Geophysical Union. Reproduced by permission of American Geophysical Union.)……...……...23

Figure 1.13. Similar as figure 1.12 but for nighttime. The average east-west drift shows more variation than during daytime. (From *Fejer*, 1985. Copyright 1985 American Geophysical Union. Reproduced by permission of American Geophysical Union.)……...23

Figure 2.1. Retarding Potential Analyzer sensor cross section (from *Holt*, 1995)……...31

Figure 2.2. Ion Drift Meter sensor cross section (from *Holt*, 1995)…….....33

Figure 2.3. ROCSAT-1 orbit mapped projection for 24 hours. The latitude coverage range is from -35 to 35 geographic degrees. The local of ascending and descending passes is approximately fixed for a specific latitude (http://sscweb.gsfc.nasa.gov/cgi-bin/sscweb/Locator_graphics.cgi).....35

Figure2.4. DMSP-F13 orbit mapped projection for 24 hours. The orbit inclination is about 98 degrees and it is fixed in local time when it crosses the equator near 1800 LT for the ascending node and near 0600 LT for the descending node. (http://sscweb.gsfc.nasa.gov/cgi-bin/sscweb/Locator_graphics.cgi).....36

Figure 2.5. Spacecraft reference frame system of ROCSAT-1……37

Figure 2.6. ROCSAT-1 orbit (blue line) with a space bin representation 5º wide in latitude and 30º wide in longitude (red box). The average vector velocity is determined for each bin and for each ion drift component ($V_x$, $V_y$, $V_z$) in the spacecraft reference frame……..……...41

Figure 2.7. Scatterplot of the ion drift measurements in the spacecraft reference frame (Vx, Vy, Vz) for ascending passes distributed in local time. The period corresponds from November 2001 to February 2002. The red line represents the mean values of 30 minutes local time intervals shifted every 15 minutes.……....44

Figure 2.8. Figure 2.8. Scatterplot of the ion drift measurements in the spacecraft reference frame (Vx, Vy, Vz) similar as Figure 2.7 but for descending passes distributed in local time. The period corresponds from November 2001 to February 2002. The red line represents the mean values of 30 minutes local time intervals shifted every 15 minutes…….……...45

Figure 2.9. Ion drift vectors $V_x$ and $V_y$ projected on the horizontal plane for the ascending pass (a) and descending pass (b). These vectors can be derived from the geographic zonal drift component $V_\Phi$ and the north south component $V_{NS}$……..47

Figure 2.10. Ion drift measurements distributed in local time in the spacecraft reference frame after processing the data shown in Figure 2.7 for ascending passes. The blue line illustrates the values of the drifts before removing the biases and the small black circles indicate the values after extracting the bias.……...49

Figure 2.11. Ion drift measurements distributed in local time in the spacecraft reference frame after processing the data shown in Figure 2.8 for descending passes. The blue line illustrates the values of the drifts before removing the biases and the small black circles indicate the values after extracting the bias.……...50

Figure 2.12. Horizontal ion drift vector components $V_x$ and $V_y$ for ROCSAT-1 projected on the horizontal plane. "δ" is the angle in between the magnetic meridian and the south-north direction……..52

Figure 2.13. Schematic representation of the satellite ascending (a) and descending (b) pass with orbital inclination i′. The spherical triangle defined by the north-south meridian, the geographic equator, and the orbital projection on the Earth shows its corresponding angles i′, β, γ when the satellite position is indicated by P. P is located at a geographic latitude $L_0$. For the descending pass β is negative (clockwise), β = -(90 – γ)……...53

Figure 2.14. A three dimensional schematic representation of the magnetic field vector B at the point "a". The declination angle is indicated by δ. "I" represents the inclination angle. The drift vectors $V_x$ and $V_y$ are situated on the horizontal plane "abcd". The segment "ab" indicates the south-north direction. The segment "ad" illustrates the west-east direction and the segment "ae" indicates the local vertical direction toward the center of the Earth……54

Figure 2.15. Ion drift measurements versus local time after converting the drift values without bias (shown in Figures 2.10 and 2.11) to ion drift values in the reference frame parallel and perpendicular to **B**. The first panel indicates the drift values in the direction parallel to **B** (positive when the drift is northward). The second panel shows the ion drift perpendicular to **B** in the magnetic meridian plane (positive when the drift is upward). The third panel shows the **E**x**B** drift in the zonal or east-west direction (positive when the drift is eastward).……..55

Figure 3.1. Configuration of the electric fields in the ionosphere and magnetosphere system in the equatorial plane in order to illustrate the undershielding and overshielding effects. The sun is located at the left of the figure. E>E′ = undershielding, E<E′= overshielding.…….....58

Figure 3.2. Vertical ion drift perturbations registered during the storm event on July 15, 2000. The first panel shows the Dst index. The second panel shows the interplanetary magnetic field (IMF-Bz). The following panels illustrate the vertical drift perturbations measured by the DMSP-F13, DMSP-F15 and ROCSAT-1. At the right side of the DMSP observation is indicated the satellite, its local time for observations and the longitude that corresponds to the point marked with the dashed line…….59

Figure 3.3. Vertical ion drift perturbations registered during the storm event on November 6, 2001……62

Figure 3.4. Vertical ion drift perturbations registered during the storm event on October 30, 2003……64

Figure 3.5. Vertical ion drift perturbations registered during the storm event on April 6, 2000……66

Figure 3.6. Vertical ion drift perturbations registered during the storm event on April 11, 2001……67

Figure 3.7. Vertical ion drift perturbations registered during the storm event on November 23, 2001……69

Figure 3.8. Evolution of the storm time event with temporal variations of the IMF-Bz, Dst index and the vertical drift perturbation. A southward turning IMF and a decreasing Dst index mark the onset of the main phase of the storm. Undershielding, overshielding and disturbance dynamo processes affect the resultant vertical drift perturbation……73

Figure 4.1. Meridional ion drifts distributed in local time at the magnetic equator during December solstice (November to February) correspondiong to the 0º (upper panel), 160º (middle) and 250º (bottom) CGM longitude sectors. Also indicated is the relative position of the maximum and minimum values by the dashed and dash-dot lines and their magnitudes for each longitude sector. The black circles represent the total average from the years 1999 to 2003. The purple, blue, turquoise and orange color lines indicate the meridional drifts for the periods 1999-2000, 2000-2001, 2001-2002, 2002-2003 respectively……78

Figure 4.2. Meridional ion drifts distributed in local time at the magnetic equator during June solstice correspondiong to the 0º (upper panel), 160º (middle) and 250º (bottom) CGM longitude sectors. The black circles represent the total average from the years 2000 to 2003. The purple, blue, turquoise and orange color lines indicate the seasonal meridional drifts for the years 2000, 2001, 2002 and 2003 respectively……79

Figure 4.3. Meridional ion drifts at the magnetic equator during equinox corresponding to the months of March, April, September and October. The purple, blue, turquoise and orange color lines indicate the seasonal meridional drifts for the years 2000, 2001, 2002 and 2003 respectively……...80

Figure 4.4. Latitudinal and local time dependent quiet time ion drifts in the direction perpendicular to B contained in the magnetic meridional plane. The panels from top to bottom indicate the Pacific Central American, South American-Peruvian, South American-Brazilian, African, Indian and Pacific regions corresponding to the 270º, 290º, 310º, 0º, 90º, 180º geographic longitudes. The averaged ion drift values are obtained for the November-February period from 1999 to 2003 (left column), the equinox period from 2000 to 2003 (middle column) and the May-August period from 2000 to 2003 (right column)……..82

Figure 4.5. Average total ion density distribution in local time and CGM latitude obtained from ROCSAT-1 for the December solstice 1999-2003 (left), the equinox 2000-2003 (middle) and the June solstice 2000-2003 periods (right). The longitude regions are the same as indicated in figure 4.4……..90

Figure 4.6. Meridional ion drifts near 1200 LT vs. apex-height for the same seasons and longitude sectors illustrated in figures 4.1-4.5……...93

Figure 4.7. Meridional ion drifts near 1900 LT vs. apex-height……..94

Figure 4.8. Meridional ion drifts near 1100 LT vs. apex-height……..96

Figure 4.9. Meridional ion drifts near 1830 LT vs. apex-height……..97

Figure 4.10 Schematic representation of the polarization charges, electric field and neutral wind configuration in the bottomside F-region ionosphere during nighttime….107

Figure 5.1. Latitudinal and local time dependence of quiet time ion drifts in the direction perpendicular to B in the east-west direction for the 270º, 290º, 310º, 0º, 90º and 180º longitude sectors during the years 1999-2003 (solar maximum). The average ion drift values are obtained for the northern winter solstice (left panel), the equinox (middle panel) and the northern summer solstice (right panel)……113

Figure 5.2. Net superrotation effect obtained from averaging the east-west drift values in local time. Results for the northern winter solstice (top), equinox (middle), and the northern summer solstice (bottom) are shown. The longitudes correspond to the longitude regions shown in Figure 5.1……...117

Figure 5.3. Latitudinal variation of the net eastward and westward ion drifts averaged in local time for different longitude sectors……..119

LIST OF TABLES

Table 1 Magnetic field declination and angles between the terminator and the magnetic field for the studied longitude sectors……....12

# ABBREVIATIONS

ACE - Advanced Composition Explorer

AE-E – Atmospheric Explorer - E

CGM - Corrected Geomagnetic

CTIPe - Coupled Thermosphere Ionosphere Plasmasphere Electrodynamic

DE - Dynamic Explorer

Dst – Disturbance Storm Time index

DMSP - Defense Meteorological Satellite Program

EIA - Equatorial Ionization Anomaly

EUV - Extreme Ultra-Violet

GSWM - Global Scale Wind Model

HWM – Horizontal Wind Model

IDM - Ion Drift Meter

IGRF – International Geomagnetic Reference Field

IMF - Interplanetary Magnetic Field

IRI - International Reference Ionosphere

IPEI - Ionospheric Plasma and Electrodynamics Instrument

Kp – Geomagnetic Planetary Index

LT – Local Time

NAIC - National Astronomy and Ionosphere Center

NCAR - National Center for Atmospheric Research

NSF - National Science Foundation

NSSDC - NASA's National Space Science Data Center

PRE - Prereversal Enhancement

ROCSAT-1 - Republic of China Satellite

RPA - Retarding Potential Analyzer

SSIES - Special Sensor-Ions, Electrons, and Scintillation

TIEGCM – Thermosphere Ionosphere Electrodynamics General Circulation Model

UT – Universal Time

# CHAPTER 1

# INTRODUCTION AND BACKGROUND

## 1.1 INTRODUCTION

Over the last 50 years important benefits have been seen from the use of space-based assets to transmit radio signals from distant places for diverse use such as radio, television, satellite communications and global positioning systems. Our society is becoming ever more dependent on spaced-based communication and navigation systems which emit radio waves that propagate through the ionosphere. Of particular interest to space agencies is the effect of the Sun on the ionosphere since it can create hazardous situations for humans and equipment in space. Therefore a better understanding of our space environment can result in more efficient and improved use of these systems. This is especially true during solar storms due to the increased amounts of radiation coming to the Earth. There are still many questions concerning the variability of the ionosphere produced by its interaction with the Sun and a more detailed and accurate description of the parameters and behavior of the region is required.

Most of what we know about the ionosphere comes from ground-based radars. The limitation in number and location, since the radars are fixed to a specific longitude and latitude, restrict our knowledge of the global variations in the physical dynamics we want to investigate. Satellites can provide better latitudinal and longitudinal coverage of the region, therefore the use of in situ measurements provides advantages for the purpose of achieving a global description of the region. In particular, the ion drift motion is a key parameter in the description of the ionosphere because it controls the distribution of the charged particles in the ionosphere. The

Republic of China Satellite (ROCSAT-1) and the Defense Meteorological Satellite Program (DMSP) are satellites that have measured ion drifts and densities in the topside ionosphere, giving a large database for the period of 1999-2004 that we use in our investigation.

In this study we describe the quiet-time latitudinal variations of the ion drifts for different longitudinal sectors using the database provided by the satellites ROCSAT-1 and DMSP. In the ionospheric region we are studying, the ion drift and electric fields are simply related by the expression $\mathbf{V}=(\mathbf{E}\mathrm{x}\mathbf{B})/B^2$. Electric fields map unattenuated along the Earth's magnetic field thus allowing a single measurement of the ion drift to specify the electric field at every location along the magnetic field above 200 km. Using this feature and quiet time satellite measurements we may describe the global distribution of ion drifts in the ionosphere. In addition, we study perturbations in the vertical plasma drift at low latitudes during storm-time conditions at different longitudes. These studies provide information that is useful for physics-based and assimilative models that are used for specification and prediction of the ionosphere.

A more detailed knowledge of the electric fields and plasma drifts is important for a complete understanding of the electrodynamics of the ionosphere. Since these parameters are relevant inputs to many physics-based models, a more accurate description of the variations in the fields and velocities will produce better predictions and will allow us to infer the main input drivers for variations in ion densities. Self-consistent models have been developed to simulate the coupled ionosphere/thermosphere system such as the National Center for Atmospheric Research (NCAR) thermosphere/ionosphere/electrodynamics general circulation model (TIEGCM) [*Richmond et al.*, 1992, 1987] and the coupled thermosphere/ionosphere/plasmasphere (CTIP) model [*Fuller-Rowell et al.*, 1996, 2002]. However, little is known of the longitude and latitude variations in the neutral winds and ion

drifts in the F-region at low and middle latitudes. Thus detailed validation of the model inputs and outputs is largely missing. At a fixed altitude a description of the longitudinal and apex-height (latitudinal) variations of the ion velocities will be of great value to advancing a more accurate description of the behavior of the ionosphere.

## 1.2 BACKGROUND

### 1.2.1 The Ionosphere

The ionosphere is a region of the upper atmosphere that contains charged particles (ions and electrons). These charged particles are produced by ionization of the neutral atmosphere by solar extreme ultra-violet (EUV) radiation and energetic particle impact. The lower altitude of the ionosphere appears near 60 km, where the electron density is of order 10 $cm^{-3}$ during the day. There is no distinct upper limit but a height of about 2000 km is arbitrarily set for practical applications as the upper limit.

The ionosphere is composed of a series of charged particle density peaks produced by the ionization of atmospheric gases such as $N_2$, $O_2$ and O. The ionosphere density peaks are named D, E and F. The highest is subdivided into the F1 and the F2 layers. The vertical structure of the ionosphere changes from day to night, with season, and with latitude. It is also affected by solar activity, but the differences between daytime and nighttime are the most dramatic variations. As shown in Figure 1.1, we can detect the presence of two major peaks in ion concentration during the day, in the E and F regions. At night, the D region vanishes; chemical losses significantly reduce the E region peak while the F region peak is maintained by downward diffusion of particles produced during the day.

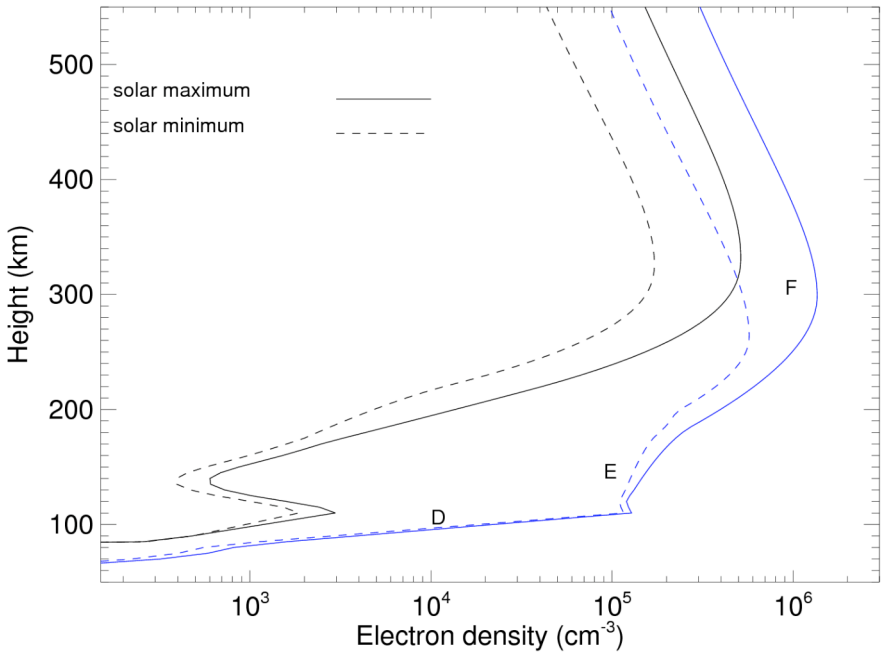


Figure 1.1. Typical density profile of the ionosphere derived from the International Reference Ionosphere (IRI) model. Regions D, E and F during the day (blue curves) and night (black curves) for high (solid curves) and low solar activity conditions (dashed curves).

In general the ionosphere is charge neutral and the total ion number density is equal to the electron number density. The concentration of ions is determined by a balance between production, loss and transport, described in a continuity equation of the form

$$\partial N / \partial t = P - L - \nabla \bullet (N\mathbf{V}) \qquad (1.1)$$

Here, N is the ion density, P is the production rate of ions, L the loss rate to recombination or charge exchange, and the last term indicates the change in ion density by transport, where **V** is the mean drift velocity.

### 1.2.2 Ion drifts in the ionosphere

Among the forces that move charged particles we consider the following: a momentum exchange force due to collisions between charged and neutral particles (neutral wind), the Coulomb force, the Lorentz force, the plasma pressure gradient force and the gravity force. Since we are considering large-scale systems that evolve over time scales of several hours or more it is acceptable to ignore acceleration of the ions and electrons so that the forces are in equilibrium. Thus, the equation of motion for the ions and electrons can be written as follows:

For ions:

$$-\frac{1}{N_i}\nabla(N_i k T_i) + m_i \mathbf{g} + e(\mathbf{E} + \mathbf{V_i} \times \mathbf{B}) - m_i \upsilon_{in}(\mathbf{V_i} - \mathbf{U}) = 0 \tag{1.2}$$

For electrons:

$$-\frac{1}{N_e}\nabla(N_e k T_e) + m_e \mathbf{g} - e(\mathbf{E} + \mathbf{V_e} \times \mathbf{B}) - m_e \upsilon_{en}(\mathbf{V_e} - \mathbf{U}) - m_e \upsilon_{ei}(\mathbf{V_e} - \mathbf{V_i}) = 0 \tag{1.3}$$

Here N is the species number density, m is the mass, T the temperature, and **V** the velocity, $k$ is Boltzmann's constant, **g** the acceleration due to gravity, $e$ the electron charge, **E** the electric field, $\nu_{in}$ the collision frequency with neutral particles, and **U** the neutral wind. The subscripts "i" and "e" denote quantities for ions and electrons, respectively.

We can derive from equations 1.2 and 1.3 the ion and electron velocities in the parallel (||) and perpendicular (⊥) directions with respect to **B**. The expressions for the ion velocities are shown in the following equations:

$$\mathbf{V}_i^{\parallel} = \frac{\mathbf{F}_i^{\parallel}}{m_i \upsilon_{in}} + \mathbf{U}^{\parallel} \tag{1.4}$$

$$\mathbf{V}_i^{\perp} = \frac{1}{\left[m_i \upsilon_{in}\left(1 + \left(\frac{\Omega_i^2}{\upsilon_{in}^2}\right)\right)\right]} + \left[\mathbf{F}_i^{\perp} + (\mathbf{F}_i^{\perp} \times \hat{\mathbf{b}})\frac{\Omega_i}{\upsilon_{in}}\right] + \mathbf{U}^{\perp} \tag{1.5}$$

where $\mathbf{F_i} = -\frac{1}{N_i}\nabla(N_i k T_i) + m_i \mathbf{g} + e(\mathbf{E} + \mathbf{U} \times \mathbf{B})$.

Here the gyrofrequency is denoted by $\Omega_i = (eB)/m_i$ and $\hat{\mathbf{b}}$ is the unit vector along the direction of the magnetic field. In a similar way we can derive the expressions for electrons but in that case the collisions with ions should be included.

At all altitudes the ions move parallel to **B** in response to a force along **B** as indicated in equation 1.4. At low altitudes where the ratio of the gyrofrequency to the collision frequency $K_j = \Omega_j / \upsilon_j$ is low, the charged particles move parallel to a force that is perpendicular to the magnetic field as shown in equation 1.5. On the other hand, at high altitudes, where the ratio of the gyrofrequency to the collision frequency is high, the charged particles move in a direction mutually perpendicular to the force and the magnetic field. Figure 1.2 illustrates the values of the ratio $\Omega/\upsilon$ as a function of altitude for ions and electrons. For the electron case over our altitude of interest, $K_e >> 1$, so electrons move mainly in the direction normal to the force and the magnetic field. In the lower ionosphere, $K_i << 1$, so the ions move along the direction of the force perpendicular to the magnetic field. At higher altitudes, where $K_i >> 1$, the drift is perpendicular to the force and the magnetic field.

The electrons are less affected by the neutral wind motions in the ionosphere since the gyrofrequency is very large compared to the collision frequency. However, electric fields drift the electrons in the $\mathbf{E} \times \mathbf{B}$ direction at all altitudes above 100 km. By contrast, the ions move along the direction of the wind force perpendicular to the magnetic field at low altitudes and perpendicular to the that same wind force and the magnetic field at higher altitudes. Moreover, at low altitudes, the ions have a very small velocity in the direction of the electric force but move

with a larger velocity at higher altitudes in the direction perpendicular to the electric and the magnetic field.

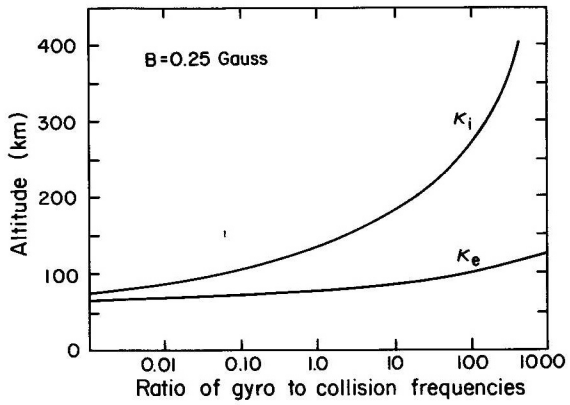


Figure 1.2. Values of the ratio of the gyrofrequency to the collision frequency with respect to altitude, for ions ($K_i$) and electrons ($K_e$). (From *Kelley*, 1989. Copyright 1989 Elsevier. Reproduced with permission of Elsevier.)

Any force that produces a relative motion between the ions and electrons will drive a current:

$$\mathbf{j}=\mathrm{Ne}(\mathbf{V_i}-\mathbf{V_e}), \tag{1.6}$$

where N is the particle number density, e is the charge of the particle, $\mathbf{V_i}$ is the velocity of the ions and $\mathbf{V_e}$ is the velocity of the electrons.

The current produced by the difference in the velocities of ions and electrons due to the forces is represented by equation 1.6. Neglecting the effect of a plasma pressure gradient force and gravity we may then find the current due to the net electric field and the neutral wind:

$$\mathbf{j}=\tilde{\sigma}(\mathbf{E}')\approx\tilde{\sigma}(\mathbf{E}+\mathbf{U}\times\mathbf{B}) \text{ or} \tag{1.7}$$

$$\mathbf{j}=\sigma_0(\mathbf{E}'^{\parallel})+\sigma_P(\mathbf{E}'^{\perp})-\sigma_H(\mathbf{E}'^{\perp}\times\hat{\mathbf{b}}) \tag{1.8}$$

The matrix $\tilde{\sigma}$ is called the conductivity tensor, and its components are the Direct ($\sigma_0$), Pedersen ($\sigma_P$) and Hall ($\sigma_H$) conductivities. The conductivities can be used to describe the components of the current with respect to the forces and the magnetic field.

An altitude profile of these conductivities is shown in Figure 1.3 for daytime and nighttime. The conductivity is used to express the components of the current with respect to the force (electric field) and the magnetic field. An electric field that is parallel to the magnetic field line drives a current defined by the parallel conductivity. For electric fields perpendicular to the magnetic field two conductivities determine currents flowing respectively parallel and perpendicular to the electric field (and magnetic field). The conductivity parallel to the electric field is the Pedersen conductivity while the conductivity perpendicular to the electric field and the magnetic field is the Hall conductivity. The direct conductivity is much higher than the Pedersen and Hall conductivity at all altitudes in the ionosphere allowing us to consider the magnetic filed lines approximately as electric equipotentials. At night the E-region conductivity becomes very low in comparison with the F-region conductivity. At about 100 km altitude, the Hall conductivity is larger than the Pedersen conductivity during the day but the Hall conductivity becomes lower than the Pedersen conductivity with increasing altitude. In the F region between 200 and 400 km, the Pedersen conductivity dominates.

From the condition for a divergence free current that must be satisfied in the ionosphere, $\nabla \bullet \mathbf{J} = 0$, we can derive the so-called dynamo equation relating the neutral wind to the electric field. Integrating the perpendicular current driven along the magnetic field line from the base at the southern foot to the base at the northern foot we have:

$$\int_s^n \nabla_\perp \bullet (\tilde{\sigma}(\mathbf{E}^\perp))ds = -\int_s^n \nabla_\perp \bullet (\tilde{\sigma}(\mathbf{U}\times\mathbf{B}))ds + \mathbf{j}^{\parallel}{}_s - \mathbf{j}^{\parallel}{}_n \qquad (1.9)$$

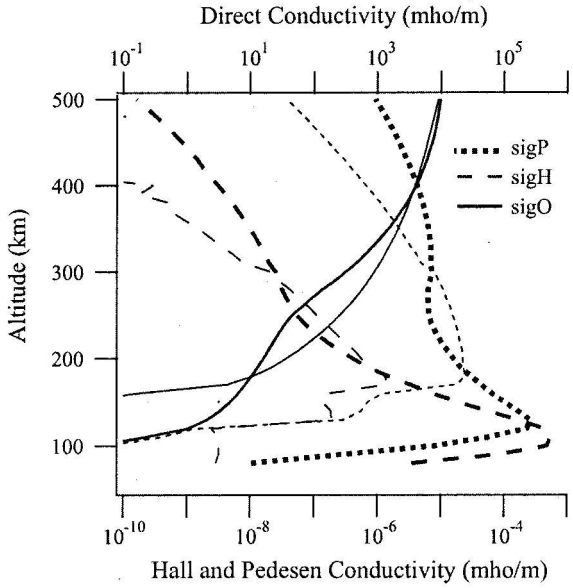


Figure 1.3. Representation of the altitude variation of the conductivities. The heavy curves indicate daytime values while the lighter curves indicate nighttime values. The direct conductivity is represented by the curve sigO, the Pedersen current corresponds to the dotted line sigP, and the Hall current is the dashed line sigh. (From *Heelis*, 2004. Copyright 2004 Elsevier. Reproduced with permission of Elsevier.)

Here $\mathbf{j}_s$ and $\mathbf{j}_n$ are the field aligned currents in the direction parallel to the magnetic field. At the base of the conducting ionosphere we may assume that $\mathbf{j}_s^{\parallel}$ and $\mathbf{j}_n^{\parallel}$ are zero. Thus, knowing the value of the neutral wind **U** it is possible to calculate the value of **E** using this dynamo equation. It is usual to express **E** in terms of the electric potential, $\mathbf{E} = -\nabla\varphi$, to accomplish this task [*Richmond*, 1995].

At middle and low latitudes, the quiet time ionosphere plasma drifts perpendicular to the Earth's magnetic fields are driven mainly by the dynamo action of neutral winds in the E region and the F region [*Rishbeth*, 1971b; 1997]. The E-region dynamo is the main source of electric fields during the daytime while the F-region dynamo contributes with more significance during the nighttime and particularly near the sunset and sunrise local time periods. The observed

electric fields on the dayside and nightside result principally from conductivity gradients at the terminators. The electric fields map throughout the F and E region along the magnetic field lines and are associated with upward and westward ion drifts during the day and downward and eastward drifts at night. The zonal drifts are generally much larger than the vertical velocities. However, the vertical drift is often enhanced just after sunset in a feature called the prereversal enhancement (PRE) [*Eccles*, 1998; *Fesen* et al., 2000].

Assuming a uniform neutral wind and magnetic field in altitude and latitude, the contribution of the F-region can be expressed in terms of the flux tube integrated Pedersen conductivity in the F- and E-region as follows:

$$\mathbf{E} \approx -\frac{\sum_F^P}{\sum_E^P + \sum_F^P}(\mathbf{U} \times \mathbf{B})$$

Here $\sum_E^P$ and $\sum_F^P$ are the flux tube integrated Pedersen conductivity in the E- and F-region respectively, **U** is the neutral wind and **B** the magnetic field line.

The electric field produced by the F-region dynamo is created when there is a divergence in the meridional wind driven current. This divergence is caused by altitude gradients in the flux tube integrated Pedersen conductivity. At the dusk terminator the zonal wind is eastward. The wind then produces a vertical current proportional to $\Sigma p(\mathbf{U} \times \mathbf{B})$ which produces a vertical downward polarized electric field. Near the dusk terminator and during the night, negative polarization charges will accumulate at altitudes below the apex height corresponding to the maximum value of the flux-tube-integrated Pedersen conductivity and similarly positive charges will accumulate above that apex height. On the east side of the negative polarization charge a fringing zonal electric field is produced and directed towards the negative charge. The electric

field is eastward producing an upward **E**x**B** drift that is the principal cause of the prereversal enhancement [*Rishbeth*, 1971; *Eccles* et al., 1998].

The downward electric field produced at the dusk terminator is mapped along the magnetic field lines from the F region to the E region. This electric field in the E region is equatorward and a westward current is driven by that electric field and the Hall conductivity. This current is directed to the west and since there is a gradient in the zonal current between the dayside and nightside of the dusk terminator a negative polarization charge at the terminator is produced. An electric field is then generated pointing towards the negative charge, being eastward on the dayside and westward on the nightside. This zonal electric field is mapped from the E region to the F region, adding to the effect of the fringing zonal electric field in the production of the PRE [*Farley et al*., 1986].

Previous studies showed that the magnitude of the PRE is largest when there is a better alignment of the dusk terminator with the magnetic meridian. This alignment depends on the longitude since the declination of the magnetic field varies as a function of longitude. *Ren et al*. [2009] showed the magnetic declination and magnitude of the magnetic field as a function of longitude at the dip equator at the height of 850 km. *Su et al*. [2009] also illustrated the same parameters at the height of 350 km, where the maximum negative declination is about -18º near 310º longitude and the maximum positive declination is about 10º in the longitude sector between 180º and 260º. The maximum and minimum values of the magnetic field strength are located near 100º and 300º longitude respectively. Table 1 shows the approximate value of the magnetic declination and the angles between the magnetic meridian and the dusk terminator for the longitude sector and seasons we have studied. The alignment is more uniform in the equinox season and generally the angle between the terminator and the magnetic flux tube does not

exceed 10º, except in the Brazilian sector (310º). During the northern winter and northern summer the best alignment occurs in the Brazilian (310º) and Pacific (180º) longitude sectors respectively.

Table 1. Magnetic field declination and angles between the terminator and the magnetic field for the studied longitude sectors.

| **Longitude** | **Declination (degrees)** | **Angle between terminator and magnetic meridian** | | |
|---|---|---|---|---|
| | | December solstice | Equinox | June solstice |
| 270º | 7 | 30.4 | 7 | -16.4 |
| 290º | -4 | 19.4 | -4 | -27.4 |
| 310º | -18 | 5.4 | -18 | -41.4 |
| 0º | -4 | 19.4 | -4 | -27.4 |
| 90º | -2 | 21.4 | -2 | -25.4 |
| 180º | 10 | 33.4 | 10 | -13.4 |

Figure 1.4 shows observations compared with numerical simulation of the equatorial F-region vertical and zonal plasma drift variations as a function of local time. The modeled ion drifts are compared with measurements from the Jicamarca radar. The numerical simulations by *Crain et al*., [1993a] used Dynamic Explorer-2 satellite (DE-2) zonal wind measurements in the F region. There is general agreement between the observations and the model using the dynamo equation (Equation 1.9). The general features we can notice are upward drifts during the day and downward drifts during night. The prereversal enhancement is present near 1800 LT before the vertical drift becomes downward at night. The zonal plasma drifts are westward during the day and eastward during night. The Jicamarca measurements show that the eastward drifts are larger

in magnitude than the westward ion drifts as a result of the dominant F-region dynamo at night [*Fejer*, 1991].

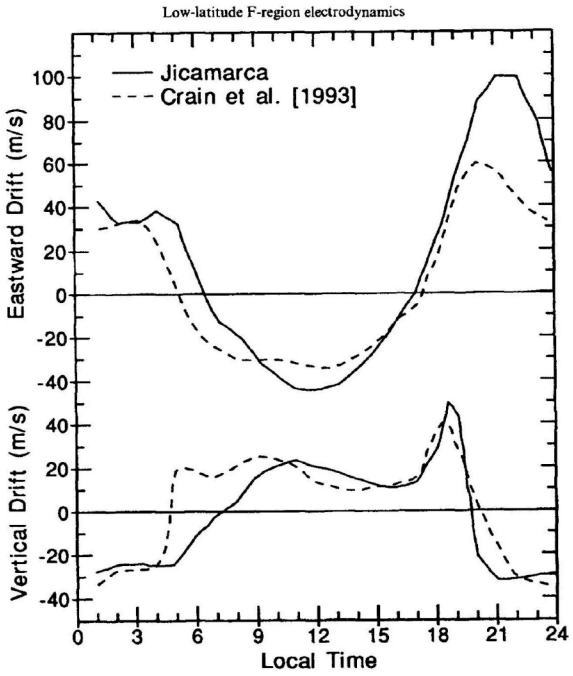


Figure 1.4. Local time distribution of the equatorial vertical and zonal plasma drifts observations from Jicamarca (solid line) and a numerical simulation model by *Crain et al.*, 1993a. The measurements correspond to equinox solar maximum conditions. (From *Fejer*, 1997. Copyright 1997 Elsevier. Reproduced with permission of Elsevier.)

### 1.2.3 Latitude, Altitude and Longitude variations in the ionospheric density

The plasma density distribution in space is strongly dependent on the plasma motion. The Equatorial Ionization Anomaly (EIA) is a clear example of the strong influence that upward ion drifts at the equator have over the distribution of the density in altitude and latitude. Also the vertical ion drift is a main factor in determining the nighttime occurrence of plasma structure at the equator known as spread-F [*Fejer et al.*, 1999]. Figure 1.5 shows the distribution in latitude and altitude of the plasma density produced by **E**x**B** drifts extracted from the results of the CTIPe model for 2000 LT [*Fuller-Rowell et al.*, 2002]. The simulation corresponds to quiet-time

conditions with a moderately high solar photon flux (10.7 cm solar flux of 160 units). The upward ion drift during the day produces an equatorial ionization anomaly that is most pronounced in the evening sector, when peaks in the ion number density are displaced almost symmetrically about 20º on each side of the magnetic equator. This figure shows results for the 90º longitudinal sector that passes through 20 LT at 14 UT. In this case we notice that the magnetic equator is displaced to the north. The density peaks are observed at geographic latitudes of about -10º and 30º, and at altitudes near 380 km.

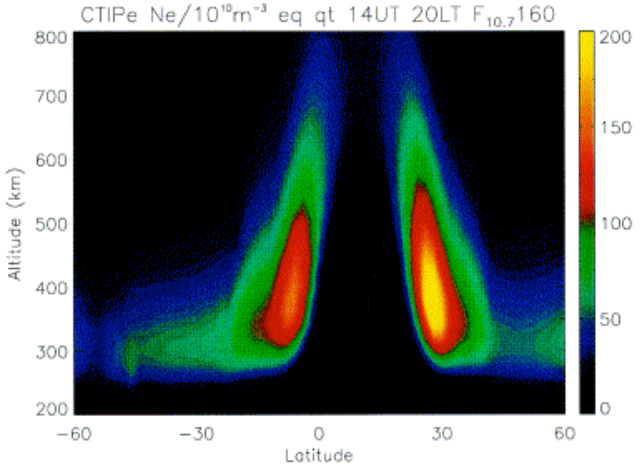


Figure 1.5. Height/Latitude structure of plasma density using the Coupled thermosphere ionsophere plasmasphere electrodynamic model (CTIPe). Altitude coverage is from 200 to 800 km, through the 20 LT sector at 14 UT. This corresponds to quiet conditions and moderately high solar activity conditions with 10.7 cm solar flux of 160 units. (From *Fuller-Rowell et a*l., 2002. Copyright 2002 Elsevier. Reproduced with permission of Elsevier.)

There are also longitudinal variations in the anomaly as evidenced through observations such as those shown in Figure 1.6 [*Immel et al*., 2006]. Here the UV imager aboard the IMAGE satellite captured a periodic wavenumber-4 signature in the airglow peaks corresponding to the equatorial anomaly in the ionosphere. The observations were taken at 2000 LT in the F region. Evidence for the longitudinal variation in the ion density itself is shown in Figure 1.7. Here,

results from the averaged ion density from ROCSAT-1 (1999-2004) at 1000-1200 LT (top panel) and at 2100-2300 LT (bottom panel) are presented [*Kil et al*. 2007]. The nighttime ion density map at 2100-2300 LT differs significantly from the daytime ion density representation. The density peaks during the day are located between -10º and 10º magnetic latitude and at geographic longitudes near 90º, 190º and 250º, while during the night there is a stronger peak in the northern hemisphere at about 10º magnetic latitude and the main peaks are observed near 300º and 360º geographic longitude. These data suggest that longitude and latitude variations may result from a range of poorly described sources, thus stimulating the studies proposed here.

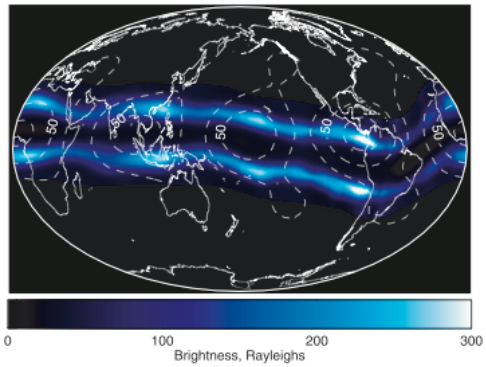


Figure 1.6. IMAGE-FUV observations of nighttime ionospheric emissions at 2000 LT. The longitudinal variability of the equatorial ionospheric anomaly can be noticed. The southern anomaly is represented with a mirror image of the northern anomaly due to a poor sampling of the southern observations. The amplitude of the diurnal temperature variation at 115 km is represented in white dashed contour lines. (From *Immel et al*. 2006. Copyright 2006 American Geophysical Union. Reproduced by permission of American Geophysical Union.)

### 1.2.4 Ion drift latitude variations

Ground-based observations show significant differences in the ion drifts for different latitudes. The Jicamarca and Arecibo observatories are near the same longitude but separated by 29 degrees in magnetic latitude. The Jicamarca radar is located nearly at the magnetic equator

(latitude 11.95° South, longitude 76.87° West, 1°N magnetic). The Arecibo radar is at magnetic latitude of 30° N (18.30°N geographic latitude, 66.75°W geographic longitude).

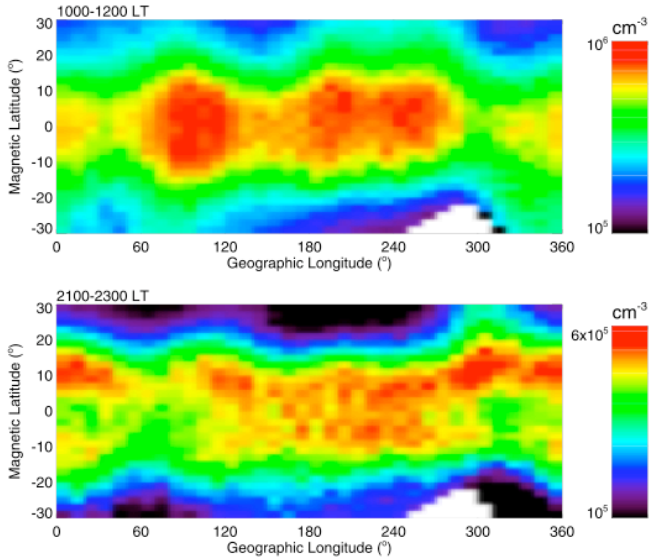


Figure 1.7. Ion density maps at 1000-1200 LT (top) and 2100-2300 LT (bottom). The averaged density in each bin of 10° longitude by 2° latitude is calculated from ROCSAT-1 data during March 1999 to June 2004. (From *Kil et al*. 2007. Copyright 2007 American Geophysical Union. Reproduced by permission of American Geophysical Union.)

Figure 1.8 shows the most noticeable differences between the ion drifts at Jicamarca and Arecibo. The left panel shows the quiet time Jicamarca average F-region vertical drifts for equinox (March to April, September to October), winter for the southern hemisphere (May to August) and summer for the southern hemisphere (November to February) for different levels of solar flux ranging from low to high solar activity. In all the seasons the pattern is similar, following a 24-hour periodic waveform with positive values during the day and negative values during the night, with an ion drift peak near 1800 LT followed by a reversal [*Fejer*, 1991].

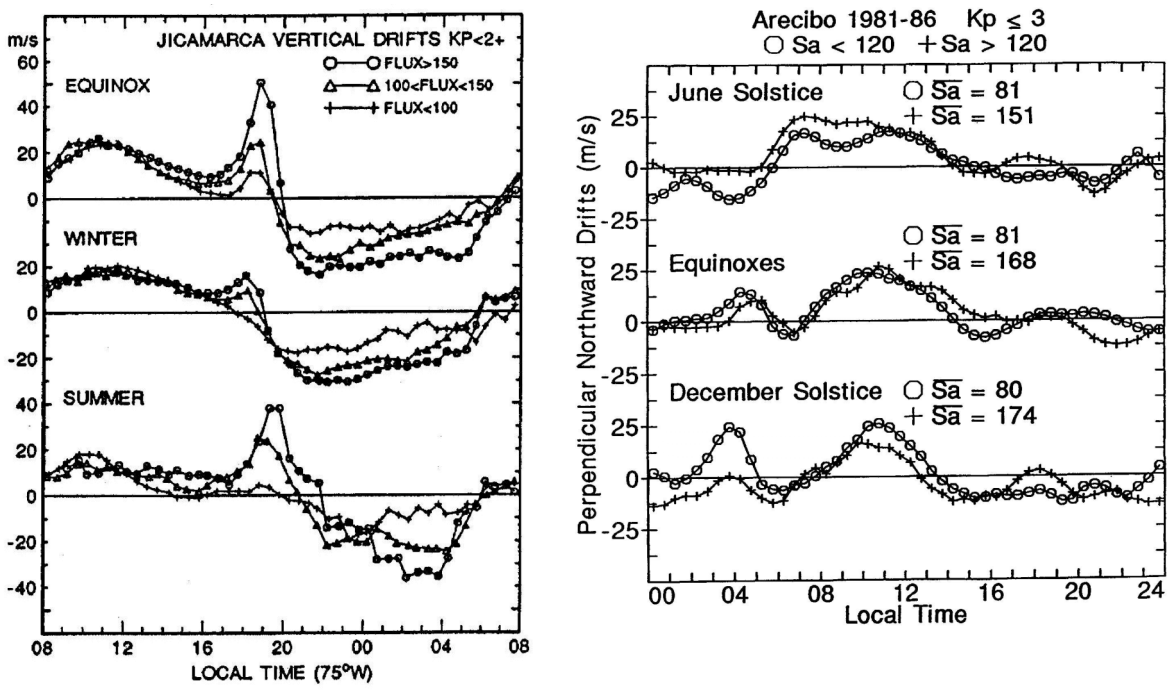


(a) (b)

Figure 1.8. (a) Vertical ion drift at Jicamarca for different seasons and solar flux conditions during quiet time (from *Fejer et* al., 1991b, copyright 1991 American Geophysical Union, reproduced by permission of American Geophysical Union); (b) Perpendicular/north F-region plasma drifts over Arecibo for different seasons during quiet times (Kp≤3). The averaged 10.7 cm solar flux values (Sa) are also shown. (From *Fejer*, 1993. Copyright 1993 American Geophysical Union. Reproduced by permission of American Geophysical Union.)

The right panel shows the seasonally averaged perpendicular/northward drifts at Arecibo during quiet times for low and moderate-to-high solar flux conditions. Notice the axes for this period differ from those in Figure 1.8 (a). The local time starts at 0800 LT in Figure 1.8(a) while Figure 1.8(b) starts at 0000 LT. At Jicamarca the daytime drifts are upward showing a single diurnal oscillation with a peak appearing slightly before local noon. In contrast, at Arecibo the daytime drifts show minima in local time near 0600 and 1500 LT indicative of the presence of a semi-diurnal oscillation. The peaks observed after midnight and before dawn during the equinox and December solstice are also another relevant difference with respect to the Jicamarca drift

features. Large conductivity changes in the conjugate ionosphere are considered the reason for these peaks [*Fejer*, 1993]. The perpendicular/northward drifts do not change much with solar flux. Nevertheless significant changes in magnitude and sign exist at these two locations for a fixed local time.

Zonal drifts at Jicamarca and Arecibo are presented in Figure 1.9. Figure 1.9(a) shows the Jicamarca zonal drifts for two different solar flux levels (<120 and >120) and for different seasons. They have a shape similar to the zonal drifts described in Figure 1.4. The eastward drifts at night have larger amplitude than the daytime westward drifts. Figure 1.9(b) shows the zonal ion drift over Arecibo for the same conditions as in Figure 1.8 (b). These drifts are generally westward from midnight to early afternoon and eastward from the afternoon to midnight. The nighttime eastward drifts increase with solar activity especially during equinox and the June solstice. The largest westward drift occur during the December solstice and there is not a significant variability in the westward drift with respect to solar activity [*Fejer*, 1993]. The nighttime zonal drift at Arecibo is significantly smaller than that seen at Jicamarca. Thus, again there are significant variations in magnitude and sign at these two locations for fixed local time.

### 1.2.5 Ion drift longitude variations

There are different possible sources of longitude variations in the ion drift including longitude variations in the driving neutral winds, variations due to the magnetic field orientation, the displacement between the geographic and geomagnetic equators, and variations in the wind-driven current due to longitude variations in the ionospheric conductivities. *Fejer et al*. [1995] studied observations from the Atmospheric Explorer-E satellite (AE-E) for quiet times ($Kp \leq 3$) around the magnetic equator.

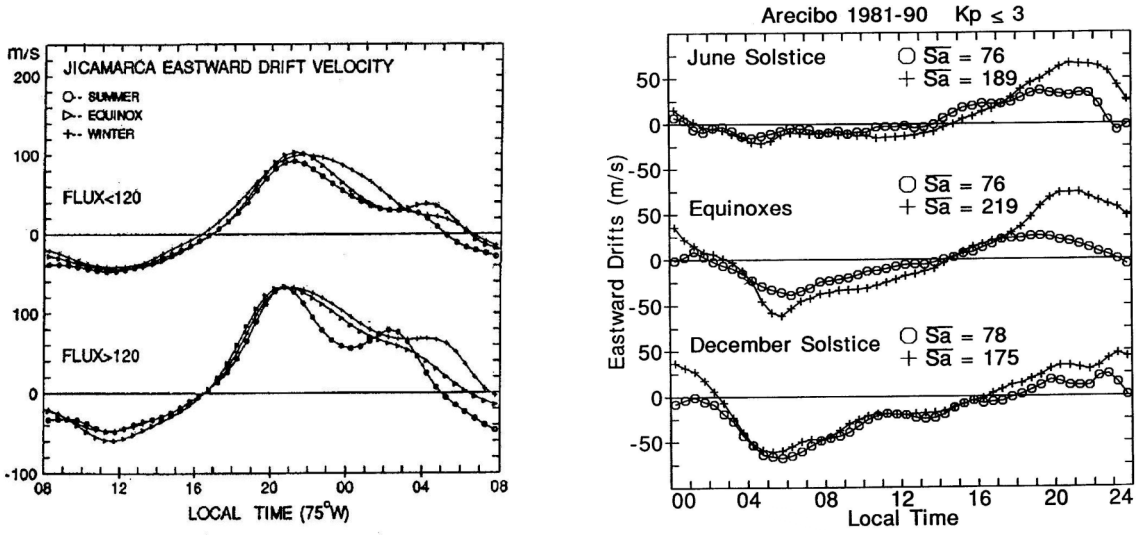


(a) (b)

Figure 1.9. (a) Zonal plasma drifts observed by the Jicamarca radar for different solar flux conditions and seasons (from *Fejer et al*., 1991b, copyright 1991 American Geophysical Union, reproduced by permission of American Geophysical Union); (b) Zonal plasma drifts over Arecibo for the same conditions as in Figure 1.8(b). (From *Fejer*, 1993. Copyright 1993 American Geophysical Union. Reproduced by permission of American Geophysical Union.)

Figure 1.10 shows variations in the averaged vertical ion drifts during the period May to August (solstice) for the post-sunset period and for different longitudinal sectors. The post-sunset upward velocity peak is an important parameter for controlling the height of the evening equatorial F layer and the presence of equatorial spread-F. The largest upward drift is observed in the longitude sector 160º-200º corresponding to the Pacific sector, but this sector has the lowest post-sunset downward vertical drift. The longitude interval 230º-310º corresponding to the Pacific-South American sector presents the lowest upward drift but the largest downward drift. The latest reversal occurs in the Brazilian-African sector. It has been suggested that the longitudinal variability of the evening vertical drifts is related to the differences in the alignment of the sunset terminator with the local magnetic meridian as a result of changes of the magnetic declination with longitude [*Hartman and Heelis*, 2007].

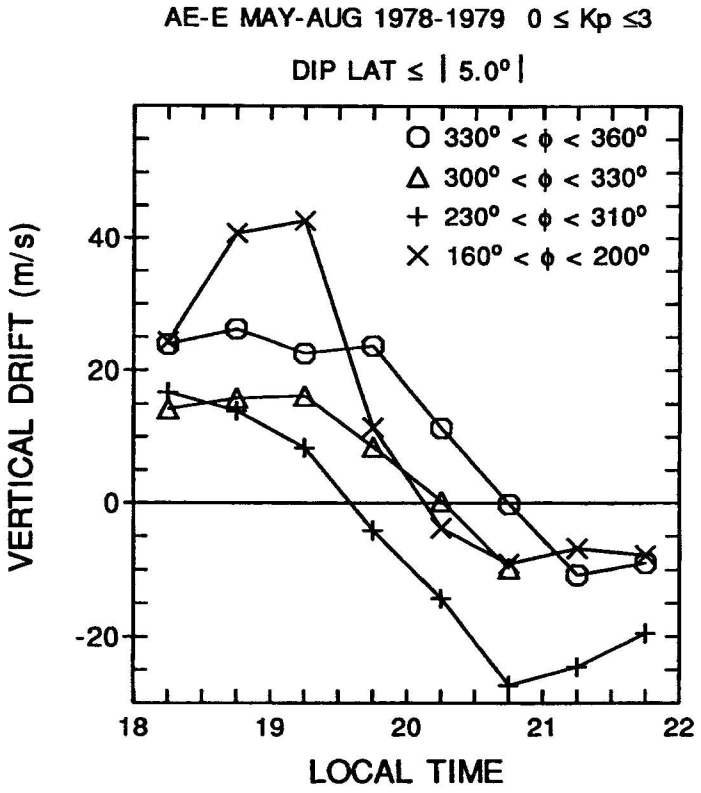


Figure 1.10. Vertical drifts measured by AE-E satellite near the magnetic equator in different longitude sectors after sunset. (From *Fejer et al.*, 1995. Copyright 1995 American Geophysical Union. Reproduced by permission of American Geophysical Union.)

*Hartman and Heelis* [2007] examined longitudinal variations of the vertical ion drifts in the topside ionosphere at the equator for the years 2001 and 2002 during quiet times. They used measurements from the ion drift meter on DMSP F15 where the local time is fixed near 0930. They suggest that the observed drifts are influenced by F region meridional winds that drive zonal currents at the feet of flux tubes that cross the equator in the topside ionosphere. Figure 1.11 shows the vertical drift from DMSP F15 from June to December of the year 2002 near 0930 LT. Each panel illustrates the vertical drifts for a month, and the solid line is the result of fitting the points using a series of periodic functions of longitude representing the first five terms in a discrete Fourier series. A local minimum appears in the region of positive magnetic declination

in northern summer and in the region of negative declination in northern winter. A seasonally dependent variation as a function of longitude is also observed. A wavenumber-4 longitudinal variation is present throughout the year that may be related to tropospheric sources but is more evident in the fall equinox.

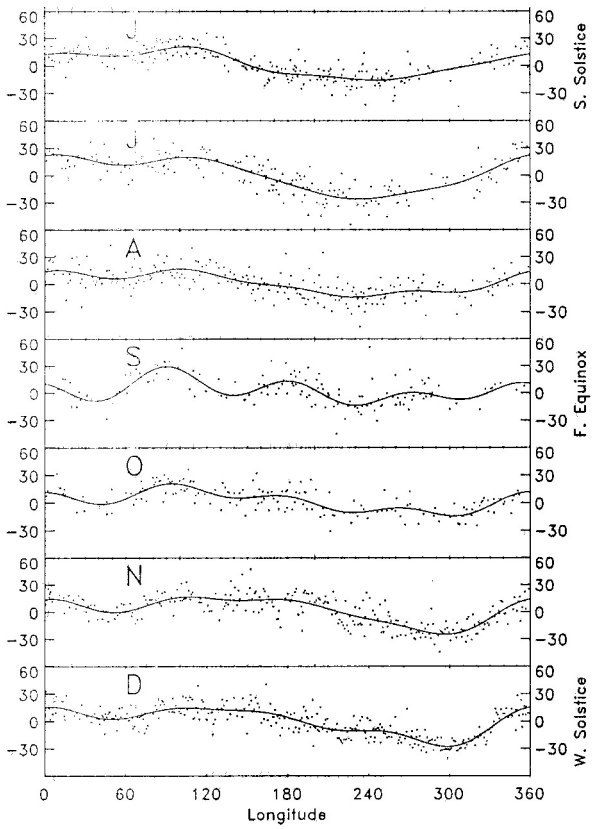


Figure 1.11. Monthly vertical ion drift versus longitude. Measurements obtained from DMSP F15 near 0930 LT for the year 2002 corresponding to the month period from June to December. The solid line represents the fitting of the distribution using the first five elements of the Fourier series. (From *Hartman and Heelis*, 2007. Copyright 2007 American Geophysical Union. Reproduced by permission of American Geophysical Union.)

### 1.2.6. Ion drift altitude variations

Information about ion drift velocities from a given radar is generally limited to altitudes below about 1000 km. In fact, the Jicamarca radar usually focuses particularly on altitudes near

the F peak between 300 and 400 km where the signal to noise ratio is highest, giving the most accurate results [*Fejer*, 1985]. Generally the only reliable data exist for altitudes below 500 km. Some observations of zonal drift changes with respect to altitude at low latitudes [*Fejer*, 1985] in the F region using Jicamarca data are shown in Figure 1.12 and 1.13. In Figure 1.12 we see the east-west F-region ion drifts for daytime near 1300 LT. Even though they present a large variation over times scales of 5-10 minutes, the average profiles obtained with integration times of 20-30 minutes only show a small variation with height. This suggests the presence of short period waves. Figure 1.13 shows a similar height profile as in Figure 1.12, but the measurements correspond to nighttime. There is a larger variation in the averaged zonal drifts than in daytime with a reversal in the zonal drift near 250 km altitude. With the satellite data from ROCSAT-1 and DMSP we are able to extend the apex-height variability description from altitudes above 600 km up to altitudes greater than 3000 km by mapping the drifts and electric fields from a broader range of latitudes along the magnetic field lines to the respective apex-height.

### 1.2.7. Ion drift storm time perturbations

The ion drifts are also affected by influences from high latitudes, particularly during periods of strong geomagnetic activity. The ionospheric motions are affected by a combined effect of two sources: direct penetration of magnetospheric potentials, also known as penetration electric fields [*Spiro et al,* 1988; *Wolf*, 1995] and disturbance dynamo electric fields [*Blanc and Richmond*, 1980]. The first process is driven by changes in the polar cap potential that are unshielded from the plasmasphere and produce prompt penetration of ion motions at low latitudes. Changes in the global circulation induced by Joule heating at auroral latitudes during storm time cause the disturbance dynamo.

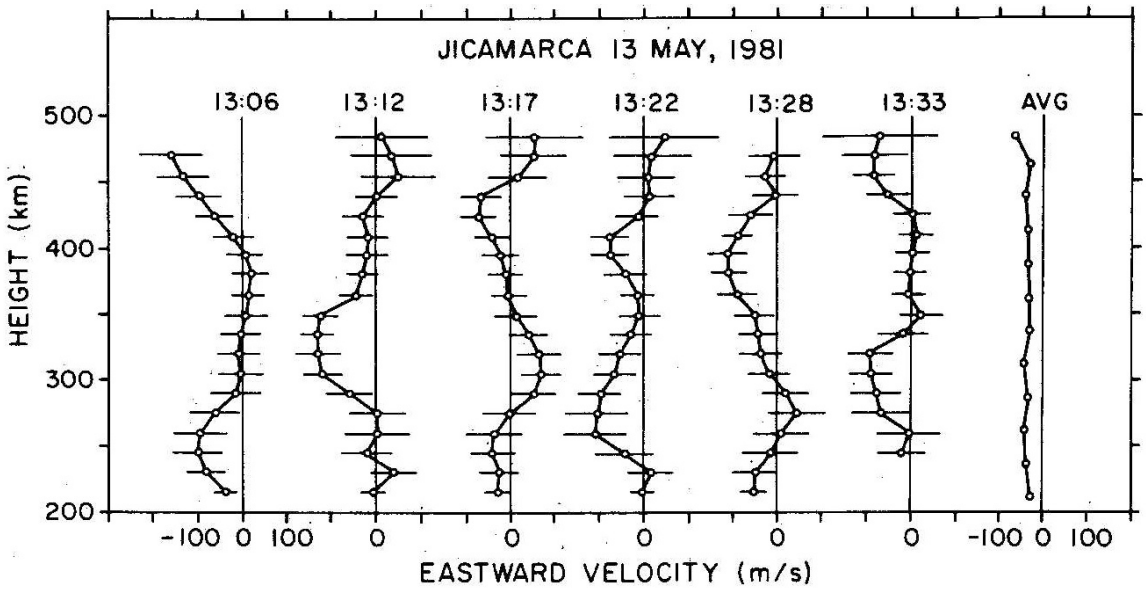


Figure 1.12. Altitudinal profile of the zonal plasma drifts over Jicamarca with an integration time of about 5 minutes during daytime. The average profile (AVG) is obtained with integration time of 20-30 minutes. (From *Fejer*, 1985. Copyright 1985 American Geophysical Union. Reproduced by permission of American Geophysical Union.)

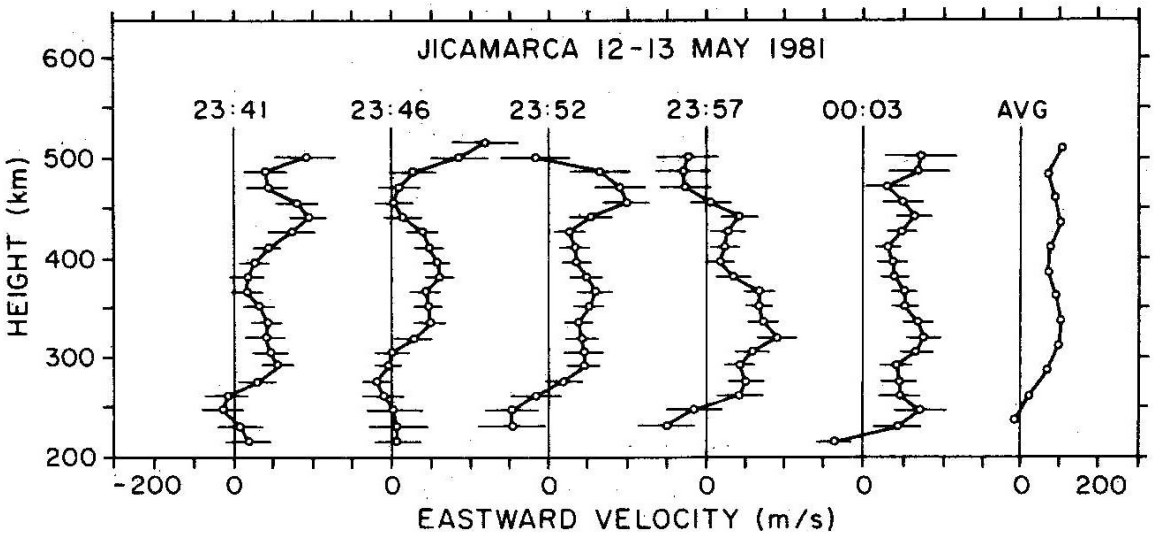


Figure 1.13. Similar as figure 1.12 but for nighttime. The average east-west drift shows more variation than during daytime. (From *Fejer*, 1985. Copyright 1985 American Geophysical Union. Reproduced by permission of American Geophysical Union.)

## 1.3 Objectives

There are good reasons to expect latitude (apex-height) variations in ion drifts that are produced by the action of winds. The large variability of the winds in latitude is therefore expected to be reflected in the ion drifts. In addition, there are external magnetospheric influences that decrease with decreasing latitude. Another factor to consider is the change in the magnetic field orientation with respect to the geographic equator at different latitudes and longitudes and the offsets in latitude of magnetic field foot points on each side of the geographic equator.

Our main research goal is to study the ion drifts and electric fields in the ionosphere at low- and mid- latitudes using satellite measurements (ROCSAT-1 and DMSP). We separately consider different aspects during disturbed and quiet time conditions. Since ground-based stations have the limitation of being in a fixed location, the use of satellite measurements is vital to study the latitude variation in ion drifts at all longitudes and between the latitudes of Jicamarca and Arecibo for different local times, and to provide appropriate resolution in latitude (apex-height) and longitude. First we investigate storm time ion drift perturbations at the magnetic equator and their local time and longitudinal dependence. In addition, we describe the quiet time latitudinal variations of the ion drifts between ± 25º magnetic latitude as a function of local time and longitude.

From all the evidence shown we conclude that a more detailed description of the latitudinal and longitudinal variations of the ion drifts improves our understanding of the dynamics of the ionosphere. This new knowledge will be useful in ionosphere/thermosphere modeling and the prediction of the behavior of the region.

# CHAPTER 2

# APPROACH

## 2.1 DATA SELECTION

We use ion drift measurements from the DMSP F15, DMSP F13 and ROCSAT-1 satellites during the solar maximum period of 1999-2003. These satellites are three-axis stabilized with one axis aligned along the local vertical direction. In addition to the in situ measurements we compare and complement our observations with data at lower altitudes from ground-based measurements using the Jicamarca and Arecibo radars. First we separate the storm-time data from the quiet-time measurements. The storm-time index (Dst), the interplanetary magnetic field (IMF) and the Kp index are used as parameters to distinguish the disturbed times from the quiet times during the entire period of study. For the perturbed time measurements, we identify major storm events from 2000 to 2004 and study the vertical and the zonal ion drift perturbations near the magnetic equator. For quiet times, the ROCSAT-1 data are selected for the period 1999-2003 and the sample space is divided in latitude, longitude and local time bins in order to find average representative values of ion drifts inside those bins. We investigate the ion drifts in the direction parallel and perpendicular to **B** and describe the quiet time variations of the **E**x**B** drifts in local time and latitude (apex-height) for different longitude sectors and seasons.

### 2.1.1 DMSP data

For our storm-time investigation we utilize the ion drift measurements near 830 km altitude from the DMSP F15 and DMSP F13 for the years 2000-2004. The data files contain the universal time (UT), local time (LT), the ion drift velocity in the ram direction ($V_X$), the ion drift velocity in the upward direction away from the center of the Earth ($V_Z$), and the ion velocity ($V_Y$) in the direction perpendicular to both $V_X$ and $V_Z$ that constitutes a right hand coordinate system. Also, the geographic latitude and longitude, and the magnetic latitude and altitude of the satellites for each measurement point are included in the data files. The data have a four-second cadence.

Each file contains data for a complete orbit that starts and ends when the satellites are located at the ascending node at zero geographic latitude. The files are in HDF format and are located at the server CSS20, which is administrated by the William B. Hanson Center for Space Sciences at the University of Texas at Dallas.

The F13 satellite crosses the equator near 1830 LT during the ascending pass and near 0630 LT during the descending pass. The F15 satellite crosses the equator near 2130 LT during the ascending pass and near 0930 LT during the descending pass. For data with a four-second cadence the eastward flow component due to the rotation of the Earth is calculated at the spacecraft's altitude and removed from the horizontal ion flow data ($V_X$ and $V_Y$) to obtain the velocity measurements in a corotating reference frame.

### 2.1.2 ROCSAT data

The ROCSAT data files include measurements for the years 1999-2004. The variables that are important to our study are the ion drift velocity in the ram direction ($V_X$), the ion drift

velocity in the direction downward toward the center of the Earth ($V_Z$), and the ion drift velocity in the direction perpendicular to $V_X$ and $V_Z$ to complete a right hand coordinate system ($V_Y$). In addition to these measurements, the files contain the universal time, local time, total ion concentration, geographic latitude and longitude, magnetic dip latitude and altitude of the spacecraft. The data have a one-second cadence.

Each file has measurements for a complete day of 24 hours, starting when the UT for that day is zero. The data files are stored in ASCII format made available by the National Central University of Taiwan and reside on the CSS20 server at UTD.

### 2.1.3 Additional data

In order to distinguish the ion drift or electric field data at storm-time periods from the quiet periods we use the disturbance storm time index (Dst), the interplanetary magnetic field (IMF) and the magnetic index Kp values for the years 1999-2004. We obtain the Dst and Kp from the OMNI database (http://nssdcftp.gsfc.nasa.gov/spacecraft_data/omni/) and the IMF from the Advanced Composition Explorer (ACE) (http://ftpbrowser.gsfc.nasa.gov/ace_merge.html) database; both provided by NASA's National Space Science Data Center (NSSDC). The Dst, Kp and IMF are provided with 1 hour, 3 hour and 4 minute resolution respectively.

## 2.2 INSTRUMENTATION

### 2.2.1 Defense Meteorological Satellite Program (DMSP)

The Defense Meteorological Satellite Program (DMSP) is a system of weather satellites operated by the United States Department of Defense. Each of these satellites has a Sun-synchronous near-polar orbit at an altitude of 830 km above the surface of the Earth. The orbit

has an inclination of 98° with a period of about 101 minutes, and the orbit path on the Earth's surface moves westward about 25° longitude for each pass. The DMSP-F13 orbits with equatorial crossings near 0600 and 1800 local time, and the DMSP-F15 orbits with equatorial crossings near 0930 and 2130 local time. The DMSP satellites contain space environment sensors that include the Special Sensor-Ions, Electrons, and Scintillation (SSIES) package, which consists of thermal plasma instruments including a Retarding Potential Analyzer (RPA), an Ion Drift Meter (IDM) [*Heelis and Hanson*, 1998; *Holt*, 1995], a Langmuir probe, and a scintillation meter. We use the observations from the RPA and the IDM to obtain the ion drift velocity and the ion density. For the SSIES data we use a coordinate system where +x is in the direction of the spacecraft motion, +y is in the cross-track horizontal direction, and +z is directed vertically upward away from the center of the Earth. All data provided have a 4-second sample rate. That means that the velocities are measured approximately every 32 km along the satellite track. The IDM samples the cross track ion velocities 6 times per second for both the horizontal and vertical flows, and 24 samples for each component are averaged to match the 4-second sample rate of the RPA. The scintillation meter samples the ion density 24 times per second and 96 samples are averaged to match the 4-second sample rate of the RPA. The drifts are measured with a sensitivity of around 5 m/s but with a larger uncertainty in the absolute value due to a less stringently specified sensor look direction.

### 2.2.2 ROCSAT

ROCSAT-1 (FORMOSAT-1) is the first scientific satellite program of the Republic of China (Taiwan, R.O.C.). It was launched on January 27, 1999 from Cape Canaveral, Florida, and ended its mission on June 17, 2004. ROCSAT-1 is a low-earth-orbit scientific experimental

satellite. It has a near-circular orbit with an altitude of about 600 km, an inclination of 35° and a period of 97 minutes. In addition, the ROCSAT-1 mission took place during the active phase of Solar Cycle 23, when space weather phenomena were most intense [*Yeh et al*., 1999b].

The major mission of ROCSAT-1 included three scientific experiments for measuring the effects of ionospheric plasma and electrodynamics, observing the ocean color image and conducting Ka-band communication experiments. On board ROCSAT was the Ionospheric Plasma and Electrodynamics Instrument (IPEI). The IPEI is a joint project of the National Space Program Office of the Republic of China, the University of Texas at Dallas, The National Central University, and the National Chiao-Tung University.

The IPEI sensors consist of an ion trap (IT), a pair of ion drift meters (IDM) and a retarding potential analyzer (RPA) [*Chang et al*., 1999]. The instrument is designed to measure the ion density, temperature, composition and drift velocity in order to study the large-scale electrodynamics, plasma distribution, and the small-scale plasma structure in the low-latitude ionosphere. IPEI was operated with a 100% duty cycle and was capable of taking data at a sampling rate of 1 kHz in selected regions. Large-scale electrodynamics but also small scale plasma structures in the topside ionosphere at middle and low latitudes can be studied using the IPEI data.

The design of the IPEI instrument is similar to those used on board the Atmosphere Explorer (AE), Dynamics Explorer (DE) and DMSP satellites since the sensors have the same principles of operation. In the case of ROCSAT the RPA has a sampling rate of 32 Hz in the NORMAL mode of operation and 64 Hz during the FAST mode providing the measured parameters at 1 Hz or 2 Hz rate during the NORMAL mode and 2 to 4 times each second during the FAST mode. This rate depends on the number of steps of the retarding potential used to

obtain the characteristic curve of potential versus ion current. The IDM, which consists of the horizontal drift meter (HDM) and the vertical drift meter (VDM), and the IT instruments have a sampling rate of 32 Hz in NORMAL mode and 1024 Hz in the FAST mode. The data files we use have a sample rate of 1 Hz that results from averaging the values to obtain the parameters at a one-second cadence regardless of the operational mode. The ion velocities are measured approximately every 8 km along the satellite track. The accuracy of the ion drift measurements is about +/- 10 m/s [*Su et. al*, 1999; *Yeh et. al*, 1999a].

### 2.2.3 Instruments

**Retarding Potential Analyzer**

The Retarding Potential Analyzer (RPA) is a planar electrostatic probe. It has a circular aperture and a series of co-planar grids that precede the ion collector. The aperture faces approximately along the spacecraft velocity vector. The ion collector is a flat solid metal conductor, which allows measurement of the ion current using a sensitive electrometer. A system of internal grids controls the energy of the ions that can reach the collector. The grid and collector configuration are shown in Figure 2.1. A grid that covers the aperture has the same potential as the aperture plane and the sensor housing. A second aperture grid is also held at this potential. This assures that the potentials from other grids inside the RPA do not escape outside the sensor and affect the external plasma. This first pair of grids is represented in Figure 2.1 by G1. Following the aperture grids there is a pair of retarding or swept grids labeled G2. They act as energy filters for the ions that pass through the entrance when a sequence of voltages is applied to them. The next grid G3, called the suppressor grid, stops the incoming electrons with energies less than 12 eV. Adjacent to G3 there is a shield grid G4 which has a potential of -1.5V

that decouples the retarding grids from the collector and reduces the noise from the suppressor grid. From the current-voltage characteristic of the RPA, the velocity of the ions along the sensor look direction, the temperature of the ions, the total ion density and the fractional composition of the plasma in $H^+$, $He^+$, and $O^+$ can be derived.

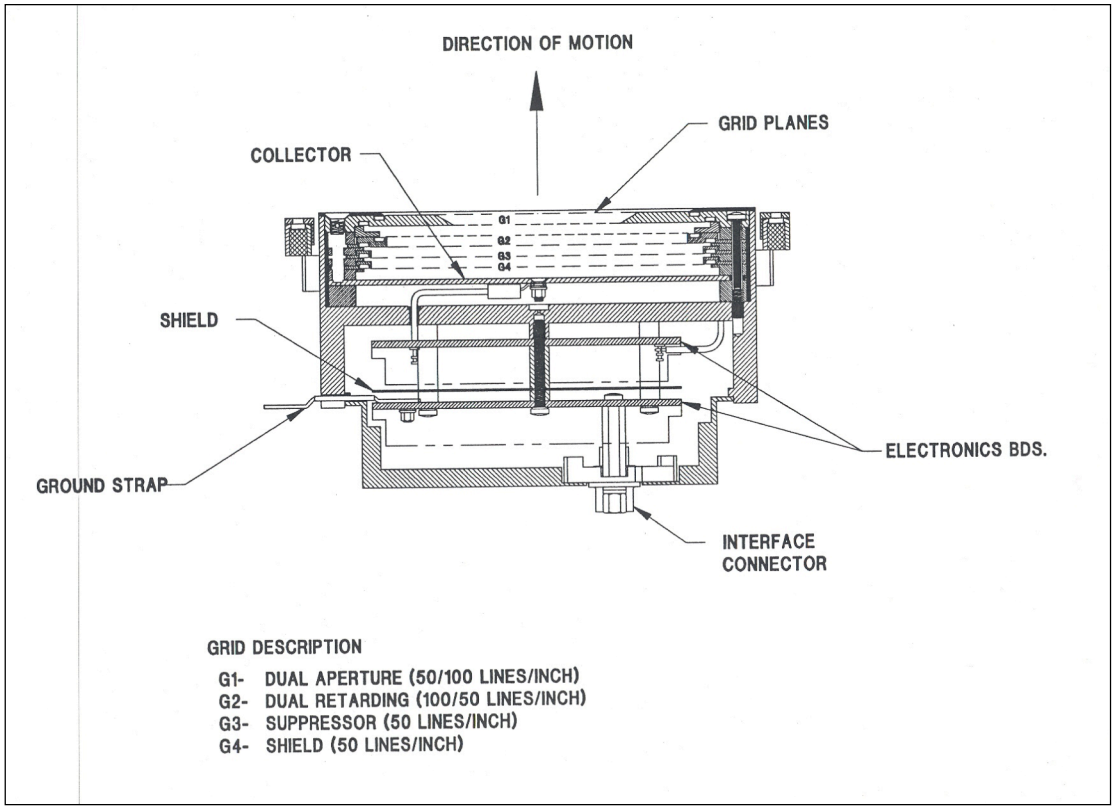


Figure 2.1. Retarding Potential Analyzer sensor cross section (from *Holt*, 1995).

**Ion Drift Meter**

The Drift Meter (DM) is also a planar electrostatic collector with a square aperture that faces into the direction of the satellite's motion. The arrangement of the grids that provide a field-free drift space prior to a segmented collector allows the ion arrival angle to be determined. Using the value of the ion ram velocity provided by the RPA together with the angle of arrival it

is possible to determine the two (horizontal and vertical) ion velocity components normal to the satellite velocity. Figure 2.2 provides a schematic representation of the cross section of the IDM. In front of the aperture there is a pair of grids, G1 and G2. Grid G1 has the same potential as the aperture, and the repeller grid G2 can be set to the same potential as the aperture or to small positive potential that is used to bias out light ions while allowing $O^+$ to pass to the collector. A pair of grids, G3, is attached to the aperture having the same potential as the sensor housing and the aperture. Adjacent to G3 are located shield grids, G4 and G5. The last grid is called the suppressor grid and its purpose is to stop the incoming electrons and repel the photoelectrons and secondary electrons emitted by the collector. The collector is located behind the grid stack and it is divided in four quadrants. The ratio of ion currents to vertically and horizontally arranged collector halves are alternately measured, each being directly proportional to the ion arrival angle. Then given the speed of the satellite and the dimensions of the sensor it is possible to convert the measured current ratios into the transverse velocities for the plasma.

**Ion Trap**

The ion trap measures the total ion concentration. The sensor is made up of a series of grids and a collector. The aperture grid and the collector are held at the ambient plasma potential. The suppressor and shield grid are biased to negative potentials to repel thermal electrons and suppress photoemission from the collector. The ion current is measured by a logarithmic electrometer. The measurements are proportional to logarithm of the ion flux which is proportional to the ion concentration, the ion collecting area and the incoming ion velocity relative to the satellite. If the incident velocity is approximated by the spacecraft velocity then

the total ion concentration can be obtained with an accuracy of approximately 5%. Then a direct measurement of the ion trap electrometer provides the ion concentration Ni.

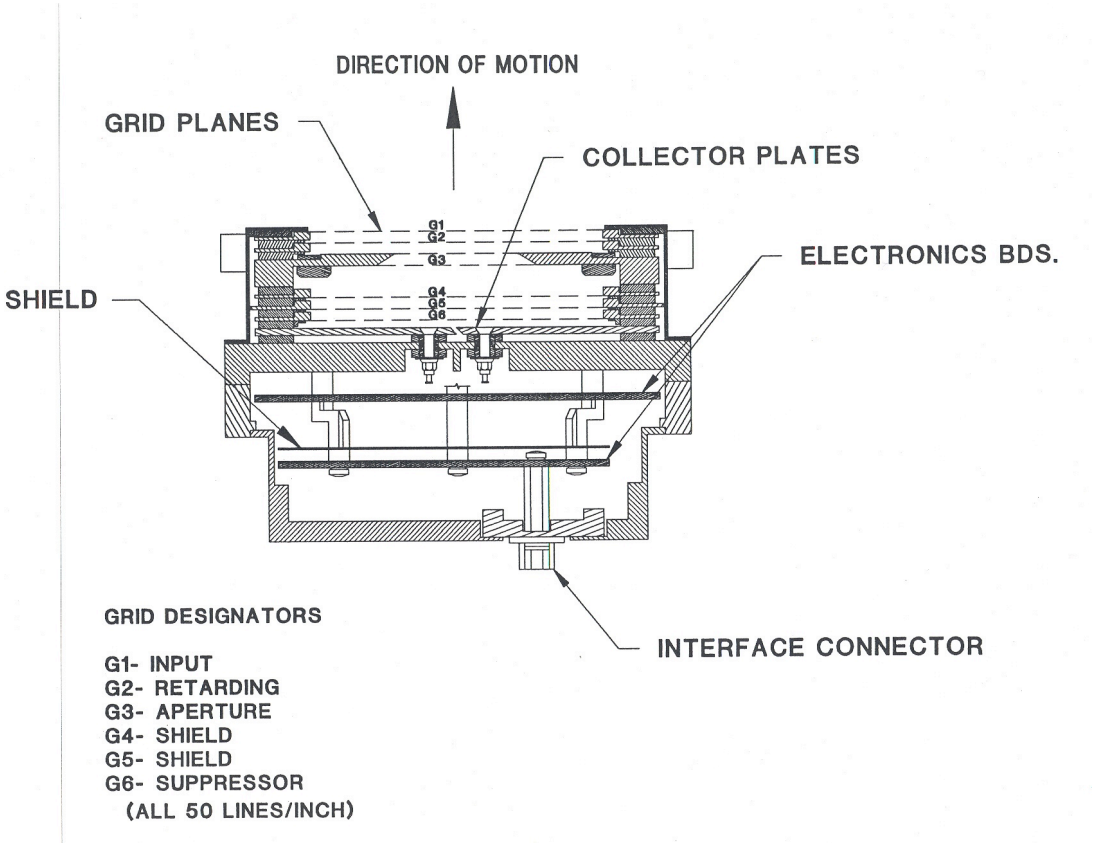


Figure 2.2. Ion Drift Meter sensor cross section (from *Holt*, 1995).

### 2.2.4 Jicamarca and Arecibo radars

Additional data sources provided by radar instruments can be used to compare our results with observations at a fixed position in longitude and latitude. In particular, ion drift observations from the Jicamarca and the Arecibo Observatories from previous studies allow us to compare our observations at low and middle latitudes, respectively. The radar data provide full local time and some altitude variations but at a fixed latitude and longitude.

Most of the features of the electric fields and ion drifts in the equatorial F-region can be described from incoherent scatter radar measurements at the Jicamarca Radio Observatory (JRO) located east of Lima, Peru (latitude 11.95° South, longitude 76.87° West, 1°N magnetic) where the earth's magnetic field is nearly horizontal over the site.

Jicamarca has a modular, phased array antenna designed to operate at 49.92 MHz. The beam of the radar main antenna array can be directed perpendicular to the magnetic field and also oriented 3° from the vertical axis. The incoherent scatter radar typically measures the vertical F region drifts between about 250 and 700 km, with a height resolution of typically 15 km and an integration time of 5 minutes. The vertical drift values near and above the F-region peak (usually between 300 and 500 km) have the highest signal-to-noise ratio. The accuracy of these measurements is usually about 1-2 m/s [*Woodman*, 1970].

The Arecibo Observatory is part of the National Astronomy and Ionosphere Center (NAIC), a national research center operated by Cornell University under a cooperative agreement with the National Science Foundation (NSF). The incoherent scatter radar is located 9 miles from the town of Arecibo, Puerto Rico (18.30°N geographic latitude, 66.75°W geographic longitude, 30°N geomagnetic latitude). The incoherent radar operates at 430 MHz and the antenna dish is 305 m in diameter. The ionospheric drift measurements were changed in 1981 from a three-position mode to a continuously scanning mode over 360° in azimuth at a fixed elevation of about 75°, with a cycle period of about 16 minutes. Ion drift velocities are typically measured near the F-peak with a typical error of about 10 m/s [*Isham et al*., 2000; *Fejer*, 1993].

## 2.3 Data Analysis

ROCSAT measurements of ion drift velocities provide full coverage in longitude and local time near 600 km altitude in the latitude range -35 to +35 degrees geographic. This global coverage is obtained from northbound and southbound passes in about 26 days. Consecutive passes move westward in longitude by about 24 degrees. Figure 2.3 shows the ground track of the ROCSAT-1 orbit for a complete day where we can observe the ascending and descending passes as a function of latitude and longitude.

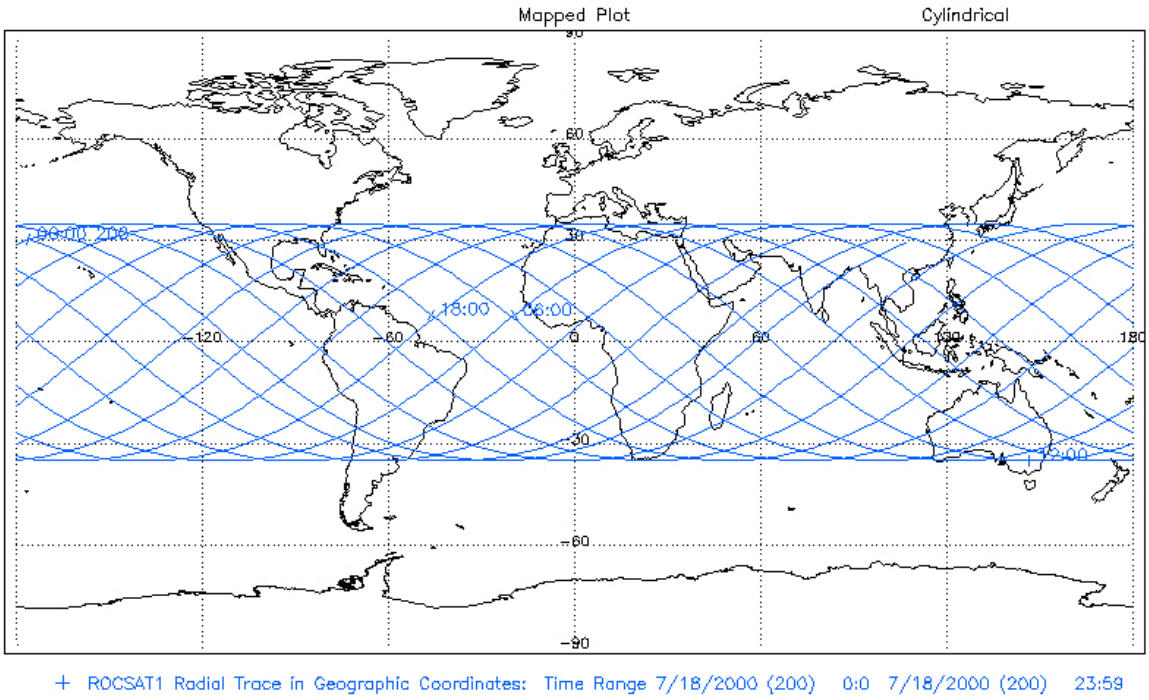


Figure 2.3. ROCSAT-1 orbit mapped projection for 24 hours. The latitude coverage range is from -35 to 35 geographic degrees. The local time of ascending and descending passes is approximately fixed for a specific latitude (http://sscweb.gsfc.nasa.gov/cgi-bin/sscweb/Locator_graphics.cgi).

We utilize the satellite data for our studies and the radar data as single point verification and validation of our findings. The DMSP data provide the same ion drift and density parameters

as ROCSAT-1 but at fixed local times near 830 km altitude. Figure 2.4 shows the ground track of the DMSP-F13 orbit for a complete day.

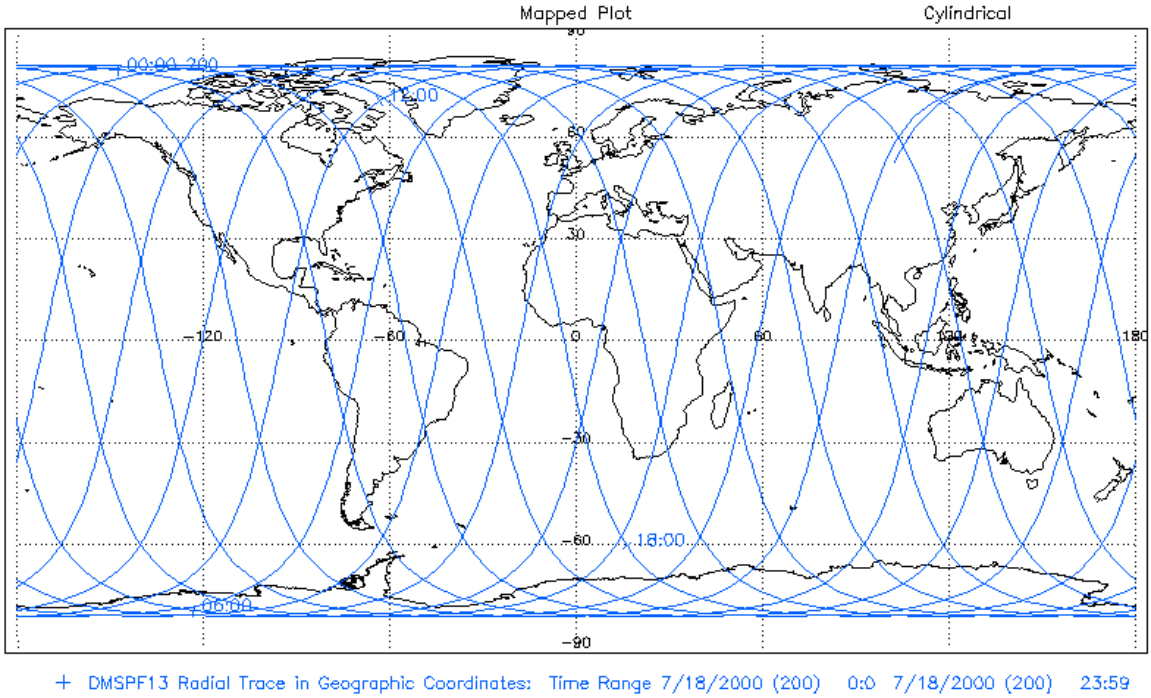


Figure 2.4. DMSP-F13 orbit mapped projection for 24 hours. The orbit inclination is about 98 degrees and it is fixed in local time when it crosses the equator near 1800 LT for the ascending node and near 0600 LT for the descending node. (http://sscweb.gsfc.nasa.gov/cgi-bin/sscweb/Locator_graphics.cgi)

Ion drifts from DMSP and ROCSAT are gathered in the spacecraft reference frame. Figure 2.5 shows this frame of reference defined with a positive X-axis in the ram direction, the positive Z-axis in the nadir (pointing in the vertical direction inward to the Earth) and the Y-axis completing a right handed coordinate system.

The representation of this reference frame shown in Figure 2.5 is directly applicable to ROCSAT-1 but applies equally to DMSP which has a much higher orbital inclination. The DMSP satellites have an orbit inclination of about 98º and thus the measured vertical and horizontal drifts near the magnetic equator are very nearly the same as the **E**x**B** drift motions in

the zonal and meridional direction. For ROCSAT-1 more processing of these drift components is required to yield the **E**x**B** drifts.

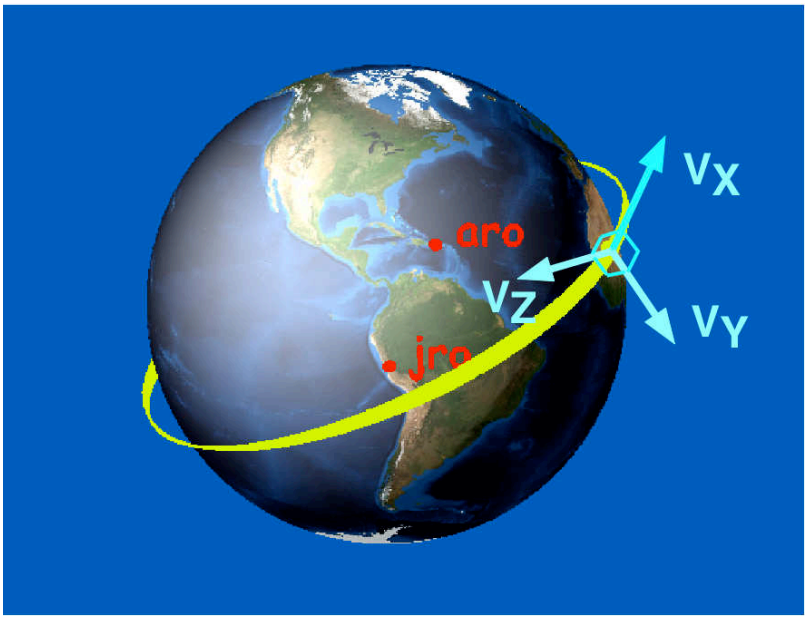


Figure 2.5. Spacecraft reference frame system of ROCSAT-1.

### 2.3.1 Storm-time drift perturbations

In order to investigate the longitudinal dependence in perturbations of the ion drifts during storm times we use DMSP F13, F15 and ROCSAT measurements of the ion drift velocities at the magnetic equator. We first study the variations in the vertical and zonal drifts. Storms are identified using the Dst index, and a time span of 20 hours before and 20 hours after the Dst minimum is examined to characterize the drift perturbations. The behavior of the vertical ion drifts and the zonal drifts within one degree of the magnetic equator are averaged to obtain a single representative point for the respective pass of the satellite across the magnetic equator. The local vertical ion drift is provided directly from measurements by the IDM. The zonal ion

drift is obtained by combining the IDM and RPA measurements, with knowledge of the orbital inclination angle and the local magnetic declination. A baseline is calculated by considering the first 10 hours of the total 40 hour time interval. Either the end of the time period is used or an earlier time period is used to establish the baseline in the event that these first hours do not constitute a period when the Dst index remains between +/- 20 nT. We subtract the value of the baseline from the total magnitude of the ion drifts to obtain only the perturbations produced by the storm events. The DMSP F13 data are taken near 1800 and 0600 LT, while the DMSP F15 satellite samples data near 2100 and 0900 LT. ROCSAT-1, due to its precessing orbit, provides data at other local times or near the local times measured by the DMSP satellites but at 600 km altitude. We then examine the nature of the perturbations at different local times and different longitudes.

### 2.3.2 Latitude variations during quiet times

In order to find the latitudinal (apex-height) variations of the ion drift velocities we utilize only the ROCSAT data set described before. This investigation is restricted to the solar maximum period of 1999 to 2003. The data processing to study the ion drifts at latitudes different from the equator is not trivial, since it requires decomposing the ion drifts in the directions parallel and perpendicular to **B**. These steps include the calculation of the corotation velocity components, the removal of biases present in the satellite measurements, and the conversion of the ion drift components from the spacecraft reference frame to a magnetic reference frame.

We first separate the quiet time data from the storm time by establishing a limit for a quiet time condition that satisfies $Kp < 3$ and $Dst > -100$. Then we characterize the ion drift

velocities in the spacecraft reference frame and derive the components parallel and perpendicular to **B**. To determine these components we use the International Geomagnetic Reference Field (IGRF) model of the magnetic field for the appropriate epoch and for the corresponding geographic latitude and longitude at an altitude of 600 km.

In order to study the velocities in the north-south, east-west, and up-down directions, it is necessary to make a transformation from the spacecraft reference frame to a reference frame that has components parallel and perpendicular to the magnetic field lines. For this data set the spacecraft velocity must be removed from $V_x$ and the corotation velocity must be removed from the horizontal ion drift components so measurements in the corotating frame of reference may be easily compared to ground based measurements.

The velocity $V_x$ is given by:

$$V_x = V_{x\text{-}raw} + V_{S/C} - V_x^{cor}$$

Here, $V_x$ is the velocity in the x-direction in the corotating reference frame, $V_{x-raw}$ is the raw velocity measurement in the same direction. $V_{S/C}$ is the spacecraft velocity assumed as a constant value of 7545 m/s. $V_x^{cor} = \omega_e r \cos i$=418.19 m/s, is the component of the corotation velocity of the plasma in the x-direction at the altitude of the satellite, $\omega_e$ is the rotational velocity of the Earth, $i$ is the inclination of the orbit (35º for ROCSAT-1) and $r$ is the radial distance from the center of the Earth [*Su et al.*, 1999]. The altitude of the satellite varies by about ±40 km from 600 km but we assume a constant altitude near 600 km since that variation produces a small change of the corotation velocity in the x-direction. The largest estimated variation is about -5 m/s when the altitude lowers to 550 km.

To determine the velocity in the y-direction of the ROCSAT reference frame, we use the relation:

$$V_y = V_{y-raw} \mp V_y^{cor}.$$

Here $V_{y-raw}$ is original ROCSAT measurement of the ion velocity in the y-direction, $V_y^{cor}$ is the velocity of the plasma due to the corotation in the same direction, the negative sign is for the north-bound orbit and the positive sign is for the south-bound orbit, and

$$V_y^{cor} = \omega_e r\left(\cos^2 L - \cos^2 i\right)^{1/2}.$$

In this expression, $L$ is the geographic latitude, and $\omega_e$, $r$, and $i$ are the same parameters as in the previous equation for $V_x^{cor}$. We again assume a constant altitude since the largest estimated variation in $V_y^{cor}$ due to a change in altitude is -3.5 m/s when the altitude lowers to 550 km.

After removing the corotation and spacecraft velocity a new data base of quiet time ambient ion drift measurements in spacecraft coordinates is created for each month. A more detailed analysis is then undertaken to find the latitudinal distribution of the ion drifts for different longitudinal sectors and local time periods.

For initial processing, we consider measurements between ±34.5º geographic latitude in the period from December 1999 to December 2003. We divide the space in corrected geomagnetic coordinates (CGM) with a latitude resolution of 2.5º. For a specific magnetic longitude and latitude we find the corresponding geographic coordinates and in a similar way we obtain the geographic location of the conjugate point. We then distribute the data at these geographic coordinates in bins of 30º longitude, 5º latitude and 30 minutes in local time. By dividing the space in this manner all northbound and southbound satellite tracks inside each bin have the same orientation with respect to the geographic meridian as shown in Figure 2.6. Thus we may straightforwardly average the data in spacecraft-coordinates for the northbound and southbound passes.

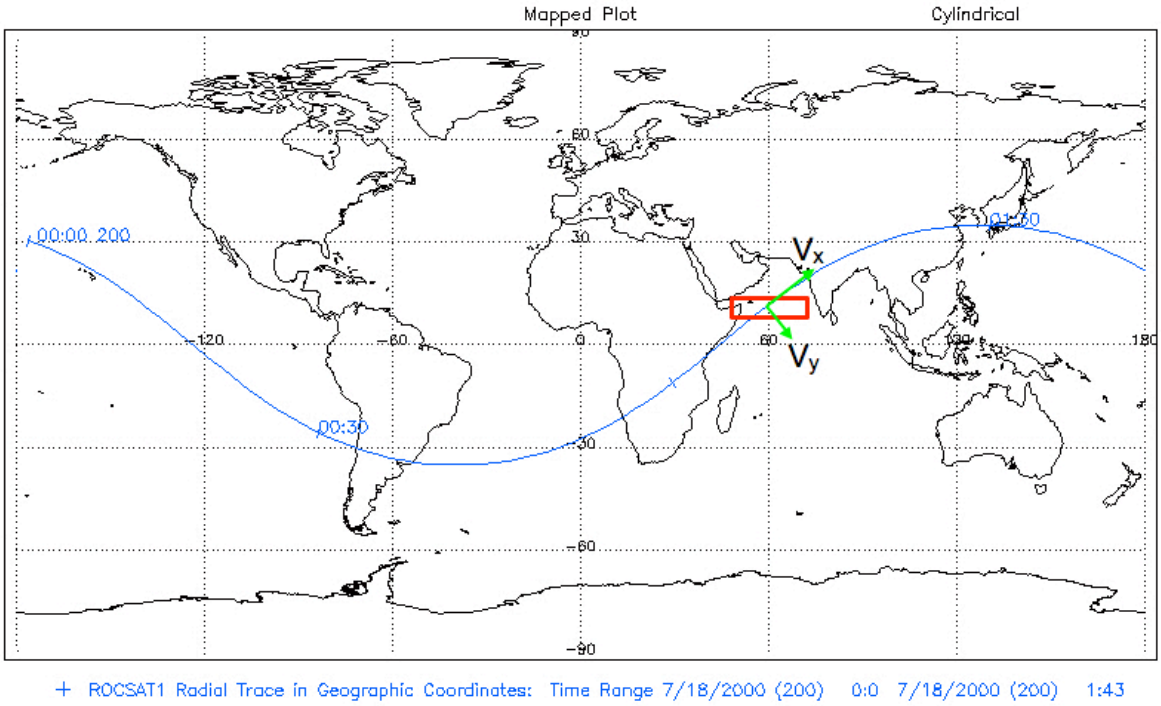


Figure 2.6. ROCSAT-1 orbit (blue line) with a space bin representation 5º wide in latitude and 30º wide in longitude (red box). The average vector velocity is determined for each bin and for each ion drift component ($V_x$, $V_y$, $V_z$) in the spacecraft reference frame.

We use measurements when the total ion density is higher than $10^4$ $cm^{-3}$ to minimize the measurement errors that occur during times of plasma depletions. Ascending or descending passes provide complete coverage in local time every 52 days. If we combine both passes, all local times are covered in 26 days. We utilize both ascending and descending node data in intervals of four months (December-February, March-April-September-October, May-August) to characterize the average ion velocities for different seasons.

Acceptable data points within the entire 24 local time period are selected by specifying upper and lower bounds for the entire data set. First we calculate the median and the standard deviation in each 30-minute local time bin. The maximum standard deviation encountered during the 24-hour period is then determined. Upper and lower bounds for the entire data period are calculated using the maximum median value plus the maximum standard deviation and the

minimum median value minus the maximum standard deviation respectively. The mean value within these bounds is found for each local time bin. Finally a cubic spline interpolation is applied to complete the values where the measurements are absent for a particular local time in order to determine the ion drifts for a particular longitude and latitude region distributed every 15 minutes in local time.

The $V_X$ and $V_Y$ measurements are smoothed with a running box car average of 5 points width (5 continuous local time intervals) shifting every 15 minutes in local time. The resultant $V_Z$ and the total density are obtained from the average of the ascending and descending measurements for each particular bin.

By grouping the data in s/c coordinates we avoid any convolution of different offsets in the average drift components. Biases in the original data are still present in the averages that are produced. In the case of the ROCSAT measurements there can be biases in the ion drift components as a result of variations in the orientation of the satellite, and changes in the vehicle potential. We remove the biases in the horizontal ion drift components by treating the ascending and descending passes separately before resolving the ion drifts in the directions parallel and perpendicular to **B**. The analysis technique is described in the following work and we can verify later that the ion drifts perpendicular to the magnetic field are approximately the same at magnetic conjugate latitudes. To remove the bias in the vertical ion drift component we use the property that the electric field, which drives the vertical drifts, must be irrotational, which implies no local changes in **B**, so the line integrals along the dip equator must be zero, as shown in the expression:

$$\oint E \bullet dl = \oint BV_z dl = 0$$

Then the longitudinally and local time averaged vertical ion drift at the equator must be

zero. Thus the average vertical drift over all local times and longitudes reveals the bias that we remove. To calculate the average vertical drift for a particular four-month season we restrict the measurements between -2.5º to 2.5º magnetic latitude, for total ion concentrations greater than $10^4$ $cm^{-3}$ and for values of vertical drifts between -220 and 220 m/s. A running box car average is applied to the ion drifts at all longitudes and local times to obtain the average values every 15 minutes in local time and with a box width of 30 minutes. Then a mean value, which is the resultant bias for $V_{Z,}$ is derived from the total average of the vertical drifts at different local times for that particular season.

Figure 2.7 shows a scatterplot of the ion drift measurements in the spacecraft reference frame versus local time during ascending passes. The first panel shows the component $V_z$, the second panel is the component $V_x$ and the third panel is the component $V_y$. Data are shown for the period November 2001 to February 2002, within +/- 2.5 degrees latitude of the geographic equator and for a longitude of 90º +/- 15º. Measurements are considered only when the ion density is greater than $10^4$ $cm^{-3}$ to minimize the effect of plasma depletions and poor signal quality. The red line represents running mean values in 30 minute local time intervals shifted each 15 minutes. The bias in $V_z$ has been calculated and removed by first collecting data at the dip equator and forcing the zonally averaged local time variation to be zero. General features such as upward drifts during the day and downward drifts at night are easily seen. Figure 2.8 shows the same drift components for descending passes taken over the same period as the data shown in Figure 2.7.

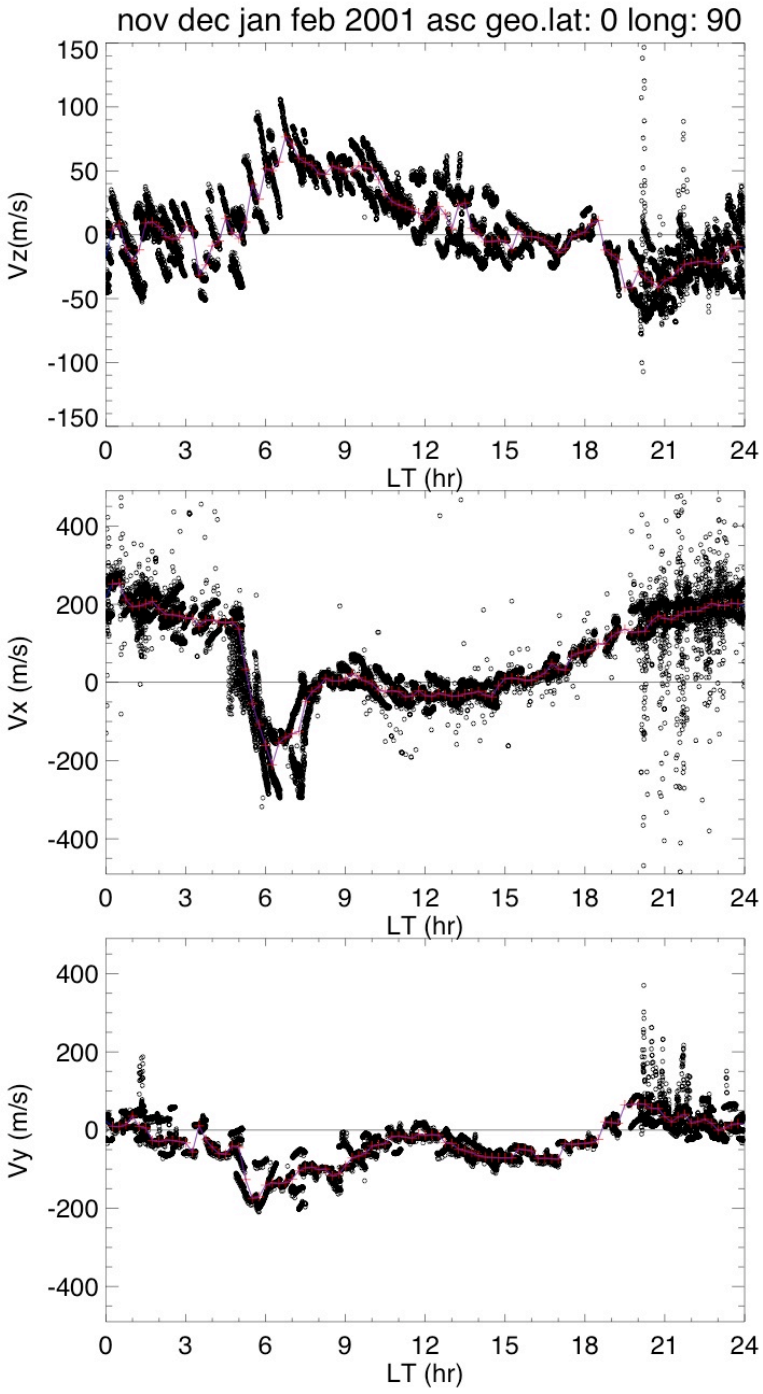


Figure 2.7. Scatterplot of the ion drift measurements in the spacecraft reference frame (Vx, Vy, Vz) for ascending passes distributed in local time. The period corresponds from November 2001 to February 2002. The red line represents the mean values of 30 minutes local time intervals shifted every 15 minutes.

The horizontal drift components $V_x$ and $V_y$ still posses biases. The large excursion in $V_x$ near sunrise is associated with a change in the vehicle potential that is poorly accommodated in the least-squares fitting procedure. Despite the erroneous data the expected features of zonal ion drifts that are westward by day and eastward by night are seen. Structured velocities seen after 2000 local time are due to the presence of equatorial spread-F.

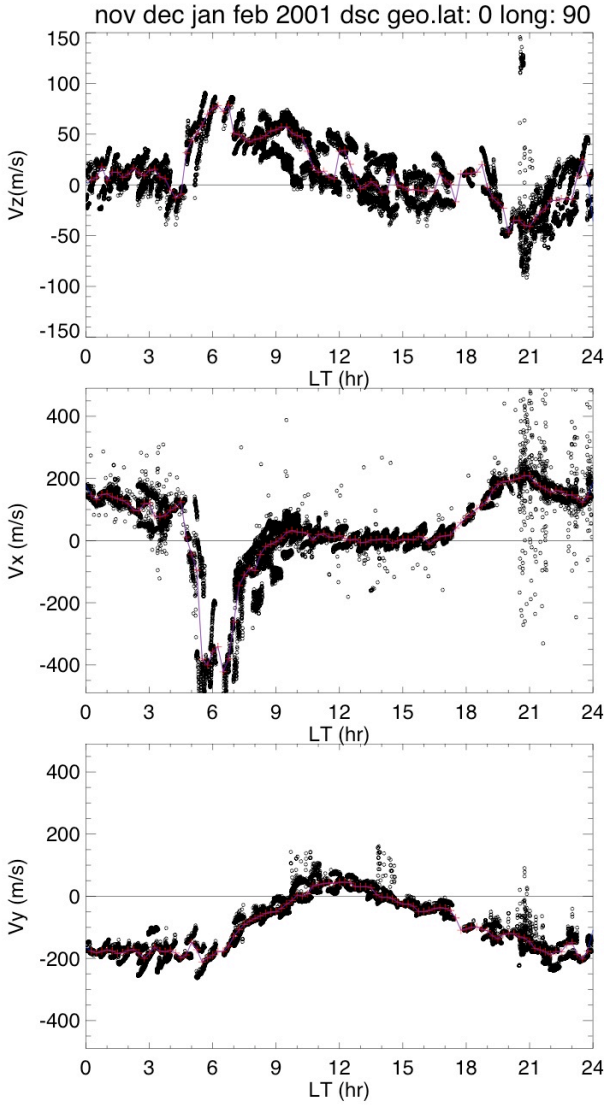


Figure 2.8. Scatterplot of the ion drift measurements in the spacecraft reference frame (Vx, Vy, Vz) similar as Figure 2.7 but for descending passes distributed in local time. The period corresponds from November 2001 to February 2002. The red line represents the mean values of 30 minutes local time intervals shifted every 15 minutes.

### 2.3.3 Derivation of the horizontal ion drift biases

The drift components in the spacecraft reference frame can be described in terms of the geographic zonal drift component $V_\Phi$ and the geographic north-south component $V_{NS}$. Figures 2.9a and 2.9b show the relationship between the measured ion drift components, $V_X$ and $V_Y$, and the geographic drift components $V_\Phi$ and $V_{NS}$ for ascending passes and for descending passes respectively. $V_x$ is rotated by an angle $\beta$ with respect to the zonal component. The drift components during the ascending pass are expressed by Equations 2.1 and 2.2.

$$\mathbf{V}_x^{asc} = \mathbf{V}_\phi \cos(\beta) - \mathbf{V}_{NS} \sin(\beta) \tag{2.1}$$

$$\mathbf{V}_y^{asc} = \mathbf{V}_\phi \sin(\beta) + \mathbf{V}_{NS} \cos(\beta) \tag{2.2}$$

Equations 2.3. and 2.4 show the relationship for these vector components for descending passes.

$$\mathbf{V}_x^{dsc} = \mathbf{V}_\phi \cos(\beta) + \mathbf{V}_{NS} \sin(\beta) \tag{2.3}$$

$$\mathbf{V}_y^{dsc} = -\mathbf{V}_\phi \sin(\beta) + \mathbf{V}_{NS} \cos(\beta) \tag{2.4}$$

If a long-term dc bias in the measurements is present then the expressions described previously are:

$$\mathbf{V}_x^{asc} = \mathbf{V}_\phi \cos(\beta) - \mathbf{V}_{NS} \sin(\beta) + A \tag{2.5}$$

$$\mathbf{V}_x^{dsc} = \mathbf{V}_\phi \cos(\beta) + \mathbf{V}_{NS} \sin(\beta) + A \tag{2.6}$$

$$\mathbf{V}_y^{asc} = \mathbf{V}_\phi \sin(\beta) + \mathbf{V}_{NS} \cos(\beta) + B \tag{2.7}$$

$$\mathbf{V}_y^{dsc} = -\mathbf{V}_\phi \sin(\beta) + \mathbf{V}_{NS} \cos(\beta) + B \tag{2.8}$$

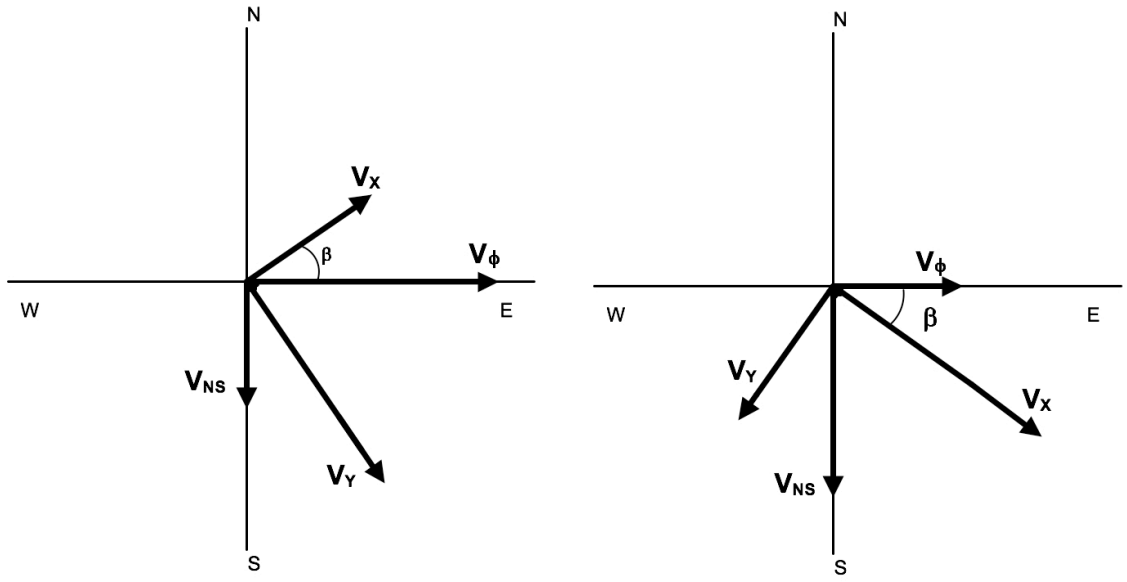


(a) (b)

Figure 2.9. Ion drift vectors $V_x$ and $V_y$ projected on the horizontal plane for the ascending pass (a) and descending pass (b). These vectors can be derived from the geographic zonal drift component $V_\Phi$ and the north south component $V_{NS.}$

Here A is the bias present in the $V_x$ measurement and B is the bias for the $V_y$ drift component. Subtracting 2.5 from 2.6 we can derive $V_{NS}$ without the need to know the bias because it is eliminated after the subtraction. The expression for $V_{NS}$ is given by

$$V_{NS} = \frac{V_x^{dsc} - V_x^{asc}}{2\sin(\beta)}$$

Similarly, subtracting equation 2.8 from 2.7 we obtain $V_\Phi$ which is expressed by

$$V_\phi = \frac{V_y^{asc} - V_y^{dsc}}{2\sin(\beta)}$$

Then replacing the values of $V_{NS}$ and $V_{\Phi}$ in Equations 2.5, 2.6, 2.7 and 2.8 we obtain the values of $V_x$ and $V_y$ without the bias.

After finding the latitude distribution of the ion drifts we can find the respective electric fields knowing the ion drift velocities and the magnetic field. Since we can consider the magnetic field lines to be electric equipotentials we can also express the electric field as a function of magnetic apex height. Finally, the results obtained can be compared with observations from ground-based stations (Jicamarca and Arecibo).

We follow the processing considering separately the ascending and descending passes to remove the biases in the ion drift measurements. Figures 2.10 and 2.11 show the ion drift values derived from the mean values shown in Figures 2.7 and 2.8. In Figures 2.10 and 2.11 the small black circles show the mean values after the biases in $V_x$ and $V_y$ have been removed. The blue curves show the original mean values including the biases. We note that the major erroneous features are removed while the features identified as characteristic of the expected **E**x**B** drift patterns remain. In $V_z$ the bias has been previously removed so it is not shown in these plots. We can observe that the bias is in general around a similar value for all local times except near 0600 LT for $V_x$. In $V_y$ the bias near 0600 LT is smaller than the bias in $V_x$ and it remains around a similar value in general for all local times except near noon.

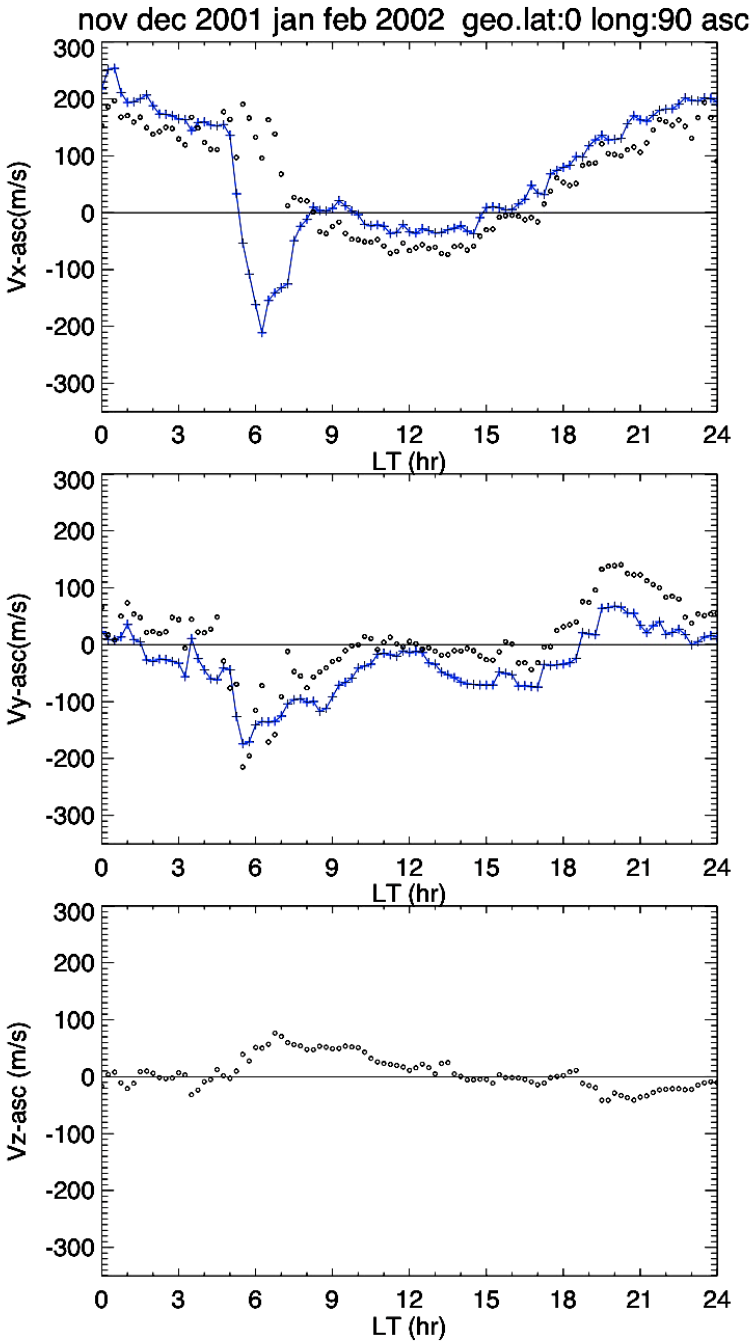


Figure 2.10. Ion drift measurements distributed in local time in the spacecraft reference frame after processing the data shown in Figure 2.7 for ascending passes. The blue line illustrates the values of the drifts before removing the biases and the small black circles indicate the values after extracting the bias.

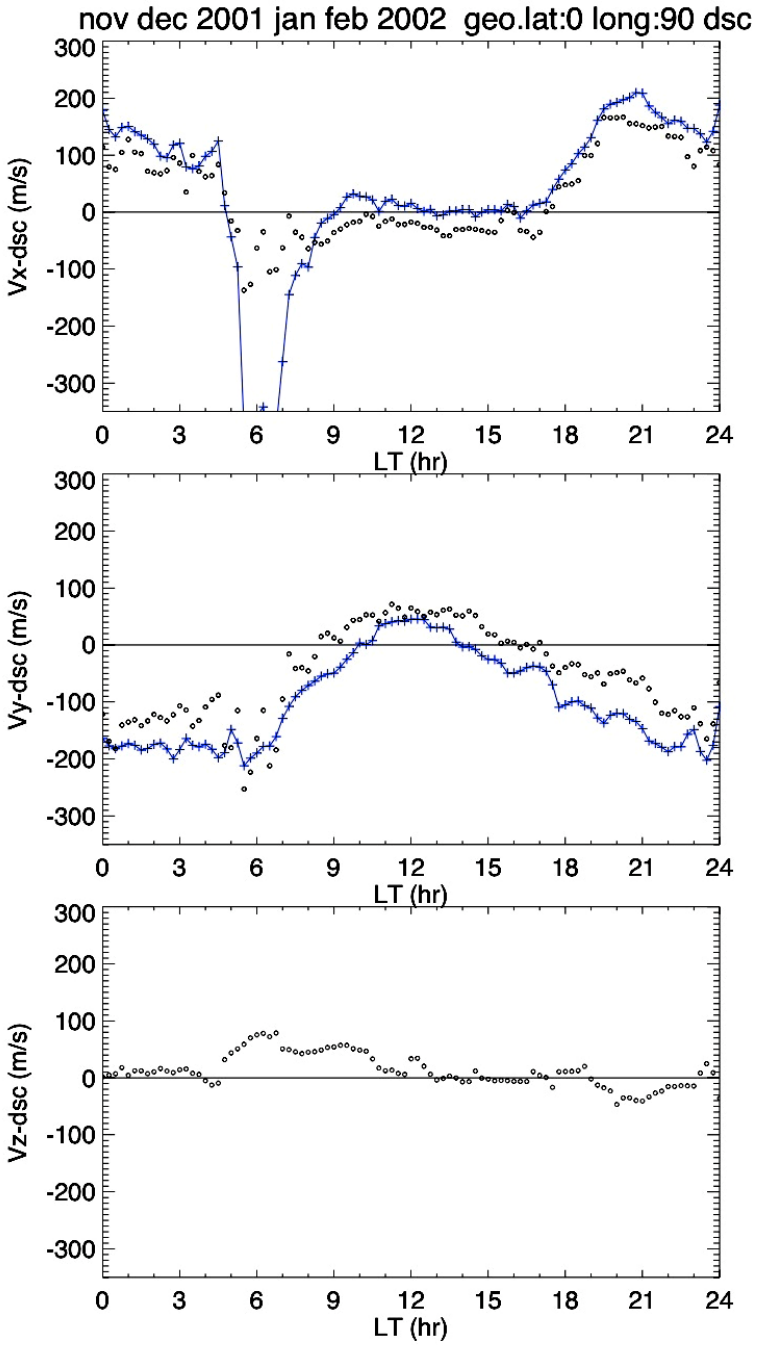


Figure 2.11. Ion drift measurements distributed in local time in the spacecraft reference frame after processing the data shown in Figure 2.8 for descending passes. The blue line illustrates the values of the drifts before removing the biases and the small black circles indicate the values after extracting the bias.

### 2.3.4 Conversion of ion drift vectors from spacecraft reference frame to geomagnetic reference frame

Following the removal of biases from the velocity measured in spacecraft coordinates we transform the ion drift components from the spacecraft reference frame to a reference frame with components parallel and perpendicular to the magnetic field line. The ion drift components $V_x$ and $V_y$ in the spacecraft reference frame are contained in the local horizontal plane. The ion drift component $V_z$ is perpendicular to that horizontal plane and is directed toward the center of the Earth. A general representation of the ion drift components $V_x$ and $V_y$ on the horizontal plane projection is shown in Figure 2.12. The magnetic meridian has a declination angle $\delta$ with respect to the geographic south-north meridian. The ion drift component $V_x$ defines the angle $\alpha$ with the magnetic meridian (or the component parallel to the magnetic field line). $\beta$ is the angle in between $V_x$ and the east-west direction.

Figures 2.13a and 2.13b illustrate the spherical angle $\beta$ during the ascending and descending pass respectively. This angle is dependent on the geographic latitude and the orbital inclination and it is determined by the following expressions:

For ascending pass:

$\beta = 90 - \gamma$

For descending pass:

$\beta = -(90 - \gamma)$,

where $\gamma = \sin^{-1}\left(\frac{\cos(i')}{\cos(L_0)}\right)$

$i'$: satellite inclination orbit (35° for ROCSAT-1)

$L_0$: geographic latitude at the satellite position

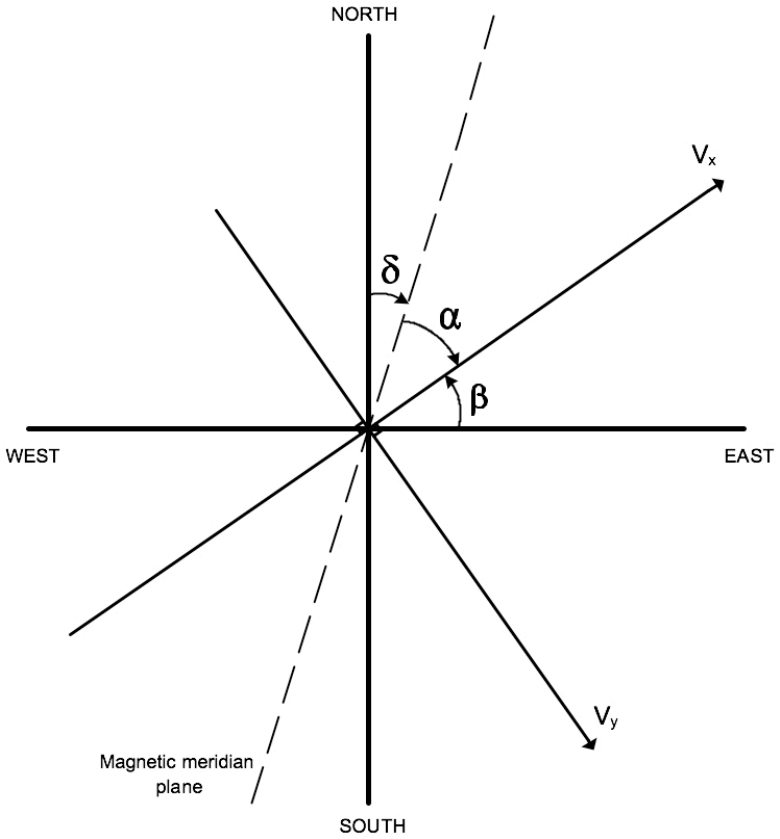


Figure 2.12. Horizontal ion drift vector components $V_x$ and $V_y$ for ROCSAT-1 projected on the horizontal plane. "δ" is the angle between the magnetic meridian and the south-north direction.

Figure 2.14 shows the declination and inclination angle of **B.** These angles determine the orientation of the magnetic field line in space and they are illustrated in a three-dimensional representation with the following definitions:

I: inclination angle of **B** with respect to the horizontal plane. It is obtained from the IGRF model.

δ: declination angle of **B** defined by the magnetic meridian plane and the south-north direction. This is obtained from the IGRF model.

α: angle measured in the horizontal plane defined by the vector $\mathbf{V_x}$ and the magnetic meridian plane

$\alpha = 90 - \delta - \beta$.

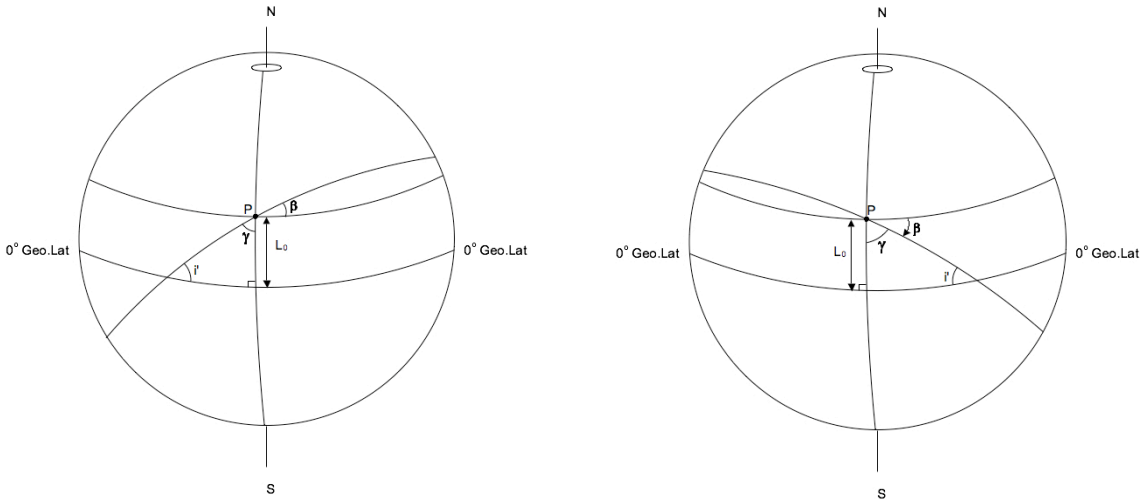


Figure 2.13. Schematic representation of the satellite ascending (a) and descending (b) pass with orbital inclination i′. The spherical triangle defined by the north-south meridian, the geographic equator, and the orbital projection on the Earth shows its corresponding angles i′, β, γ when the satellite position is indicated by P. P is located at a geographic latitude $L_0$. For the descending pass β is negative (clockwise), $\beta = -(90 - \gamma)$.

The relations to derive the parallel and perpendicular components of the ion drifts in the spacecraft reference frame are:

Ion drift component parallel to **B**:

$$\mathbf{V}^{\parallel} = [\cos(\alpha)\cos(I)\mathbf{V}_x] + [\cos(90+\alpha)\cos(I)\mathbf{V}_y] + [\cos(90-I)\mathbf{V}_z]$$

Ion drift component perpendicular to **B** in the meridian plane:

$$\mathbf{V}_M^{\perp} = [\cos(\alpha)\sin(I)\mathbf{V}_x] + [\cos(90+\alpha)\sin(I)\mathbf{V}_y] - [\sin(90-I)\mathbf{V}_z]$$

Ion drift component perpendicular to **B** in the east-west direction:

$$\mathbf{V}_z^{\perp} = [\sin(\alpha)\mathbf{V}_x] + [\sin(90+\alpha)\mathbf{V}_y]$$

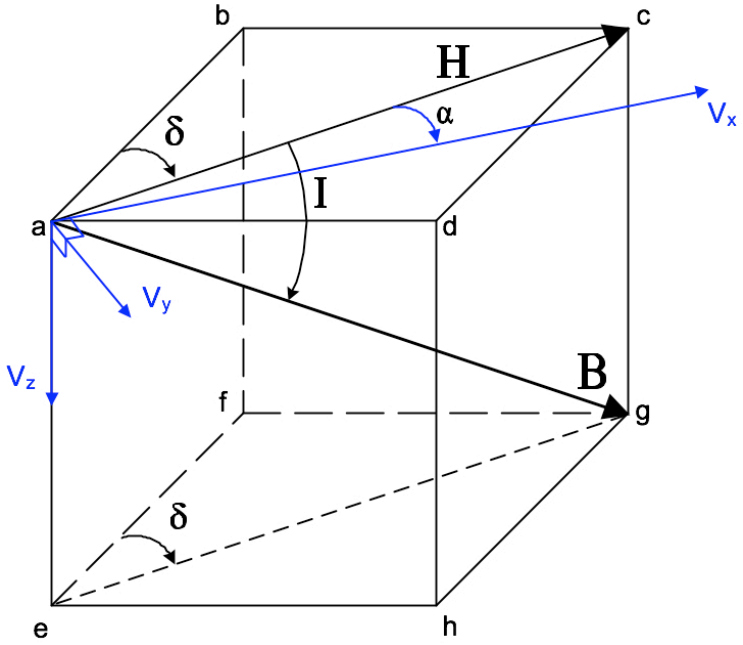


Figure 2.14. A three dimensional schematic representation of the magnetic field vector **B** at the point "a". The declination angle is indicated by δ. "I" represents the inclination angle. The drift vectors $V_x$ and $V_y$ are situated on the horizontal plane "abcd". The segment "ab" indicates the south-north direction. The segment "ad" illustrates the west-east direction and the segment "ae" indicates the local vertical direction toward the center of the Earth.

Figure 2.15 shows the resultant values using the data shown in Figures 2.10 and 2.11. The first panel shows the ion drift in the direction parallel to the magnetic field line. Here, there is a sunrise surge (positive along **B**) in the ion drift due to the ionization production below 600 km, and a southward drift due to diffusion at night after sunset. Note that the geographic equator lies southward of the magnetic equator in this longitude sector. The second panel shows the **E**x**B** component contained in the meridian plane. Here, the drift is upward during the day and downward at night. The third panel shows the perpendicular component in the zonal direction where large eastward **E**x**B** drifts are observed during the night and smaller westward ion drifts are observed during the day. These features are evidence of ionospheric superrotation.

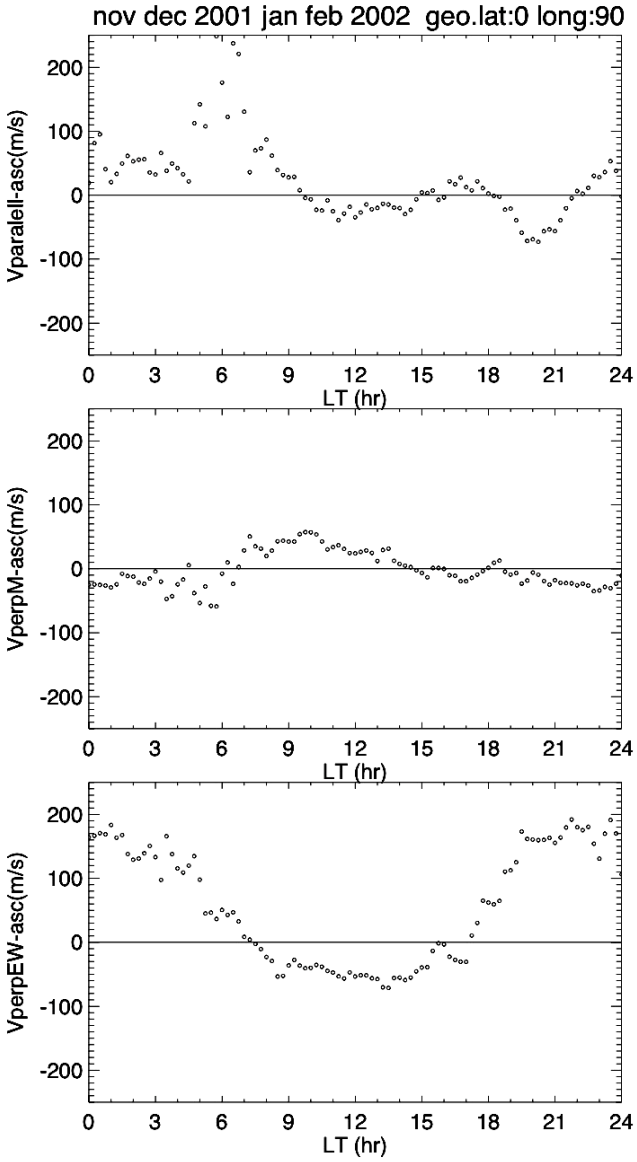


Figure 2.15. Ion drift measurements versus local time after converting the drift values without bias (shown in Figures 2.10 and 2.11) to ion drift values in the reference frame parallel and perpendicular to **B**. The first panel indicates the drift values in the direction parallel to **B** (positive when the drift is northward). The second panel shows the ion drift perpendicular to **B** in the magnetic meridian plane (positive when the drift is upward). The third panel shows the **E**x**B** drift in the zonal or east-west direction (positive when the drift is eastward).

Additional offsets are removed enforcing the conjugacy of the perpendicular drifts after calculating the average values of the drifts at the north and south conjugate latitudes. We select longitude regions where the magnetic declination and the offset of the magnetic equator with

respect to the geographic equator have different values, and describe the variations of the drifts for the northern winter solstice, equinox and northern winter seasons. These longitude regions are near the Peruvian, Brazilian, African, Indian, Pacific and Central American regions. We then describe the characteristics of the quiet time ion drifts in local time, latitude (apex-height), longitude and season.

# CHAPTER 3

# RESULTS

## 3.1 Storm Time Vertical Drift Perturbations

We studied six cases that illustrate the presence of ion drift perturbations due to storm effects. These correspond to the storm events of 6 April 2000, 15 July 2000, 11 April 2001, 6 November 2001, 24 November 2001 and 30 October 2003. Since we considered the storm events when the Dst index is more negative than -200 nT these observations from DMSP F13, F15 and ROCSAT-1 illustrate the behavior seen during so-called superstorms.

In the presence of an electric field directed from dawn to dusk, produced by the interaction of the magnetosphere with the solar wind, the plasmasphere is shielded by an electric field produced by the accumulation of polarization charges due to the gradient-curvature drift of energetic particles in the magnetosphere as shown in Figure 3.1. When the electric field from the magnetosphere ($\mathbf{E}$) is suddenly increased, then the electric field produced inside the plasmasphere $\mathbf{E}'$ is insufficient to cancel it and the undershielding effect occurs. When the magnetosphere electric field $\mathbf{E}$ decreases, then the electric field $\mathbf{E}'$ inside the plasmasphere may become greater than $\mathbf{E}$ and the overshielding effect is produced. In addition to the shielding effects the magnetospheric field also produces Joule heating at high latitudes that may modify the neutral winds at middle and low latitudes in a so-called disturbance dynamo. We suggest that the combined effect of the disturbance dynamo, undershielding and overshielding interact to produce the perturbations observed near the magnetic equator.

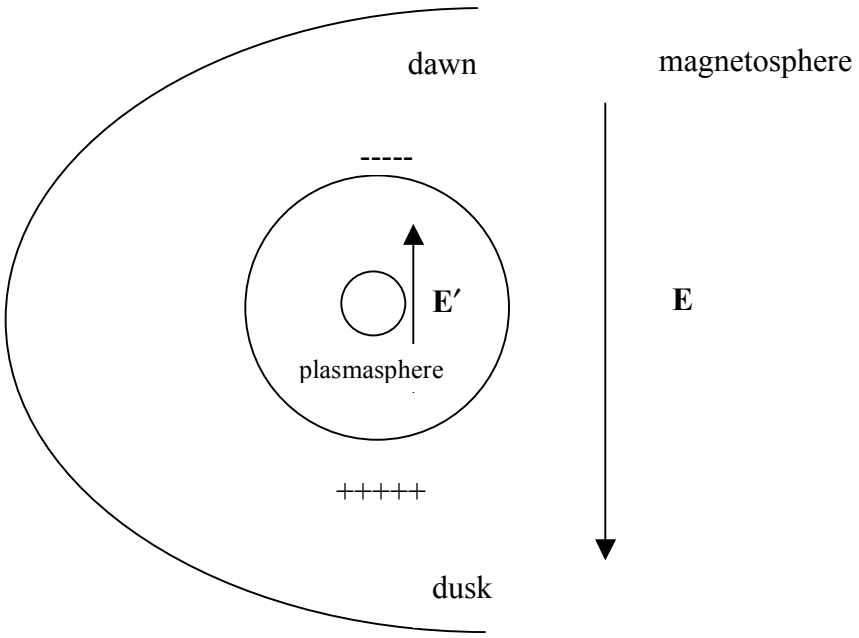


Figure 3.1. Configuration of the electric fields in the ionosphere and magnetosphere system in the equatorial plane in order to illustrate the undershielding and overshielding effects. The sun is located at the left of the figure. E>E′ = undershielding, E<E′= overshielding.

### 3.2 Observations

One of the superstorm events is illustrated in Figure 3.2. It shows the vertical ion drift perturbation near the magnetic equator during the storm time period on July 15, 2000. The upper panel shows the behavior of the Dst index versus universal time. The minimum Dst value is located at the center of this panel and we consider the behavior during a time range of 20 hours before to 20 hours after this point. The second panel shows the north-south component (Bz) of the interplanetary magnetic field (IMF). The following panels show the vertical ion drift perturbations for each pass of the satellites across the magnetic equator during the 40-hour period. An average of the vertical drift during the first 10 hours of the 40-hour period is obtained to determine a baseline that represents the ion drift during non-storm conditions. The difference with respect to this baseline is plotted for the 40-hour period. There is a dashed line on these

panels that indicates the pass closest in time to the minimum Dst in each case. The satellite, local time and longitude of these marked passes are indicated at the right side of each panel.

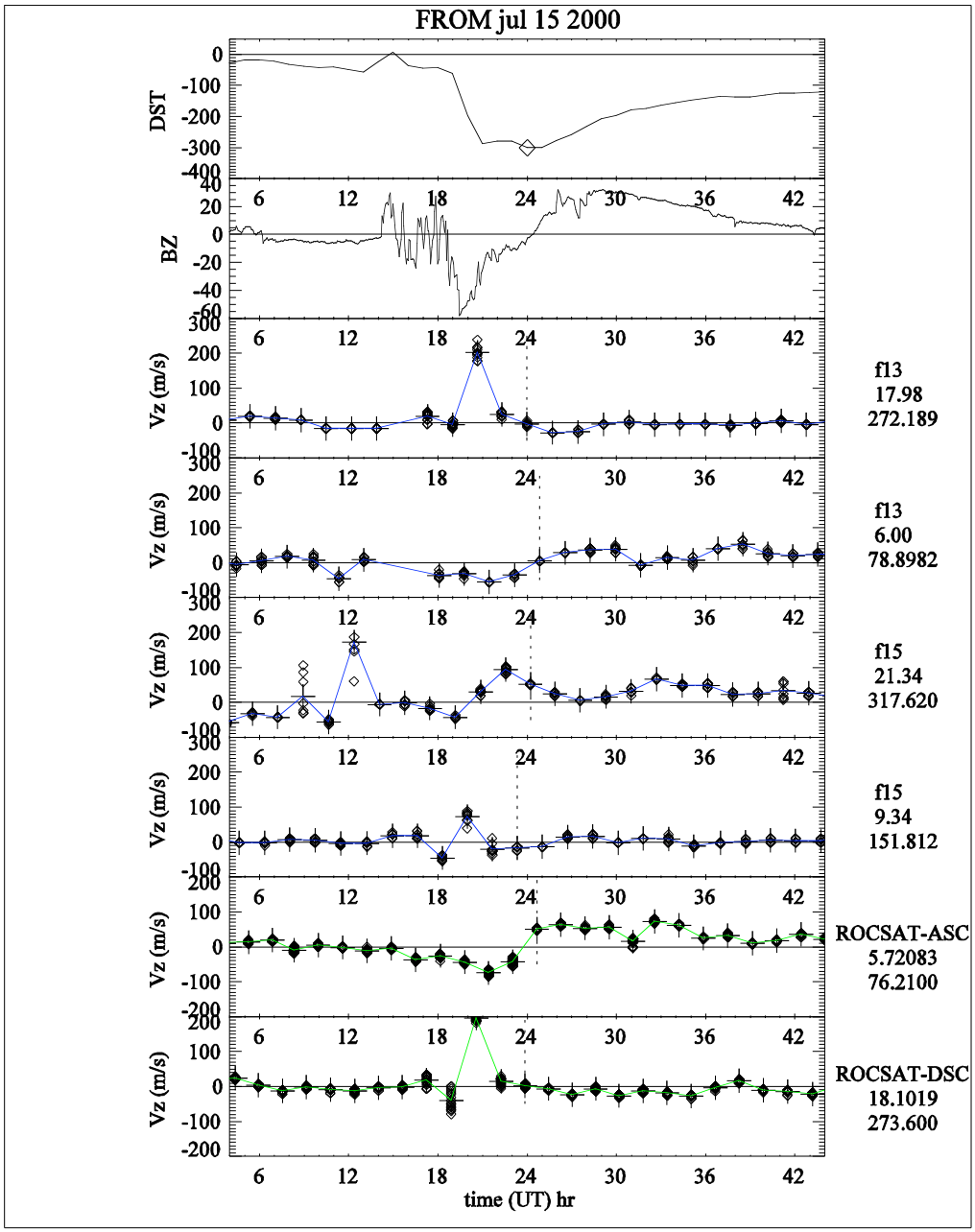


Figure 3.2. Vertical ion drift perturbations registered during the storm event on July 15, 2000. The first panel shows the Dst index. The second panel shows the interplanetary magnetic field (IMF-Bz). The following panels illustrate the vertical drift perturbations measured by DMSP-F13, DMSP-F15 and ROCSAT-1. At the right side of the DMSP observation is indicated the satellite, its local time for observations and the longitude that corresponds to the point marked with the dashed line.

The DMSP satellites provide measurements near the same local time for each event. F13 has an ascending pass near 1800 LT and a descending pass near 0600 LT. F15 has an ascending pass near 2100 LT and a descending pass near 0900 LT. For ROCSAT-1 there are about 16 orbits per day and about 28 minutes of local time span during that period. Thus, the local time moves by about 45 minutes during each storm sequence of 40 hours. Each time the satellites cross the equator, the longitude of each pass decreases by 25 degrees for DMSP and about 24 degrees for ROCSAT-1. Because of the low sampling rate (one sample per orbit in 90 or 100 minutes) we cannot resolve features that change over time scales less than this period. For this study we examine only the duration of events that last several hours and mean drifts that occur over these periods.

For the case shown in Figure 3.2, the IMF starts in a southward steady state near -5 nT, then it shows a highly structured behavior beginning near 1400 UT with an average value near 0 nT. Near 1900 UT a large southward turning of the IMF occurs in less than an hour, reaching a value near -60 nT. During this expansion phase the value of the Dst index changes from about -50 nT to -300 nT in less than 2 hours and reaches a minimum of -320 nT as the southward IMF decreases. The recovery phase is marked by a slow decrease in the southward IMF, which takes about 5 hours to reach positive values. The IMF remains northward during the remainder of the recovery phase for more than 12 hours. The Dst index decreases rapidly following the large southward turning of the IMF. Spanning the period of the southward turning, upward drift perturbations are seen at 1800 LT by DMSP F13 and ROCSAT-1 and at 0930 LT by DMSP-F15. The perturbations are seen across a time span of 3 hours but are observed for only one orbit before they are suppressed in the presence of a large and negative Bz that is decreasing.

The smallest upward drift excursion is seen near 0930 LT but from this single event it is not possible to determine if this is an artifact of the poor temporal resolution afforded by the orbit sampling. Near dawn, both the F13 and ROCSAT-1 observations show a similar temporal variation in the drift perturbations. Downward drift perturbations begin at the storm onset and peak at the minimum Dst. Near 2400 UT when the IMF turns northward the drift perturbations become small and upward and persist throughout the storm recovery phase as observed by ROCSAT-1 near 0540 LT. There is some evidence for similar signatures seen near dawn by F13, but the drift magnitudes are not generally above the uncertainty levels of the baseline. For observations near 2100 LT the baseline for the F15 observations prior to the storm is compromised by the presence of $H^+$. Following the storm, atmospheric heating restores the topside ionosphere near 830 km to wholly $O^+$ and the baseline is more reliably established. Under these conditions, which prevail for all the storm periods we examine, we are able to establish the existence of a small upward drift perturbation with an onset time that is delayed with respect to the perturbation seen near 1800 LT by DMSP F13. The vertical drift perturbations at 2100 LT also appear to have a longer duration than the perturbations seen at 1800 LT. The large and structured upward drifts seen at this local time preceding the storm period are associated with spread- F.

Figure 3.3 shows the vertical ion drift perturbations at the magnetic equator for the storm period on November 6, 2001. The panel distribution is the same as described in Figure 3.2. The storm of November 6, 2001 is preceded by a quiet period during which the IMF is first rather structured and northward and then extremely steady and southward. During the quiet period we see small-scale deviations of about 30 m/s in the vertical ion drift recorded by DMSP and by

ROCSAT. We utilize this level of perturbation as a significance threshold. This storm period is triggered by a rapid southward turning of the IMF to reach values near -80 nT. In a little over one

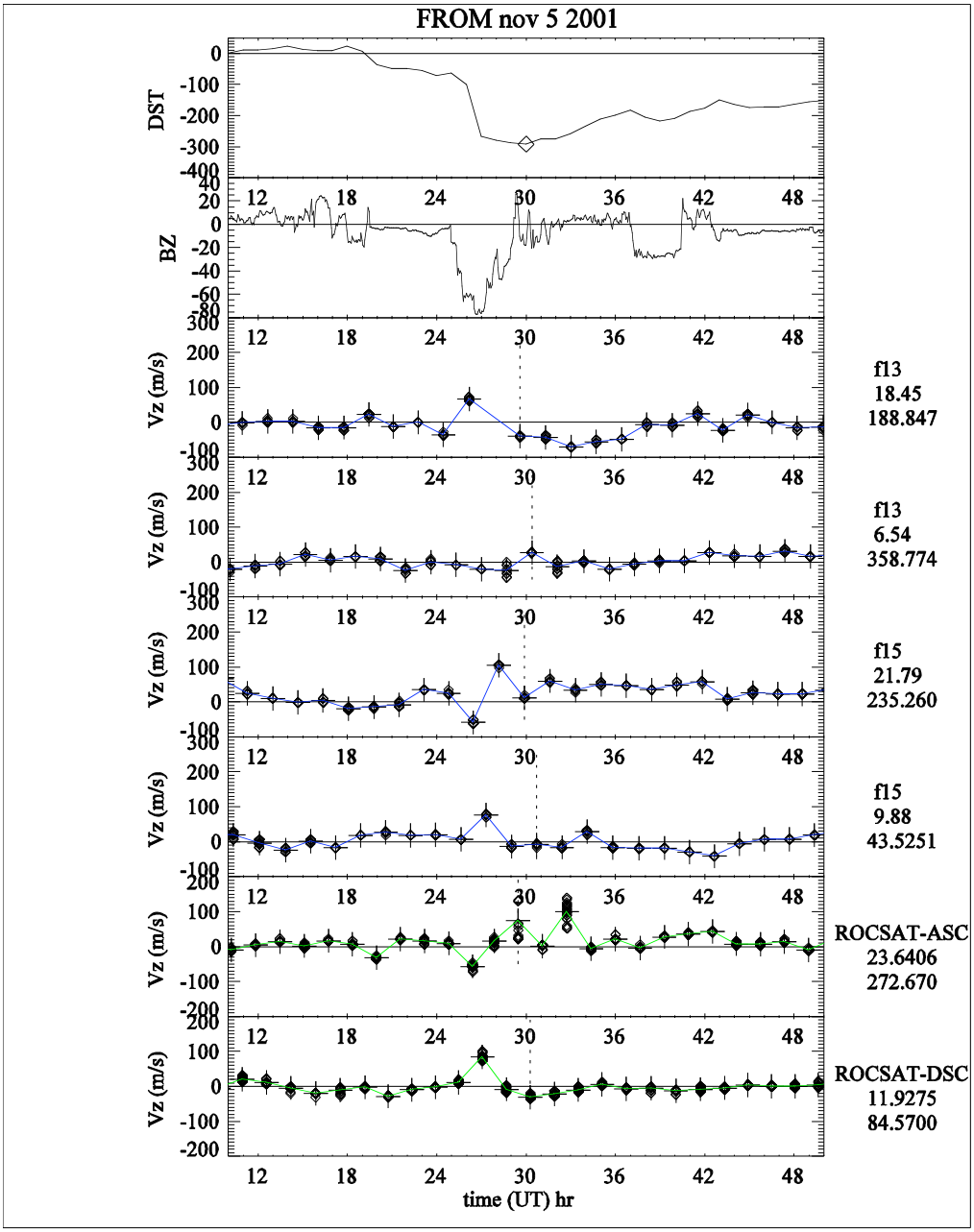


Figure 3.3. Vertical ion drift perturbations registered during the storm event on November 6, 2001.

hour the Dst index subsequently falls from about -100 nT to values near -300 nT. Over a period of about 3 hours a rapid northward turning of the IMF to values near zero marks the onset of the recovery phase. The recovery phase itself persists for almost 24 hours. Aligned with the southward turning of the IMF is a family of drift perturbations that conform nicely to our expectations for a penetration event [*Spiro et al*., 1988; *Wolf*, 1995; *Huba et al*., 2005; *Maruyama et al*., 2005]. Near 1830 local time a small upward drift perturbation is observed. Similar upward drift perturbations are also seen near 1000 local time by DMSP F15 and near local noon by ROCSAT-1. The F13 data are compromised by one missing orbit during the event but the other satellites each record a drift perturbation for only one pass. The magnitude of the peak drift is again compromised by the temporal resolution of the data. There are corresponding downward drift perturbations observed near 2140 local time from DMSP F15 and near midnight from ROCSAT-1. No significant drift perturbations are observed near dawn. Near 2140 local time, an upward drift perturbation is observed when the IMF retreats from its maximum southward excursion immediately following the downward perturbation. The drift perturbations near midnight observed by ROCSAT-1 are associated with spread-F irregularities that rotate into that local time sector and are spawned by the previous upward drifts across the dusk side.

Figure 3.4 shows the vertical drift perturbations seen at the equator for the storm event of October, 30, 2003. This is the second of two storm features that appear on October 29 and October 30 in which the drift perturbations are sufficiently extended in time to be observed by consecutive passes. As before the storm is triggered by a dramatic southward turning of the IMF to values near -30 nT in less than 1 hour. However, during the main phase the IMF remains southward for 2 to 3 hours prior to a northward turning. Under these circumstances a large upward drift perturbation is seen near 1830 local time that persists for at least 2 passes (100

minutes) and could be as long as 4 hours. A similar upward drift perturbation of smaller magnitude is seen near 0940 local time and near local noon. Downward drift perturbations exten-

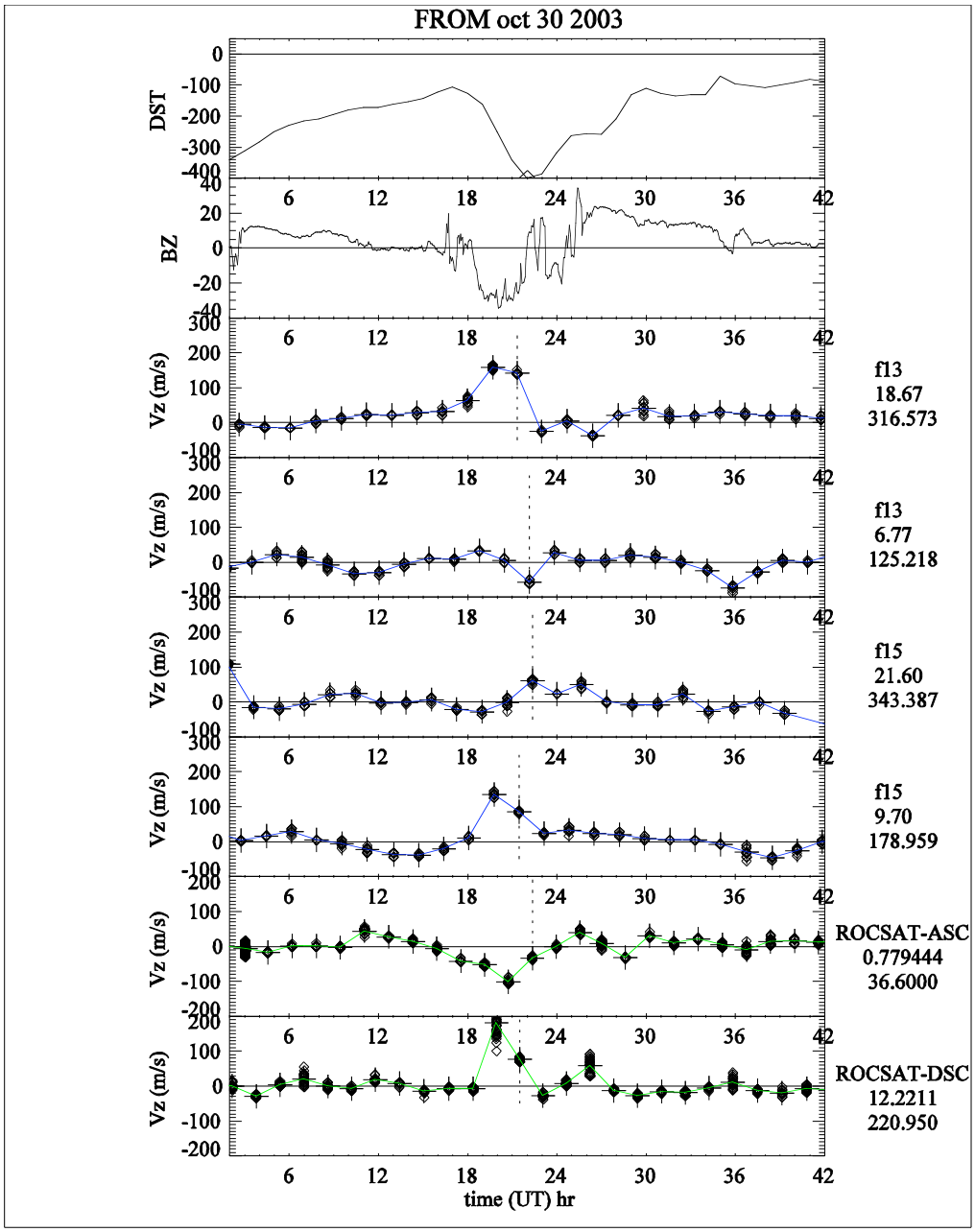


Figure 3.4. Vertical ion drift perturbations registered during the storm event on October 30, 2003.

ding over similar time periods are seen near local midnight. Over this period, corresponding to a continuous reduction in the Dst index for four hours or more no significant perturbations are seen near 2130 LT or 0640 LT.

In Figure 3.5 we show another case when the main phase of the storm coincides with a prolonged period of steady southward IMF. The observations are obtained during more modest excursions in the IMF and the Dst index, but again the reduction in Dst takes place over a period of 4 hours or more. In this case a critical pass of F13 is missing and the resolution of the samples does not allow us to determine the maximum magnitude of the vertical drift perturbations for the period between 1800 and 2000 UT, but an upward drift excursion that spans the region of decreasing Dst and across the brief northward IMF excursion is evident. Near 0930 local time (F15) and 0330 LT (ROCSAT), upward and downward drift perturbations respectively appear during the period of decreasing Dst but are terminated by the brief northward excursion of the IMF. The upward drift seen later by ROCSAT at 0330 LT is associated with equatorial irregularities that persist well into the post midnight period. Near 2100 LT, a small upward drift occurs at the later stages of the main phase.

Figure 3.6 represents a case when the IMF turns south/north/south during the expansion phase of a storm that persists for almost 8 hours. The start of the recovery phase begins with a northward turning of the IMF. DMSP F13 detected two small upward drift perturbations near 1800 LT. Both drifts follow each southward turning of IMF during the main phase.

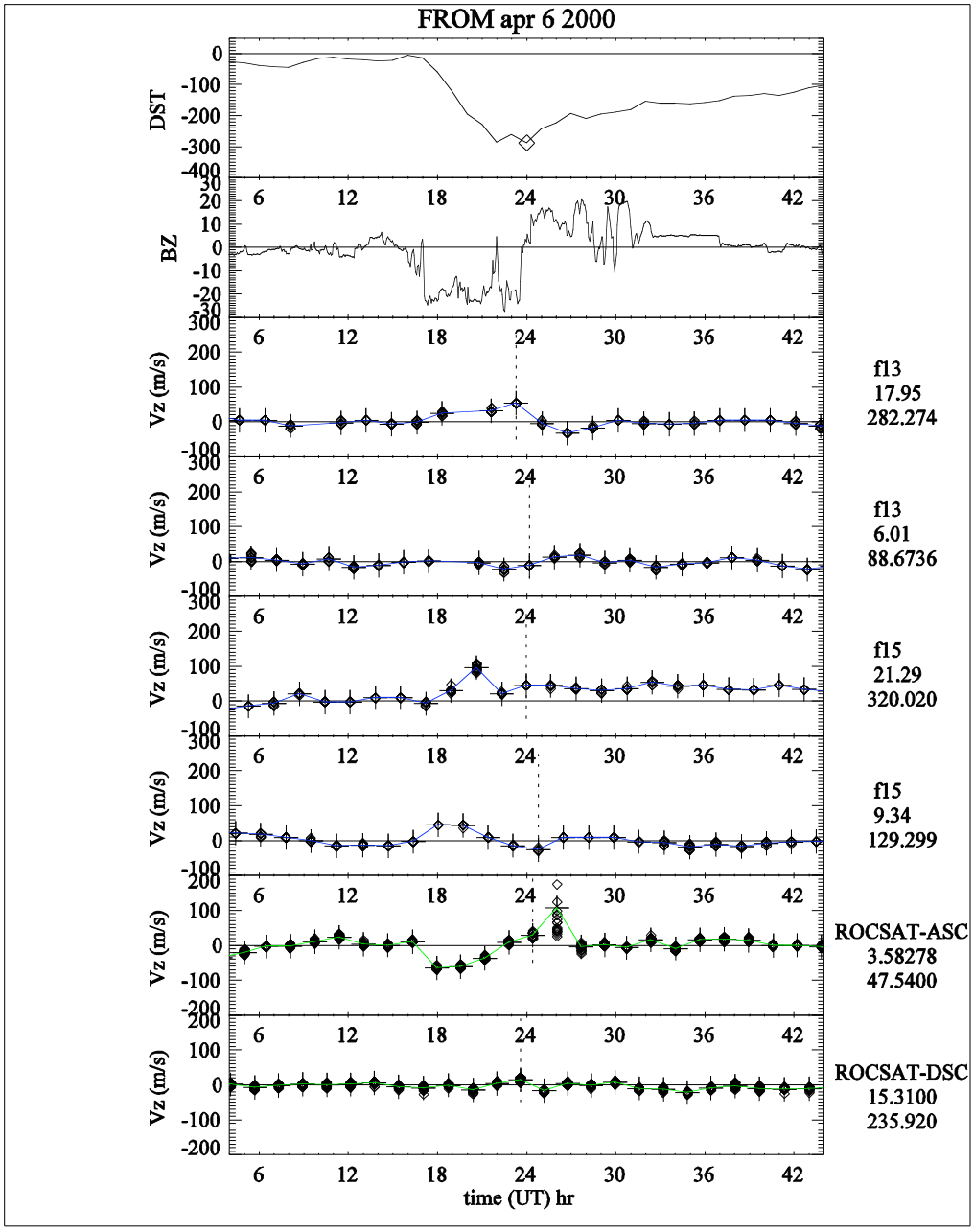


Figure 3.5. Vertical ion drift perturbations registered during the storm event on April 6, 2000.

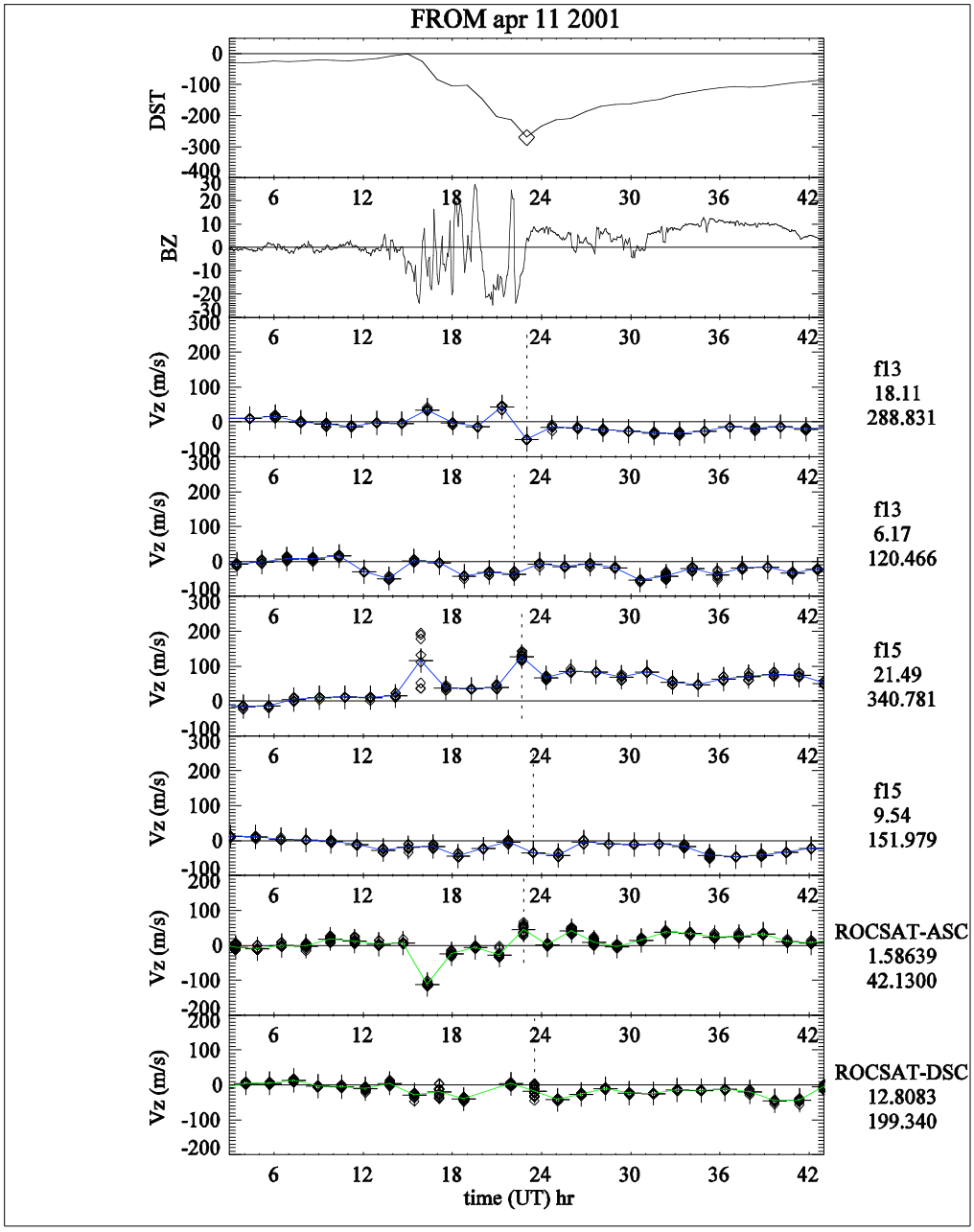


Figure 3.6. Vertical ion drift perturbations registered during the storm event on April 11, 2001.

DMSP-F15 measured a small structured upward drift around 2100 LT near 16 and 23 UT. These perturbations are associated with spread-F irregularities and not directly attributable to changes in the IMF. Almost negligible drifts variations are present around 9 LT. These variations tend to be upward during the southward periods of IMF and downward during

northward IMF. However, the available temporal resolution is insufficient for clear association to be made. ROCSAT measurements show a large, short-lived (3 hrs.) downward drift near 1.5 LT, which follows the first southward turning of the IMF, but the expected upward drift perturbation near local noon is not observed.

In Figure 3.7 we observe the vertical ion drift perturbations during a storm event on November 23, 2001. This event is distinguished by a period of northward IMF during the expansion phase. Near 1830 LT, DMSP-F13 shows an upward drift perturbation associated with the initial period of southward IMF. The drift perturbation becomes downward when the IMF turns northward, even while the Dst index is decreasing. Near 1700 LT ROCSAT-1 also shows an upward drift perturbation coincident with the initial period of southward IMF, but a downward drift associated with the following period of northward IMF is much less evident at this earlier local time.

On the dayside near 0950 LT, DMSP-F15 records a small upward drift perturbation associated with the initial period of southward IMF, but there is no significant response to the northward IMF excursion that follows. Near 0400 LT, ROCSAT also detects upward drifts associated with irregularities that corotate with the post midnight sector.

## 3.3 Discussion and Conclusions

The characteristics of storm-time vertical ion drift perturbations are studied using the DMSP and ROCSAT-1 data. In all cases we are able to investigate the vertical drift perturbations near 0600 0930, 1800 and 2130 local time. Additional local time hours such as noon or midnight are provided by ROCSAT-1 corresponding to the location of the satellite during the storm.

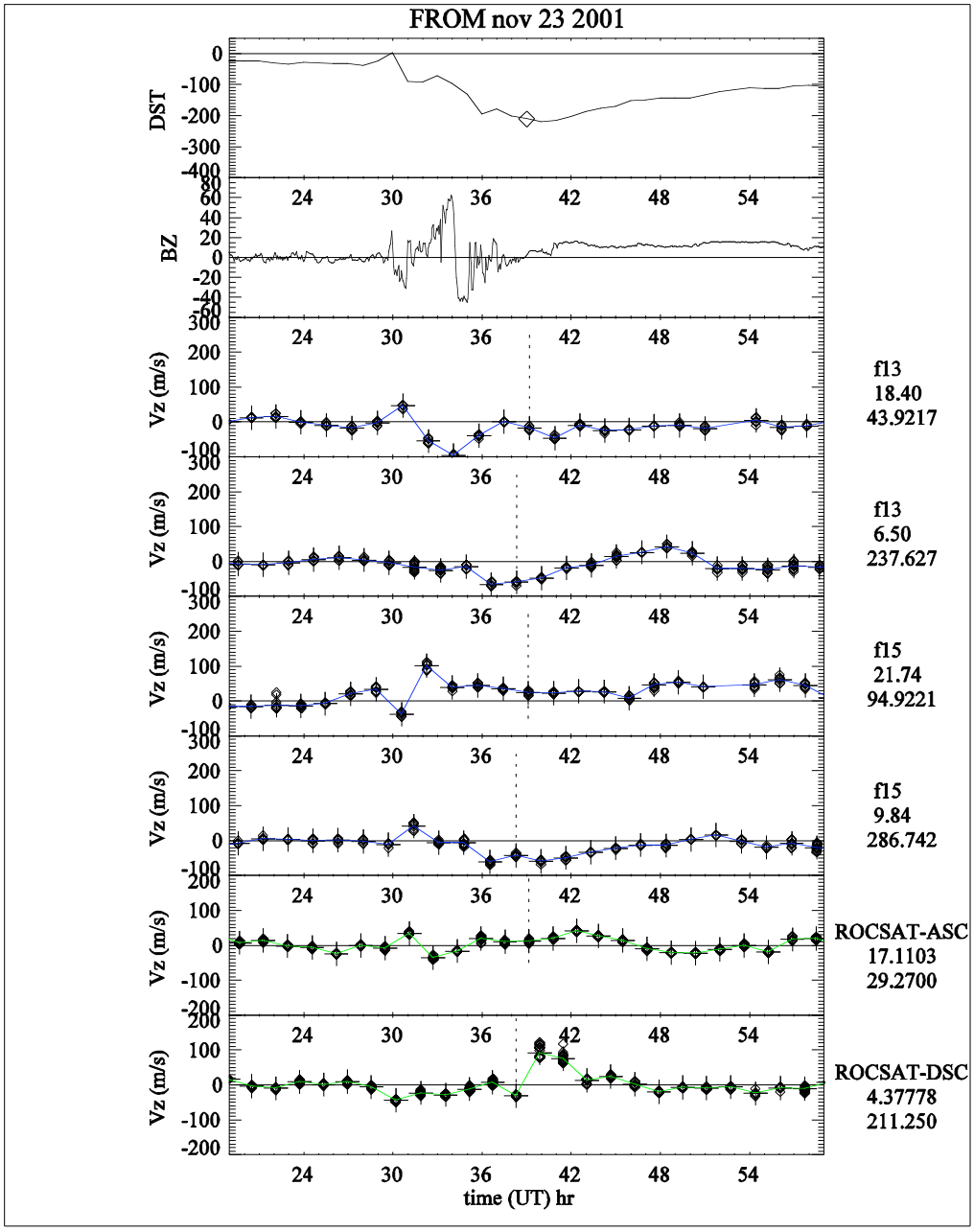


Figure 3.7. Vertical ion drift perturbations registered during the storm event on November 23, 2001.

The temporal sampling rate in our data is limited to the orbit period and is insufficient to effectively correlate the relationship between the drift perturbations and parameters such as the IMF and the ring current intensity that vary on time scales of a few minutes. However, we are able to examine the vertical drift perturbations recorded simultaneously at different local times

and to verify that the behavior in a single storm is similar to that predicted from a statistical analysis of data for many storms taken at a single location [*Fejer and Scherliess*, 1995; *Fejer and Scherliess*, 1997]. These drift perturbations are consistent with the so-called penetration electric field expected as a result of incomplete shielding of the low-latitude ionosphere (under-shielding) from the high-latitude current system [*Spiro et al*, 1988].

Even though all storms are characterized by different initial conditions and different evolution of the interplanetary magnetic field, examination of the vertical drift perturbations during these selected storm-time events reveals a number of reproducible features. We find that changes in the interplanetary magnetic field exercise the largest influence on the vertical drift perturbations. Large southward excursions of the IMF are accompanied by more negative Dst index values that identify the expansion phase of a storm. Similarly the recovery phase of a storm is most frequently marked by an excursion to northward IMF. In all the storms investigated here, the storm onset and expansion is marked by a large southward excursion in the IMF to large negative values of Bz. We find that the largest drift perturbations among these local times are always upward and occur near 1800 hours. The smallest of the drift perturbations is always near 0600 local time where the perturbation is below the detection threshold for drift perturbations. Simultaneous observations taken near 0900 and local noon show that the drift perturbations at these local times are also upward, with those at local noon being larger than those at 0900. Observations near local midnight indicate that the drift perturbation is comparable to that seen near local noon but the drift perturbation is downward. Near 2130 local time, drift perturbations associated with the southward excursion of the IMF are quite small. In fact the largest upward drift perturbations near 2130 local time are seen at times after the storm onset and associated with the appearance of equatorial irregularities [*Basu et al*., 2005].

Within the temporal resolution available from our data we find that the storm expansion, defined by the continuous decrease in the Dst index, is marked by the continual southward turning of a negative IMF or the maintenance of a large negative Bz produced by a prior southward turning. Of the storms we examine, the expansion phase may occupy between 2 and 10 hours. For those of short duration in this category we observe a vertical drift perturbation for only one pass at any local time that is encountered. For the longest duration storms, perturbations may be observed for 2 or three consecutive orbits even if the IMF is relatively stable. This supports the finding of *Basu et al* [2005] that the changes in the ring-current intensity also influence the observed vertical drift perturbations at the magnetic equator.

The storm recovery phase is always marked by a northward turning of the IMF, resulting in a prolonged period of weakly southward or northward IMF. This behavior is to be distinguished from brief northward excursions of the IMF that may occur during the storm expansion phase but are accompanied by a return to strongly southward turning IMF with negative Bz. During the storm recovery phase we rarely observe vertical drift perturbations at the equator. This study is not designed to examine the effects of northward IMF turnings from a previous quasi-steady period, the so-called over-shielded condition. Of the storms examined, only one exhibits a prolonged duration of northward IMF during the expansion phase. In this case the vertical drift perturbations are significantly smaller than those seen for comparable southward excursions of the IMF. Only a downward drift perturbation near dusk can be identified above the expected temporal variations produced by sampling at different longitudes.

In all cases the storm recovery is initiated by a northward turning of the IMF to values that are small and southward or northward. In this case the abrupt termination of vertical drift perturbations is due to the cessation of an applied high latitude current system that cannot be

shielded from low latitudes. When the storm expansion phase occupies a period in excess of 2 hours and vertical drift perturbations are seen for more than one pass, it is not possible to easily distinguish the effects of a penetration field from those produced by modification of the dynamo winds. It is interesting to note that in such cases the vertical drift perturbation observed at 0930 local time is of shorter duration that that seen near 1800 local time. Since the effects of a disturbance dynamo are significantly diminished on the dayside [*Scherliess and Fejer*, 1997; *Scherliess and Fejer*, 1998] the evidence for the influence of the disturbance dynamo is quite compelling.

In summary, the storm-time evolution of the observed vertical drift perturbations appear to be quite consistent with the presence of penetration fields, overshielding, and the disturbance dynamo, that operate with varying degrees of efficiency at different times. Figure 3.8 shows schematically how these contributions may be superimposed in a typical storm sequence illustrated by an idealized temporal evolution of the IMF Bz component and the Dst index. A period of quiet time precedes the storm event. A southward turning of the IMF is promptly followed by a drift perturbation due to an undershielded condition. The enhanced convection speeds in the auroral zone associated with the larger high latitude electric fields produce a disturbance dynamo that produces an upward drift perturbation over a time period that follows the prompt penetration, but may overlap with it and/or extend in time beyond it. The disturbance dynamo signature will depend in magnitude on the magnitude of the IMF southward component and on the duration over which the IMF remains at a consistently large southward value. The storm recovery commences with a northward turning of the IMF accompanied by a vertical drift perturbation characteristic of an overshielded state. The effect of the overshielding effect is opposite to the penetration electric field or undershielding, and a downward perturbation vertical

drift will be produced. The combined effects of these contributions give rise to the typically observed signatures in the vertical drift perturbations during the storms that we have examined. The order of magnitude of the perturbations are between 50 to 150 m/s. The time scales for the undershielding, overshielding and disturbance dynamo are generally different, with peak values observed at the beginning of the storm events coincident with the maximum effect produced by the undershielding source. The undershielding can last from a few minutes to a few hours depending on the time changes in the IMF. The disturbance dynamo lasts longer than the undershielding and the effect can remain for many hours. The overshielding mechanism has shorter duration than the disturbance dynamo and again has a duration of about two hours.

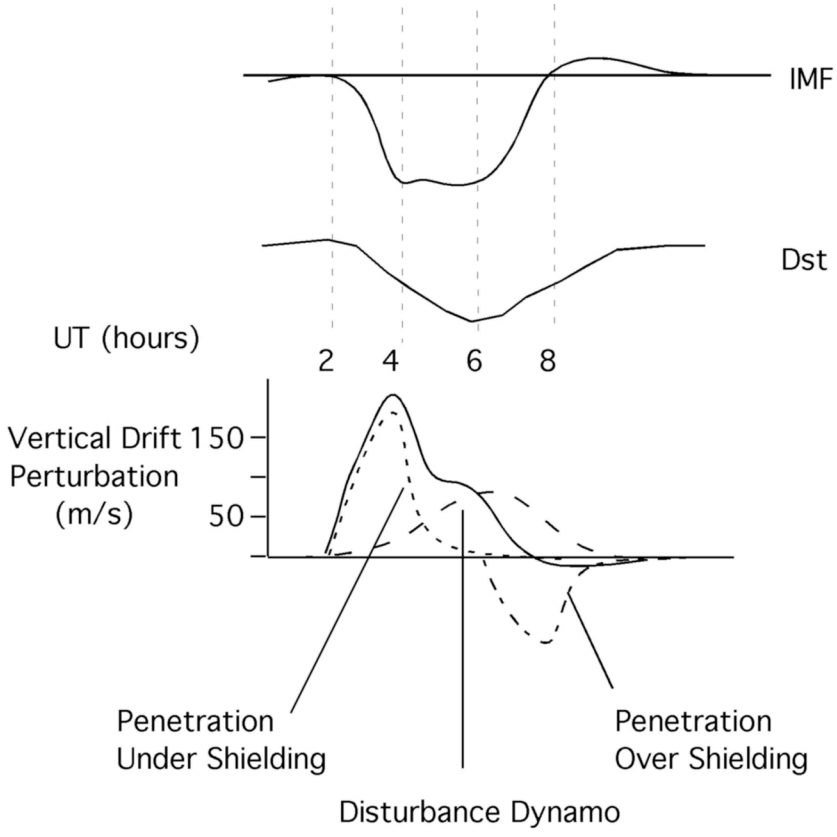


Figure 3.8. Evolution of the storm time event with temporal variations of the IMF-Bz, Dst index and the vertical drift perturbation. A southward turning IMF and a decreasing Dst index mark the onset of the main phase of the storm. Undershielding, overshielding and disturbance dynamo processes affect the resultant vertical drift perturbation.

# CHAPTER 4

# QUIET TIME MERIDIONAL ION DRIFTS

## 4.1 Introduction

The incoherent scatter radar at Jicamarca (latitude 11.95° South, longitude 76.87° West, 1°N magnetic) has provided a wealth of information on the local time variations in the meridional (vertical) and zonal drifts at the magnetic equator [*Woodman*, 1970; *Fejer*, 1991; *Fejer* et al., 1991b; *Fejer*, 1997]. These data have illustrated significant variations with season, solar activity and magnetic activity and have formed the basis for empirical models [*Scherliess and Fejer*, 1999] that are used extensively in computational models [*Huba et al*., 2000]. The availability of extensive data sets from satellite instrumentation has largely confirmed the seasonal and local time variations observed from the radars but have added additional information on longitude variations that reveal the characteristics of the neutral wind dynamos in the E region and the F region [*Fejer et al*., 1995; *Hartman and Heelis*, 2007; *Kil et al*., 2007; *Fejer et al*., 2008, *Oh et al*., 2008; *Ren et al*., 2009].

The incoherent scatter radar at Arecibo (18.30°N geographic latitude, 66.75°W geographic longitude) has also provided data that describes the local time variations of the meridional and zonal drifts driven by dynamo winds at middle latitudes [*Fejer*, 1993; *Zhou et al*., 1997]. These data also describe the dependencies on solar activity and season and, by contrast with Jicamarca, quite dramatically show the differences in local time variations at different magnetic latitudes that are apparently the result of changes in the neutral wind drivers. However, the spatial separation of ground-based radars makes it difficult to describe the latitude variations

that exist between them. For the most part this information has been derived from computational models such as the National Center for Atmospheric Research (NCAR) thermosphere/ionosphere/electrodynamics general circulation model (TIEGCM) [*Richmond et al*., 1992] that solve the dynamo equations given a specified global wind field. Since ground-based stations have the limitation of being in a fixed position, the use of satellite measurements is vital to study the latitude variation in ion drifts at all longitudes between the latitudes of Jicamarca and Arecibo for different local times. For the data considered here from ROCSAT-1, this exercise is complicated by the presence of biases in the ion drift components that must be accounted for when transforming vector measurements made in a satellite reference frame to a reference frame that is fixed with respect to the magnetic field. Thus much of the work with satellite data is restricted to the behavior of the ion drifts near the magnetic equator, which avoids the convolution of offsets from different drift components in the spacecraft reference frame [*Su et al*., 1999, *Yeh et al*., 1999b, *Kil et al*., 2007, *Fejer et al*., 2008]. Here we examine the ion drifts between ± 25º magnetic latitude using measurements from the FORMOSAT-1 (formerly ROCSAT-1) satellite in order to provide a description of the quiet time latitudinal (apex-height) variations of the ion drifts as a function of local time for different longitude sectors.

## 4.2 Methodology

A complete description of the methodology employed to produce the data is described in detail in chapter 2 and briefly summarized here for convenience. We first divide the sample space between ± 35º geographic latitude into latitude bins that are 2.5 degrees wide, longitude bins that are 30 degrees wide and local time bins that are 30 minutes wide shifted every 15

minutes. We find the average representative values of ion drifts inside those bins considering separately northbound and southbound passes. We have restricted the ion drift data set, considering only the values when the total ion concentration is higher than $10^4$ $cm^{-3}$ to minimize the measurement uncertainty in plasma depletions that occur after 1900 LT and at late night hours when the percentage of light ions is high [*Fejer et al*. 2008].

The main biases in each ion drift component are the result of variations in the orientation of the satellite and changes in the vehicle potential. A first order offset in the vertical drift is obtained by noting that the electric field is curl free and thus the longitudinal and local time average of the vertical drift at the magnetic equator is zero. The biases in the horizontal drift components are eliminated by applying the condition that geographic north-south and east-west drift components in each sample volume must be the same for northbound and southbound passes. In each bin the contributions of the drift components in the satellite reference frame to the geographic north-south and east-west drifts are weighted differently for the northbound and southbound passes. Thus we are able to determine a first order correction for offsets in the measured ion drift components by enforcing the condition that the east-west and north-south drifts must be the same for both trajectories through a given sample volume.

To convert the drifts averaged on a geographic grid to components parallel and perpendicular to the magnetic field we first re-sample the data onto a uniform grid in magnetic coordinates. The grid size is 2.5º in corrected geomagnetic (CGM) latitude, 10º in longitude and 15 minutes in local time. The location of each bin in CGM coordinates is converted to geographic coordinates using the IGRF model. The ion drift velocity components in the spacecraft reference frame are specified at each grid point and at the conjugate point. We consider ascending and descending passes to obtain average values separately for each sample

volume, and a boxcar average is applied to the measurements with a width of 30 minutes and shifted every 15 minutes in local time. The values of the ion drifts are obtained for a specific season and year. Finally the drift velocity in the spacecraft reference frame is transformed into components parallel and perpendicular to the magnetic field and further adjustments to the offsets in each component are made to enforce conjugacy in the drifts perpendicular to the magnetic field. Then the plasma drift for four consecutive years for a specific season are averaged and shown in the figures.

We note that the altitude is not constant but is near 600 km with variations of +/- 30 to 50 km. This introduces a variability of less than 5 m/s in the horizontal components of the ion drift in the corotating reference frame.

For this study we have selected six magnetic longitude sectors, the Pacific Central American, South American-Peruvian, South American-Brazilian, African, Indian and Pacific regions corresponding to the 270º, 290º, 310º, 0º, 90º and 180º geographic longitudes respectively. For each longitude sector, the magnetic equator has a different offset with respect to the geographic equator and the magnetic field has a different declination.

Figures 4.1, 4.2 and 4.3 show the derived meridional ion drifts obtained at the magnetic equator for the December solstice, June solstice and equinox period, respectively. The small black circles indicate the resultant value from averaging the drifts for each year used in our study. The top, middle and bottom panels indicate the measurements in the 290º, 90º and 180º geographic longitude sectors, respectively. These data show the same local time, seasonal and longitude variations described in detail by *Fejer et al*. [2008] near the magnetic equator. For example the previously established seasonal and longitude variations in the prereversal enhancement are verified and the agreement with the average drifts at Jicamarca provides

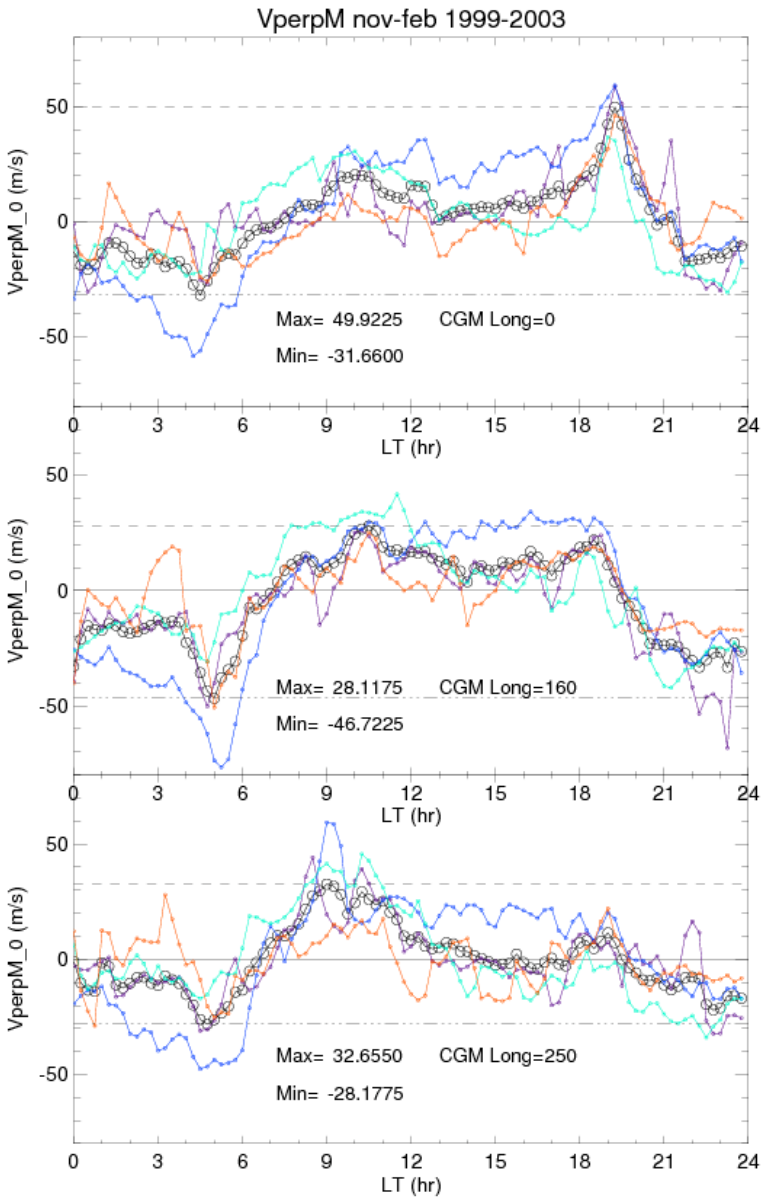


Figure 4.1. Meridional ion drifts distributed in local time at the magnetic equator during December solstice (November to February) correspondiong to the 0º (upper panel), 160º (middle) and 250º (bottom) CGM longitude sectors. Also indicated is the relative position of the maximum and minimum values by the dashed and dash-dot lines and their magnitudes for each longitude sector. The black circles represent the total average from the years 1999 to 2003. The purple, blue, turquoise and orange color lines indicate the meridional drifts for the periods 1999-2000, 2000-2001, 2001-2002, 2002-2003 respectively.

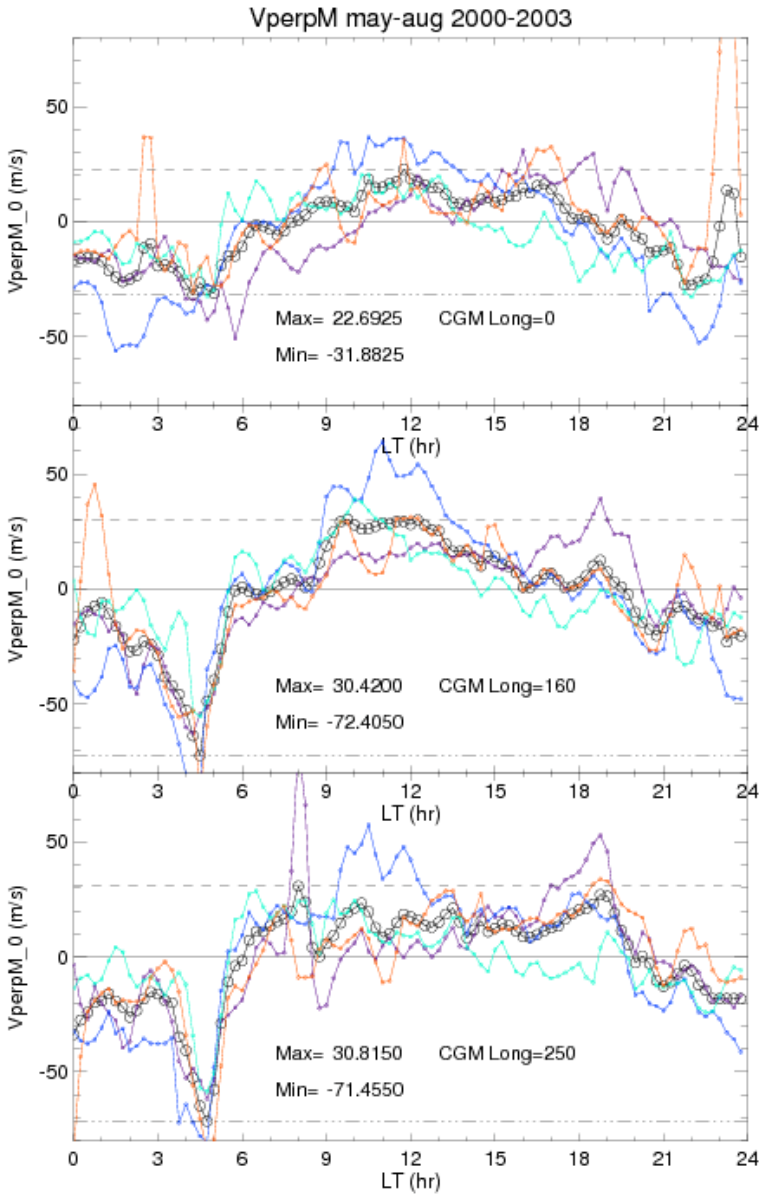


Figure 4.2. Meridional ion drifts distributed in local time at the magnetic equator during June solstice correspondiong to the 0º (upper panel), 160º (middle) and 250º (bottom) CGM longitude sectors. The black circles represent the total average from the years 2000 to 2003. The purple, blue, turquoise and orange color lines indicate the seasonal meridional drifts for the years 2000, 2001, 2002 and 2003 respectively.

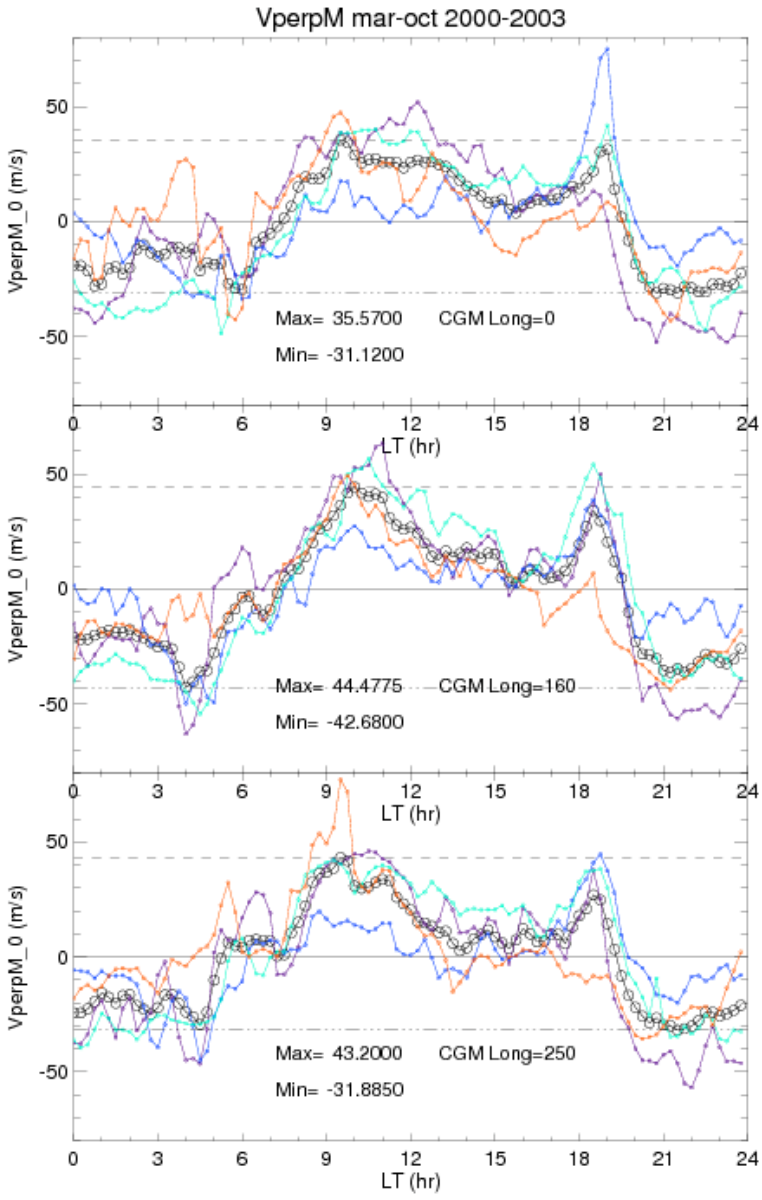


Figure 4.3. Meridional ion drifts at the magnetic equator during equinox corresponding to the months of March, April, September and October. The purple, blue, turquoise and orange color lines indicate the seasonal meridional drifts for the years 2000, 2001, 2002 and 2003 respectively.

confidence in our data set. Note however, that significant annual variability exists that could be related to variations in the solar flux for the periods over which the data are collected. Invalid measurements in 2003 are observed in the local vertical ion drift component during the northern summer. As shown in Figure 4.2, large positive values are measured in the 0º CGM longitude sector near 0300 and 2300 LT and also in the 160º CGM longitude sector near 0100 LT. These data points escaped our first order filtering and lead to large excursions over short local time regions. However, these excursions do not affect the major findings of our study.

## 4.3 Observations

Figure 4.4 shows the general characteristics of the average ion drifts perpendicular to the magnetic field in the magnetic meridian plane. The drifts are organized by season for each column and shown as a function of magnetic latitude and magnetic local time with the color scale indicating the magnitude of the drift. The red color indicates positive magnitudes or upward drifts and the blue color indicates downward drifts or negative values. These data encompass the northern winter periods (November to February) from 1999 to 2003 (left column), the equinox period (March, April, September, and October) from 2000 to 2003 (middle column), and the northern summer (May to August) for the years 2000 to 2003 (right column). The top panel corresponds to the Pacific Central American sector, the second, third, fourth, fifth and sixth panels show the ion drifts for the South American-Peruvian, South American-Brazilian, African, Indian and Pacific sectors respectively. The results for the southern hemisphere are mirrored from the northern hemisphere since the ion drifts are the same at conjugate latitudes.

Each longitude region is characterized by a different displacement between the geomagnetic and geographic equator and by a different magnetic declination. The representative

geographic longitudes are shown to the right of each panel. In each longitude the drifts are determined out to the maximum magnetic latitude accessible by the satellite in both hemispheres. Vertical lines at 0600 and 1800 local time are drawn to aid in the location of drift features.

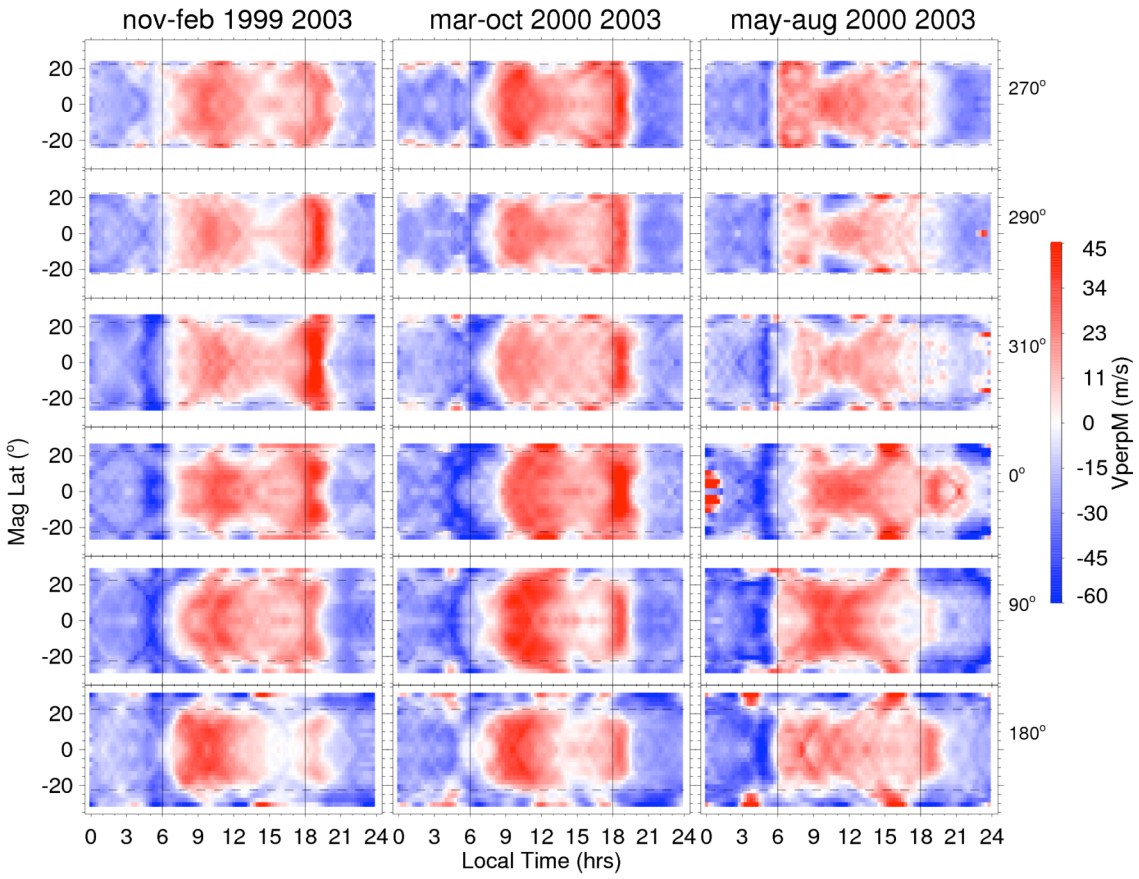


Figure 4.4. Latitudinal and local time dependent quiet time ion drifts perpendicular to **B** contained in the magnetic meridional plane. The panels from top to bottom indicate the Central American, South American-Peruvian, South American-Brazilian, African, Indian and Pacific regions corresponding to the 270º, 290º, 310º, 0º, 90º, 180º geographic longitudes. The averaged ion drift values are obtained for the November-February period from 1999 to 2003 (left column), the equinox period from 2000 to 2003 (middle column) and the May-August period from 2000 to 2003 (right column).

Three dominant features are immediately seen in these data, which show strong seasonal and longitudinal variability. First, the pre-reversal enhancement (PRE) can be seen as a relatively

confined region in local time with enhanced upward (outward) drift occurring shortly after 1800 hours. Second, the region of daytime upward drift, extending from near sunrise across local noon, is highly variable with season, longitude and local time. Finally, a sunrise downward drift enhancement that is apparent in most longitude regions and most seasons is confined in local time near 0600 hours and shows a seasonal and longitude dependence. Below we discuss each of these features.

### 4.3.1 PRE features

One of the main features observed during the December solstice is the large variability of the pre-reversal enhancement (PRE). The latitude (apex-height) extension and magnitude of the PRE change in different longitude sectors. The location of the PRE in local time also depends on latitude (apex-height) and longitude.

During the northern winter the PRE has its largest magnitude in excess of 45 m/s in the South American-Brazilian sector near 310º longitude. In this longitude sector, the PRE extends to magnetic latitudes near 20 degrees and is almost constant in magnitude and centered at the same local time. However there is some tendency for the PRE to extend over a broader local time range at higher latitudes. The PRE also extends to about ±20º magnetic latitude in the South American-Peruvian region (290º) and the Central American region (270º). However, the PRE peaks at higher latitudes occur earlier in local time than the peaks near the magnetic equator. The opposite situation occurs near 90º and 180º where the PRE occurs earlier in local time at low latitudes. The PRE magnitude decreases with increasing longitude from 0º to 180º. At 180º longitude, the PRE is extremely weak and restricted to latitudes less than 17 degrees, and a local maximum is seen near 15 degrees rather than at the equator. This local maximum in the PRE

drift also appears at later local time than the weaker feature seen at the magnetic equator. The PRE rapidly diminishes with increasing latitude beyond 15 degrees, and a reversal to downward drift is observed near 17 degrees in the Pacific sector (180º). In the African sector (0º) the enhancement is slightly smaller than the PRE in the Brazilian sector but comparable in magnitude to the PRE in the Peruvian sector. The peak of the enhancement in the African region has a tendency to appear at latitudes near 7º and decreases with increasing latitude extending to about 20º magnetic latitude. During northern winter, the evening reversal times occur between 1900 LT and 2100 LT. Near the 290º and 270º longitude sectors the evening reversal times occur earlier, near 1930 LT, at the highest latitudes and later, near 2100 LT, at the magnetic equator. Near the 310º, 90º and 180º longitude sectors, the evening reversal times at the magnetic equator are located at earlier local times, near 1930 LT. For latitudes away from the equator the reversal local times are near 2030 LT, for magnetic latitudes near 22.5º and 12.5 that correspond to the 310º and 180º longitude sectors respectively. The evening reversal time for the 90º longitude sector occurs near 2030 LT for latitudes near 17.5º.

During the equinox period the PRE appears in all longitude regions at a local time near 1830 hours. The extension of the PRE in latitude is dependent on longitude. Near 180º longitude the PRE magnitude is near 30 m/s and extends to only 15º magnetic latitude before the drift reverses to downward at higher latitudes. Near 270º and 290º, the PRE extends to latitudes beyond 20 degrees. In the African sector the PRE occupies a larger local time extent, extending the period of upward drift to near 2100 local time, while at other longitudes the transition to downward drift occurs near 2000 hours.

During the June solstice the PRE magnitude is also latitude (apex-height) and longitude dependent. The PRE is in general smaller in magnitude and latitudinal extension than at other

seasons. The PRE is largely absent in the South American sector but it is weakly present in the African, Indian regions and more strongly in the Pacific sector, where it reaches magnitudes near 25 m/s. In this last region it appears with about the same magnitude as in equinox but is significantly more restricted in latitude. In this longitude sector the PRE rapidly declines at latitudes beyond 10 degrees and the drift becomes downward beyond about 15 degrees latitude. A particular case is the African region that shows upward ion drifts with longer duration in local time than the meridional ion drifts observed at other longitudes. The reversal time occurs near 22 LT and the PRE presents a latitude extension of about 15º which is narrower than the latitude extension of the PRE at other longitudes and seasons. Observations [*Oyekola*, 2006; 2009] at Ibadan (7.4º N, 3.9ºE geographic, dip 6ºS), Nigeria, West Africa, show vertical plasma drifts in the evening region after sunset during quiet solar maximum using data from 1958 ionosonde measurements in the F-region, near 350 km altitude. The seasonal general features of the PRE agree with our results where the largest PRE is observed during equinox and the smallest during northern summer. Larger duration of the PRE in local time during the northern summer months extending from 1700 to 2200 LT with a peak value near the 1900 LT are observed with the ionosonde and ROCSAT-1 measurements. In the Indian sector the PRE is also restricted in latitude to about 10 degrees, where the drift turns downward. The PRE is preceded by very small downward drifts near 1700 LT.

### 4.3.2 Daytime upward-downward drifts features

Another significant feature observed is the region of daytime upward drift, extending from near sunrise across local noon. These drifts are highly variable with season, latitude, longitude and local time extent. Starting shortly after 0600 local time upward (outward) drifts are

seen in all longitude regions during the December solstice. Peak values are seen near 1000 local time in all longitude sectors, and the drifts decline with increasing local time until the PRE is encountered after 1800 local time. The largest morning upward drifts during northern winter are observed near the 180º longitude sector reaching values near 30 m/s between 0800 LT and 1100 LT. They occur earliest for latitudes near 17.5º. The smallest morning upward drifts, less than 20 m/s, are in the South American sector. The American and Pacific sectors coincide with the longitudes of a local minimum and maximum in the wave number-four structure of the equatorial vertical morning drifts near 1000 LT [*Fejer et al*., 2008]. These maxima and minima are clearly seen extending in latitude out to 15º. The daytime drifts show a strong latitude dependence consistent with the introduction of a semi-diurnal component into the local time behavior at higher latitudes. In the South American and African sectors, at latitudes above 12 degrees the drifts become weakly downward after local noon, with the most pronounced effects being seen near 1500 local time and 290º longitude. In the Indian sector no strong latitude dependence is seen within 20 degrees of the equator, but in the Pacific sector the latitude dependence reappears with the daytime drifts being downward after 1500 local time above 12 degrees latitude. In the Pacific sector after 1500 local time the daytime drifts are extremely weak at all latitudes and can even be downward at the equator.

During equinox through most of the day the upward drifts do not show a strong dependence on latitude out to about 20º, but there is still some evidence for changes in the local time variations at higher latitudes between 1300 and 1500 LT. The morning upward drifts are the largest during this season and maximize in the morning sector before 1300 LT. The strongest upward daytime drifts are observed in the Indian, Pacific and African sectors, where they exceed 40 m/s, and the smallest morning upward drifts at low latitudes are again observed near the

American sector. The local time of the dawn transition from downward to upward drift is highly dependent on longitude. In the African sector the onset of upward drifts begins near 0900 local time and moves to slightly later local times at latitudes above 10 degrees. In the Indian and Pacific sectors the upward drift onset retreats to near 0700 local time but becomes later with increasing latitude above 10 degrees. In the American sectors the upward drift onset begins near 0800 local time at low latitudes and at slightly later local times at higher latitudes out to 20 degrees. The largest latitudinal extension of the morning upward drifts is observed near the African and Indian sectors. In all longitude sectors there is a signature of a semidiurnal component in the ion drift during the day. This manifests itself as a small weakening of the upward drift near local noon and 1500 LT at the highest magnetic latitudes sampled.

During northern summer, the upward daytime drifts commence near 0600 local time except in the South American (310º) and African (0º) sectors where the onset time is near 0800 LT. The largest upward daytime drift is seen in the Indian sector with a peak of 35 m/s near local noon. During this season a much clearer semi-diurnal component is apparent at latitudes above 10 degrees in all longitude sectors. In the Pacific and American sectors a region of downward drift is observed in the pre-noon hours at latitudes above 10 degrees. We note that this same signature was observed in the post-noon hours in the northern winter. In the African sector a similar region of downward drift above about 15 degrees latitude is observed across local noon as it was during the December solstice.

### 4.3.3 Downward enhancement near sunrise

The final prominent feature for discussion is the appearance of a dawn side enhancement in the downward drift that precedes the onset of the usually expected upward daytime drifts.

However, the determination of the precise latitude extent of this feature is again complicated by the transition from diurnal to semidiurnal variations with increasing latitude. Our results show that during the December solstice this feature is most evident in the Indian sector; although it is sometimes weakly present, the average onset time of the downward enhancement at all longitudes is near 0500 LT. It is almost absent near the Central American and Peruvian sectors but appears dramatically near the 310º longitude and persists throughout the African sector and into the Pacific. Near the 310º longitude sector, the downward drift enhancement with magnitude near 40 m/s is observed near 0500 LT at latitudes near the magnetic equator and shifts slightly to later local times with increasing latitude. At other longitudes, the feature is largely independent of latitude but the later onset time for upward drifts at higher latitudes tends to broaden the local time extent of the downward drifts at high latitudes in the Indian and Pacific sectors. *Prabhakaran Nayar et al*. [2009] studied the electrodynamics of the pre-sunrise equatorial F-region using HF Doppler radar and a digital ionosonde. A downward enhancement of the vertical ion drift is observed around local sunrise followed by an upward turning that coincides with the start of the E-region sunrise.

During equinox the dawn downward drift enhancement is most prominent in the African sector where it extends over nearly a two-hour local time region starting near 0400 LT. In the Indian sector the downward enhancement peak lies near 0500 local time. The magnitude of this enhancement is about 40 m/s near both longitude sectors. However in the American region the downward drift peak occurs after 0600 LT with magnitudes of about 25 m/s. At all longitudes the downward drift enhancement appears at later local times with increasing latitude during the equinox period. During the June solstice the downward drift enhancement can also be seen at all longitudes but it is weakest and most narrow in local time in the American sectors. It is more

pronounced in the Pacific sector with magnitudes of about 65 m/s. The downward drift enhancement occurs at almost the same local time near 0500 LT at all latitudes out to 20º. It extends over the maximum latitude range in the African sector but more confined in local time (about 1 hour) than the same feature observed during equinox. In the Indian sector the downward drift enhancement is less apparent due to the presence of relatively large downward drifts throughout the period from midnight to 0600 hours. The dawn downward drift enhancement appears more intensely in the Pacific sector during the June solstice than during other seasons.

### 4.3.4 Ion density features

We have observed the average total ion concentration distributed in local time and magnetic latitude for the same seasons and years as in Figure 4.4. The average density, as shown in Figure 4.5, is derived from the same space bins used to obtain the meridional ion drifts. The left, middle and right panels correspond to the December solstice, equinox and June solstice periods respectively. In this case the color scale indicates the logarithm of the total ion concentration. The responsiveness of the topside ion density to the meridional drifts and F-region winds is immediately apparent in all these data. After midnight the action of interhemispheric F-region winds that blow from the summer to the winter hemisphere can be easily seen in the latitude asymmetry of the ion density minimum in the winter and summer months. Also notable is the presence of an equatorial anomaly in the post sunset hours that is directly responsive to the post sunset enhancement in meridional (vertical) ion drift. The anomaly signature is also seen during the daytime in the Indian sector during equinox and northern summer months when the daytime upward drifts are the largest.

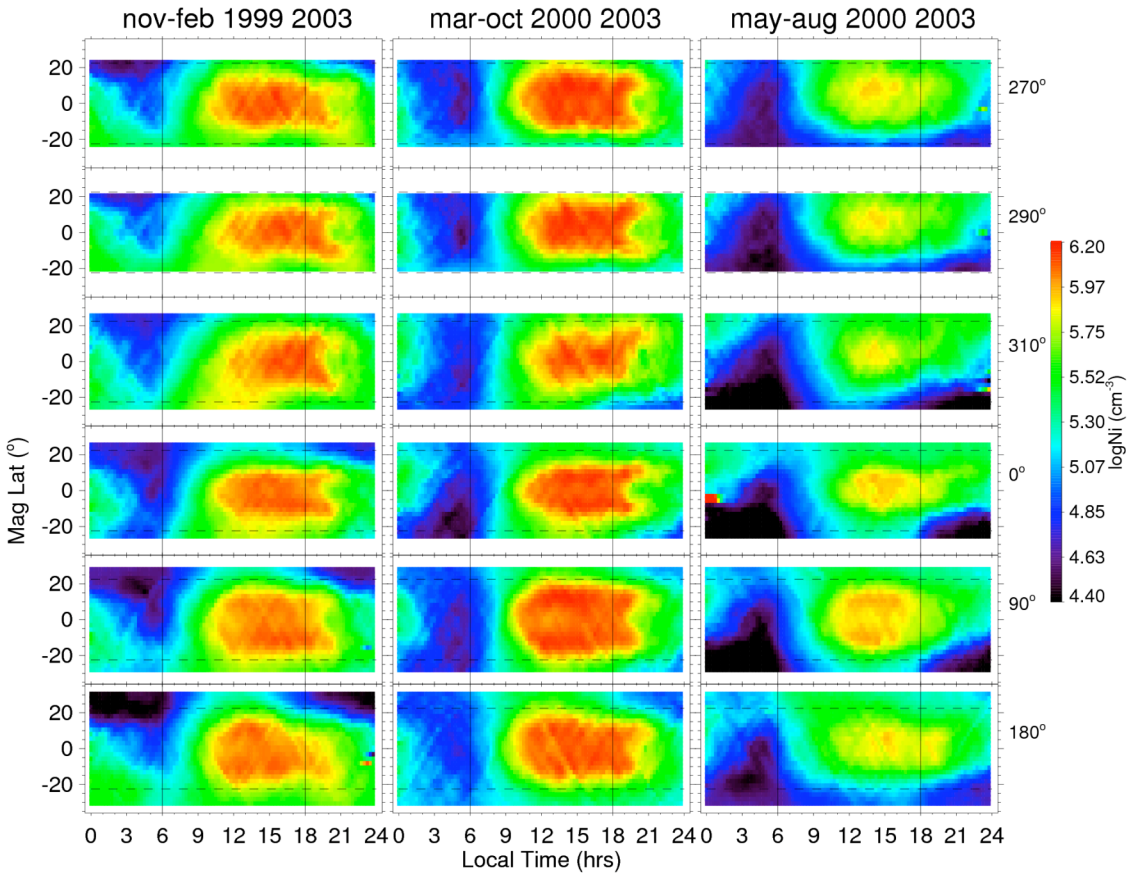


Figure 4.5. Average total ion density distribution in local time and CGM latitude obtained from ROCSAT-1 for the December solstice 1999-2003 (left), the equinox 2000-2003 (middle) and the June solstice 2000-2003 periods (right). The longitude regions are the same as indicated in figure 4.4.

Features in the ion number density may be disguised by the choice of color scale but there are two main features that respond directly to the drift. One characteristic is the latitudinal width over which low latitude density maxima are seen and the other is the latitude distribution that displays the signature of an equatorial anomaly in the topside at 600 km altitude. The transitions from green to yellow and from yellow to red in the displays of Figure 4.5 are the

easiest features with which to identify these characteristics. To relate these features to the meridional ion drift it is also necessary to appreciate that the distribution of ionization responds to the imposed ion drift with a time delay of 1 hour or so. The largest daytime density values are observed during the equinox period corresponding to the largest morning upward drifts. Broad density maxima near $10^{5.8}$ $cm^{-3}$ are located between ± 20º magnetic latitude, consistent with the ionosphere being lifted by the upward morning drifts. During the June solstice, the maximum density values are smaller than values observed during the equinox and the December solstice periods. The extent of the density maxima is directly associated with the magnitude and onset time of the meridional drift, which is more evident in the Indian sector. In this longitude sector, it is more noticeable the presence of the equatorial ionization anomaly signature. Inspection of the drift features during the northern winter months shows the maximum upward drifts appear in the pre-noon sector in the Pacific sector while the maximum PRE drifts appear in the American sector. Correspondingly, the widest latitude extent of the daytime equatorial density maxima appears in the Pacific longitude sector where there is even a signature of an equatorial anomaly in the hours around local noon. Note however that after 1600 local time the latitude extent of the density maxima becomes restricted in latitude corresponding to the appearance of weak or even downward drifts after 1400 in this longitude sector. By contrast in the American sector, the density maxima is more restricted in longitude but remains almost constant throughout the daytime, corresponding to the smaller upward daytime drifts seen in this longitude sector. However, in the post sunset hours a prominent equatorial anomaly is seen corresponding to the appearance of a pronounced PRE drift in this longitude region. Continued examination of the ion drift features and features in the ion number density during the equinox and northern-summer months provides more confidence in the relationships between these independently observed

parameters. Specifically the latitude extent over which ion densities greater than $1x10^6$ $cm^{-3}$ are observed is dependent on the magnitude and latitude extent of the daytime meridional ion drift. Comparing the ion drift and ion number density for the equinox months at longitudes near 90 and 180 degrees shows that the equatorial ion drifts are of comparable magnitude but extend further in latitude in the 90 degree sector than in the 180 degree sector. Likewise the latitude extent over which the density maximum exists is larger in the 90 degree sector than in the 180 degree sector. In the northern summer only the longitude sector near 90º shows substantial upward drifts on the dayside and only this sector shows elevated ion number densities with a signature of the equatorial anomaly at 600 km altitude.

### 4.3.5 Apex Height ion drift variability

The latitude variations in the ion drift described in the previous figures are described in more detail at specific local times by examining the variations in the ion drift as a function of magnetic flux tube apex height. Profiles of the meridional ion drifts versus apex height near noon and near the local time of maximum PRE (1900 LT) are shown in Figures 4.6 and 4.7 respectively. Each panel shows results for the northern winter solstice, equinox and northern summer solstice from top to bottom respectively. The meridional drifts for each longitude sector are represented by different colors.

Near noon and during the northern winter, the meridional ion drifts vary slightly with apex height between 600 km and 1000 km (within 14º magnetic latitude range). Previous studies of observations over Jicamarca also show small variations of the drifts for that altitude range [*Woodman*, 1970; *Fejer et al*., 1991b; *Pingree and Fejer*, 1987]. Above 1000 km, our results show evidence of decreasing meridional drifts with increasing apex height, and the drifts reverse

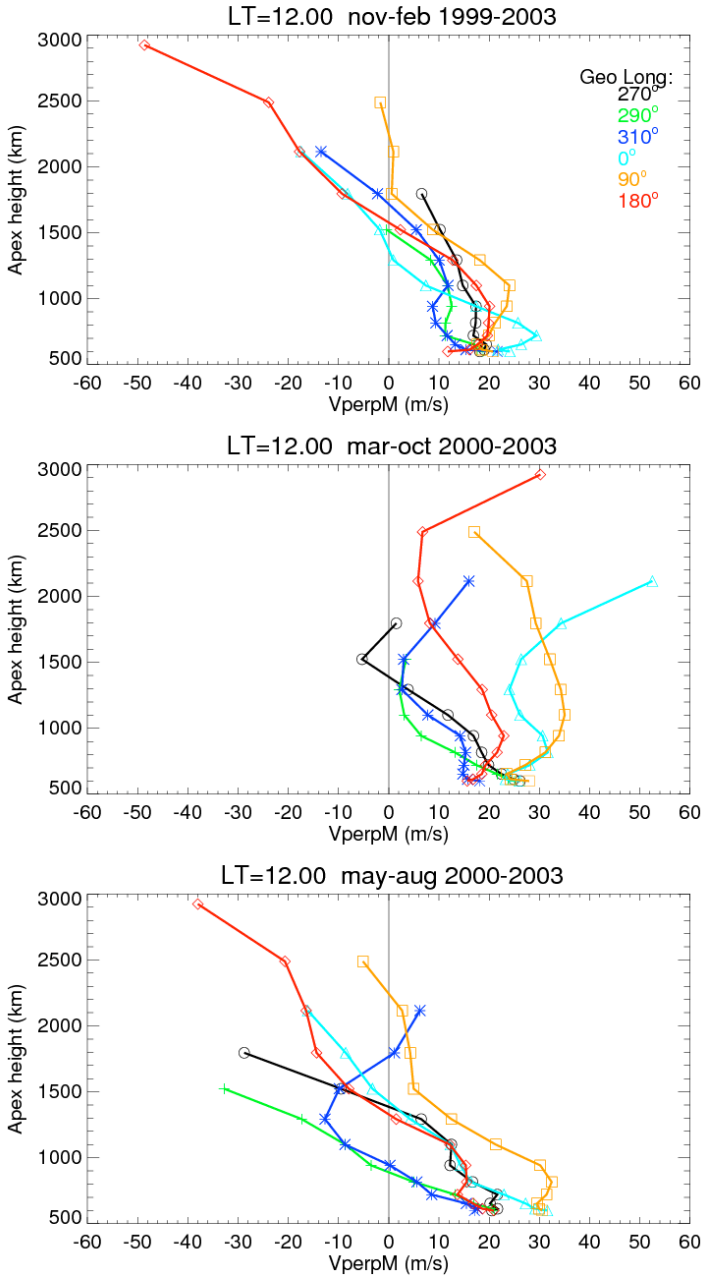


Figure 4.6. Meridional ion drifts near 1200 LT vs. apex-height for the same seasons and longitude sectors illustrated in figures 4.1-4.5.

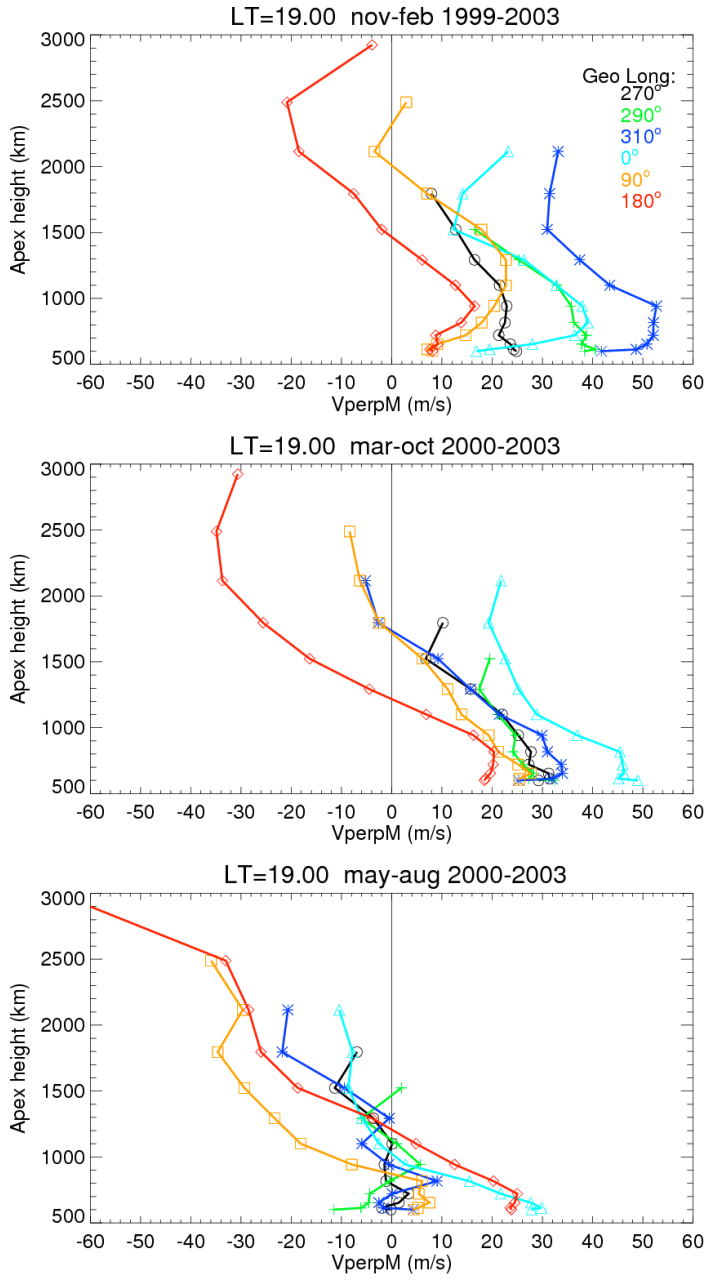


Figure 4.7. Meridional ion drifts near 1900 LT vs. apex-height.

sign and become negative at the highest altitudes. During equinox the plasma drift values tend to remain positive or upward with increasing apex height. The observations near 1900 LT show that the ion drifts maximize below 1000 km as observed in Figure 4.7, and decrease above that altitude. Generally the drifts reverse direction at lower apex height during the northern summer than during equinox and northern winter. There is a larger variability of the PRE in longitude observed during the December solstice than during the other seasons. The largest PRE is present in the Brazilian sector (310º) and the smallest in the Pacific sector (180º). Near 1900 LT the apex height variations are indicative of the factors controlling the PRE drift where it appears during the northern winter months. It is expected that the apex height variation in the PRE will reflect the altitude gradient in the flux tube integrated Pedersen conductivity. In the Pacific region, where the upward drift is small, the peak in the flux tube integrated Pedersen conductivity appears at apex height below 1500 km. However, when the ionosphere is subjected to a large upward drift the peak in flux tube integrated Pedersen conductivity appears at much higher altitudes. The same relationships between the magnitude of the upward drift and the flux tube integrated Pedersen conductivity can be seen in the equinox months when the PRE appears at all longitudes near 1900 LT. In the northern summer months the PRE is largely absent and a reversal in the upward ion drift appears at low apex height due in part to the weakness of the F-region dynamo and in part due to the influence of different E-regions winds at higher magnetic latitudes.

We have to be aware of the sensitivity of the apex height variations with respect to changes in local time, as observed in Figures 4.8 and 4.9, that show the meridional ion drifts at 1100 LT and 1830 LT, respectively. Even though the results in Figure 4.8 are separated by just

one hour in local time with respect to the results observed in Figure 4.6, there are some differences. Near 1100 LT the drifts corresponding to the Indian (90º), African (0º) and the

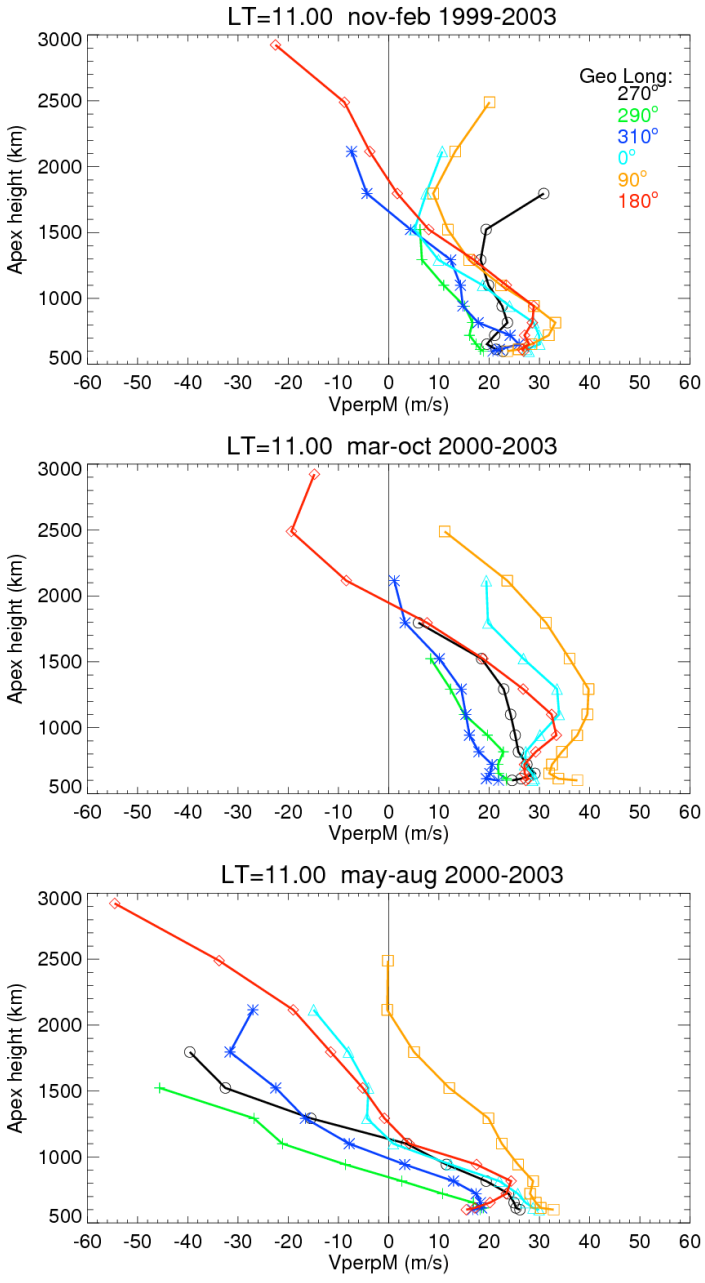


Figure 4.8. Meridional ion drifts near 1100 LT vs. apex-height.

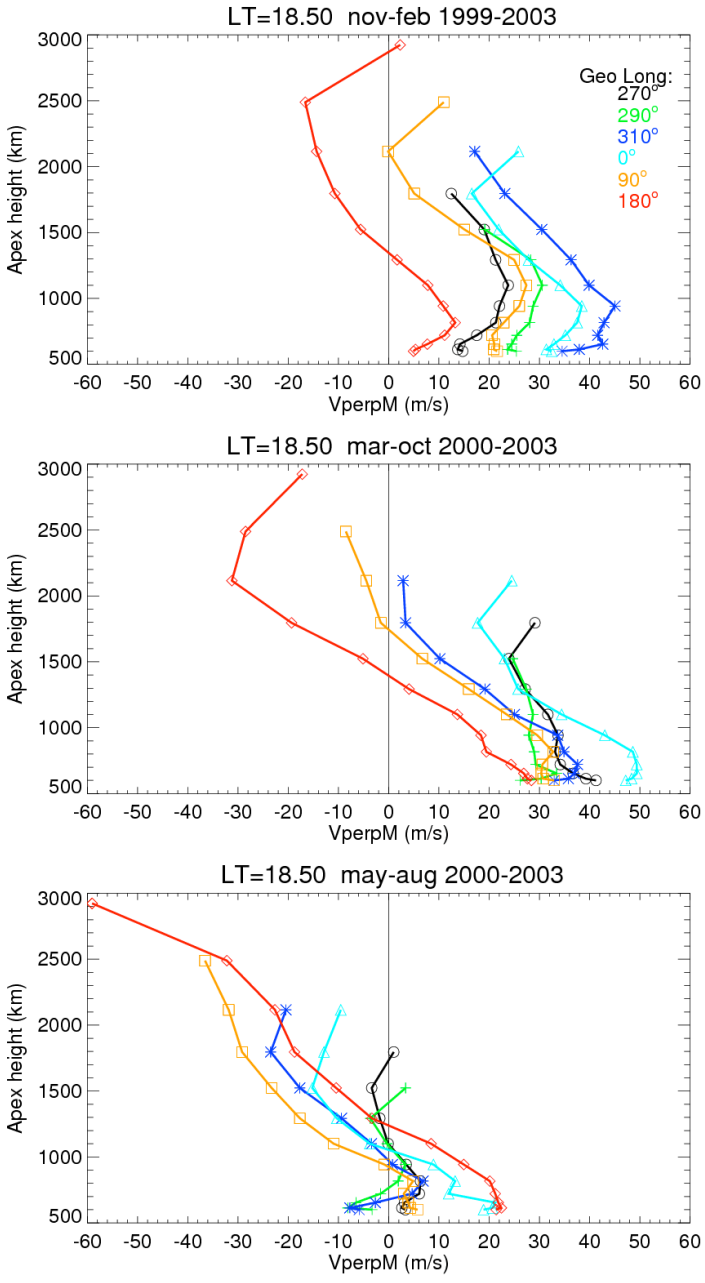


Figure 4.9. Meridional ion drifts near 1830 LT vs. apex-height.

Central American (270º) sector tend to increase in magnitude above 1500 km while during noon the drifts tend to decrease and change direction with increasing altitude for the same longitude regions. The Peruvian, Brazilian and Pacific longitude regions decrease in magnitude with increasing altitude and reverse direction above 1500 km at both local times. During equinox the most noticeable difference is the increase of the drift magnitude above an apex height of about 1700 km for the measurements near the 250º magnetic longitude at noon but a decrease and reverse of direction near 1100 LT. The meridional drifts in the American region show a higher rate of change with respect to increasing apex height at noon than at 1100 LT. Near noon, the ion velocities reach small magnitudes and reverse direction in some cases below an apex height of about 1500 km, and later increase their magnitudes above that apex height. During the northern summer, the drifts behave in a similar way at both local times, decreasing their magnitudes with increasing apex height. The rate of change is higher compared with other seasons, but the magnitude of the drifts near the Brazilian sector reaches larger negative values at 1100 LT near an apex height of about 2000 km.

The apex height variation of the meridional drifts at 1830 LT is very similar to that observed near 1900 LT. Figure 4.9 illustrates the apex height dependence of the drifts near 1830 LT and shows the same general features described before, such as the smaller variations below 1000 km and larger variations above that apex height. During the December solstice the positive peak values of the drift occur near an apex height of 1000 km, except for the Pacific sector which attains its maximum positive value is located near an apex height of about 700 km. We cannot identify features below 600 km since the satellite does not reach these lower heights. The major differences during this season are observed below 1000 km apex height in the Peruvian and

Central American regions. At 1900 LT the drifts peak at apex height near 600 km and decrease with increasing height, but at 1830 LT the drifts increase with increasing height, maximizing near 1000 km and then decrease above that apex height. During the equinox less variability with respect to apex height is observed in the Central American longitude region at 1830 LT. Another difference is that the maximum positive value in the Pacific sector occurs at an apex height of about 800 km at 1900 LT while the peak value at 1830 LT for that longitude region occurs at apex heights below 600 km. Very similar tendencies are observed near 1830 and 1900 LT during the Junes solstice with small drift magnitudes for all longitude sectors below an apex height of 1000 km. Above 1000 km, larger magnitudes are observed at both local times for the Brazilian, Indian, and Pacific regions. There is insufficient data in the other longitude regions to infer features at higher apex heights.

## 4.4 Discussion and Summary

We have described the topside ionosphere F region meridional ion drifts in the latitude range of ± 25º obtained from ROCSAT-1 from 1999 to 2003. We applied a methodology to eliminate offsets in the spacecraft measurements before deriving drifts in the directions parallel and perpendicular to **B**. We have used drifts measurements without separating the data by solar flux values. The period from December 1999 to December 2003 is during solar maxima, but the solar flux index levels are between 110 to 240 for that period. The maximum values occur between the end of 2001 and the beginning of 2002. The minimum values of solar flux appear during 2003. Thus the variability in the data is influenced by this range in the solar flux. We have calculated the average values during each year in the interval 1999-2003. Some caution should

be applied to the results at magnetic latitudes higher than 20º since above these latitudes there is more annual variability in the drift values of each individual year with respect to the mean value.

As expected, the daytime plasma drifts are generally upward and westward during the day and downward and eastward during the night. The E and F- region dynamo wind currents produce the general features of the drifts at low and middle latitudes. The results show evidence of ion drift gradients in latitude, or equivalently gradients in apex-height besides the variations in longitude, season and local time. The apex-height variations of the plasma drift may be related to latitude gradients in the neutral wind or related with gradients in the conductivities. Immediately apparent in our results is the large longitudinal and seasonal variability in the pre-reversal enhancement (PRE) drift. The PRE exhibits more variability in longitude and latitude (apex-height) during the solstices than during the equinox. Within each longitude sector it is also seen that the daytime meridional drift has significant variations in magnetic latitude or equivalently in magnetic flux tube apex height. The morning upward ion drifts are predominantly dominated by the E-region dynamo. The presence of a downward pre-sunrise enhancement is another significant feature observed in our results. The morning and evening reversal times show variations in latitude (apex- height) and longitude and could be influenced by the occurrence of the PRE and downward sunrise enhancement and by the action of neutral winds in the E-region.

It is understood that the PRE is produced by the action of an eastward F-region neutral wind that blows across the evening terminator toward the nightside. The so-called F-region dynamo supports a vertical polarization electric field that is applied across the conducting F-region defined by the apex-height profile of the flux tube integrated Pedersen conductivity. In the simplest model no current flows through the E-region at night and the electric field drives a current that exactly balances the **U**x**B** driven current. The field is applied between the bottomside

and topside gradients in the flux-tube-integrated Pedersen conductivity. During the daytime the electric field from the F-region dynamo is weak and is given in terms of the flux tube integrated conductivity in the E and F region. The E-region contribution to the flux-tube-integrated Pedersen conductivity is dominant and assuming the neutral wind and the magnetic field are almost constant in altitude and latitude in the region we are considering near the low and middle latitudes then the F-region dynamo field is given by the expression:

$$\mathbf{E} \approx -\frac{\sum_F^P}{\sum_E^P + \sum_F^P}(\mathbf{U}\times\mathbf{B})$$

This electric field is mapped to the E region, where it drives a meridional current to close the current in the F region through field aligned currents that thread the bottomside and topside ionosphere. In addition the electric field drives a zonal current toward the dayside in the E-region.

During the nighttime the E-region conductivity becomes very small and the electric field from the F-region dynamo is given by $\mathbf{E} \sim (\mathbf{U}\text{x}\mathbf{B})$. Again the electric field in the E region drives a small meridional current to close the current in the F region, but in principle this current is negligible and so is the zonal current it drives in the E region. The discontinuity in the zonal current across the dusk terminator in the E region produces zonal polarization electric fields directed toward the terminator on both the dayside and nightside [*Farley et al*., 1986]. The effect of this field also can contribute to the formation of the PRE [*Farley et al*., 1986]. These electric fields produced in the E region map to the F region and produce an upward $\mathbf{E}\text{x}\mathbf{B}$ ion drift on the dayside of the terminator and a downward ion drift on the nightside of the terminator, adding to the effect produced by the fringing field described before.

The fringing field will in addition depend on the local time gradient in the conductance across the terminator. When the terminator is aligned with the magnetic field meridian then the gradient is largest and results in the largest fringing fields. Thus, the vertical **E**x**B** ion drift and the PRE are largest. When the terminator is not aligned with the magnetic meridian then the local time gradients in the conductance are smaller. Consequently, the **E**x**B** drift and the PRE are smaller under these conditions.

From the previous considerations we expect the PRE to be most pronounced when the eastward wind across the terminator is a maximum and when the magnetic meridian is most aligned with the solar terminator. Our results show that the magnitude of the PRE is larger when they are located in regions where the magnetic meridian is more aligned with the terminator, as has been documented in numerous other studies. As expected the PRE is maximum in the region of negative declination in northern winter and only appears in the region of positive declination in northern summer. However we note that even in the most favorable conditions in the northern summer the PRE is significantly weaker than in the less favorable conditions during equinox. The annual asymmetry [*Zeng et al*., 2008] is evident in the observations of the ion drifts and ion density. We observe the largest total ion density values during the equinox and northern winter and the smallest during the northern summer at 600 km altitude. We conclude that the reversal in the zonal wind from westward to eastward occurs later in local time, much closer to the terminator, during northern summer than in the other seasons.

The latitude extension of the PRE will be affected by the latitudinal or altitudinal variation of the F-region zonal wind since it produces the meridional current. Assuming for simplicity that the zonal wind does not change much with altitude and latitude at the low and middle latitudes the gradients in the meridional current will be produced mainly by the altitudinal

gradients of the flux tube integrated Pedersen conductivities. Then the fringing field primarily responsible for the PRE is limited in altitude extent by the apex-height variation in the Pedersen conductance. It will extend across the bottomside extending up to the altitude of the peak in the Pedersen conductance. The magnitude of the PRE over this altitude range is determined by the gradient in the meridional current density, or equivalently the Pedersen conductance assuming the neutral wind is constant. Using this model we expect that the PRE will be largest at the altitude where the bottomside gradient in the flux-tube-integrated Pedersen conductivity is a maximum. We would generally expect this altitude to be below the spacecraft and thus for the PRE to be a maximum at the magnetic equator and to decrease with increasing apex height. The PRE also has a contribution from the polarization field produced by the discontinuity in the zonal current, which is in turn produced by the F-region dynamo electric field and the E-region Hall conductivity [*Farley et al*., 1986]. This mechanism acts to reinforce the PRE and make it less dependent on apex height in the region between the bottomside and topside F-region conductivity gradients. This is generally the feature that we see. Of course the upward **E**x**B** drift induced by the PRE will itself modify the F-region conductivity and raise the location of the bottomside conductivity gradient. Thus we might expect the maxima in the PRE to lie at higher apex heights (higher latitude) when the PRE has its maximum magnitude. This tendency also appears in the observations. Our data show that the PRE is consistently confined to low latitudes in the summer months, similarly suggesting that the peak in the conductance profile is lower during this season than in northern winter. We have previously noted that the peak in the fringing field will be determined by the gradients in the Pedersen conductance. We might normally expect the gradient to maximize at apex heights below the spacecraft altitude of 600 km. However, in northern winter when the peak in the conductance may be near 1100 km, it is

possible that the maximum gradient in the conductance lies above the spacecraft altitude. In this case the PRE maximum will occur at latitudes away from the equator as is seen for example in the northern winter months in the African and Indian sectors. The average ROCSAT-1 data suggest that the peaks in the conductance profile lie near 1100 km (15º) in northern winter and near 650 km (5º) in northern summer.

*Kil et al*. [2006] showed the features of the flux tube integrated F-region Pedersen conductivity deduced from the TIMED/GUVI instrument using electron density profiles in the 290-350º longitude sector at 1900-2200 LT for the months of December and August. The December flux tube integrated Pedersen conductivity has a maximum value at higher altitude and with larger magnitude than in August. The values of the peak magnitude of $\sum_F^P$ and the corresponding apex height are about 24 mhos and 1100 km for the December days and 18 mhos and 600 km for the August days. During the daytime the gradients in the conductance are very small and the E-region wind dynamo is the dominant driver of currents and electric fields.

The simplest model for the daytime electric field in the F-region depends upon the diurnally varying E-region dynamo winds [*Tarpley*, 1970] that produce a polarization electric field across the terminators and between the equator and middle latitudes. These fields produce drifts that are upward during the day, downward at night, and to the west during the daytime. Most striking in these observations is the morning/afternoon asymmetry in the meridional drifts that must be due to the local time variation in the neutral winds. In the equatorial region the local time variation appears as a local maximum in the upward drift that always appears before local noon, with the drifts in the afternoon being significantly smaller than in the morning, and sometimes even downward. Typically, the plasma drifts in the meridional plane are upward during the day and downward during the night, but there are some very small downward drifts

during the afternoon sector from about 1400 LT to 1700 LT observed particularly during the December solstice (290º and 180º longitude sectors) and the equinox period (90º and 180º longitude sectors). At higher latitudes the local time variation during the solstices includes alternating regions of upward and downward drift that indicate the presence of a semi-diurnal wind-driven current. We observe some cases of downward drifts during the day at latitudes higher than 20º that might be related to semidiurnal tides that produce divergence in the currents generating westward electric fields that could produce downward ion drifts. At magnetic latitudes above about 20 degrees the influence of semidiurnal variations in the meridional ion drift becomes apparent. Such variations are clearly seen in the average drift patterns at Arecibo [*Fejer*, 1993]. The higher-latitude variations produced by a semi-diurnal oscillation may sometimes produce features that are aligned in local time with enhancements in the lower latitude drift patterns produced from another source. Thus it is important to consider these mechanisms separately. No direct measurements of the neutral winds in the E region or F region are available to confirm the implied behavior of the winds or their variations with season, longitude and latitude. However, it is implied that the largest wind variations occur at the equinox, when the magnitude of the upward daytime drifts is a maximum and the local time of the transition from downward to upward near dawn has the largest variability. During the equinox and the northern summer the latest morning reversal times occur near the African sector. In this longitude sector is also observed the latest evening reversal time during the northern summer. The largest morning upward drifts are observed during the equinox near the Indian sector. On particular longitude regions and seasons the upward morning drifts are preceded by significant downward sunrise enhancements as observed during the northern summer solstice near the African, Indian and Pacific sectors.

An enhancement in the downward drift prior to the reversal to upward drift near dawn is the third remaining feature of note in the data. This feature is most prevalent during the solstices where it appears over a limited local time region prior to sunrise. It appears as a counterpart to the pre-reversal enhancement that occurs at the sunset terminator and rather naturally we appeal to the F-region dynamo for an explanation. The available models [*Liu et al*., 2006] and in situ measurements [*Wharton et al*., 1984; *Hererro and Mayr*, 1986; *Coley et al*., 1994] describing F-region winds suggest that a transition from eastward to westward wind is made near 0400-0500 local time. Thus, during the eclipse period the F-region dynamo will be associated with a vertically upward polarization field that also drives the plasma to the west and produces an eastward fringing field that penetrates to the morning side where it is associated with the dayside upward drift. The F-region polarization field also maps to the E region where it again drives zonal currents due to the finite Hall conductivity [*Farley et al*., 1986]. In this case the resulting polarization field in the E region opposes the fringing field in the F region, thus reducing the effect relative to that seen at dusk. It does not provide a satisfactory explanation for the observed downward drift enhancement that appears in darkness before sunrise. A possible explanation for this phenomenon lies in noting that the transition from eastward to westward in the F-region zonal wind occurs near 0400 LT. The change in direction of the F-region zonal wind produces a westward enhancement in the electric field and an associated downward plasma drift on the nightside of the dawn terminator as is observed.

Figure 4.10 illustrates the configuration of wind, current and electric field in the bottomside F-region that results only from the F-region dynamo. In this picture we notice two features of the drift enhancement at dawn that are different from that at dusk. First the fringing field, producing an upward drift in the post sunrise region is reduced by the discontinuity in the

zonal current in the E-region whereas the same field in the pre-sunrise region is enhanced. Second, in the pre-sunrise region the downward drift enhancement is not produced by a fringing field but by the reversal in the F-region zonal wind prior to sunrise. It is therefore less dependent on the local time gradient in the flux-tube-integrated conductivity than the post-sunset drift enhancement. The observations do indeed show a much weaker seasonal and longitude dependence in the pre-sunrise enhancement than in the post-sunset enhancement, but in both cases seasonal and longitude variations in the F-region zonal wind will also play a significant role. This will produce a reversal in the meridional current and induce a downward **E**×**B** drift to maintain a curl free electric field. As before, the detailed distribution of the field will depend on the apex height variation in the Pedersen conductance that will itself be modified by the drift.

The density and meridional drift observations reveal the connection between them. It is important to emphasize that the observed distribution of ion density is related to the local time history of the ion drifts and not to the instantaneous drift observed at given local time. On a day to day basis we expect significant variability in the local time variation of the **E**×**B** drift [*Woodman*, 1970; *Fejer et al.*, 1989] and thus the average features that we illustrate in the data will contain only the most general of the reproducible attributes that we have described.

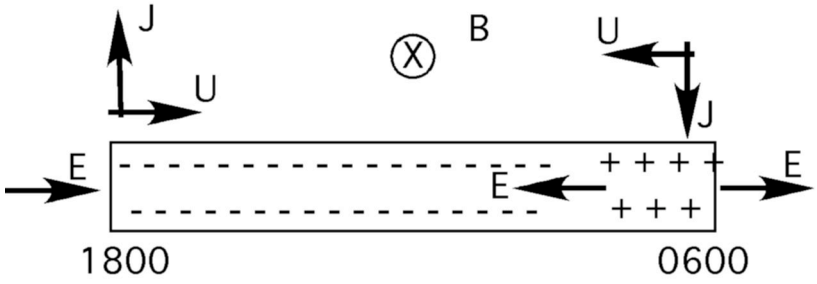


Figure 4.10 Schematic representation of the polarization charges, electric field and neutral wind configuration in the bottomside F-region ionosphere during nighttime.

In particular, we note that the magnitude of the daytime upward drift and the PRE directly determine the extent to which an equatorial anomaly signature is seen at 600 km and the local time extension of that feature beyond the PRE toward midnight. Similarly, the rate of decrease in the density at 600 km after local midnight is directly correlated with the magnitude of the downward drifts and the appearance of the pre-sunrise drift enhancement.

Finally, we point out the relationship of the ion drifts with the wave number-four structure of the ionosphere. Large values of morning meridional ion drifts during the equinox measured in the Indian, African, Pacific and Central American sectors correspond to the peak values in the wave number-four feature of the vertical ion drifts observed by *Fejer et al*. [2008], and *Kil et al*. [2007] at the magnetic equator near the 100º, 190º, 260º and 0º longitude regions, while a local minimum is located in the Brazilian sector which is the region where our morning upward drifts show the smallest values during the equinox. We observe a smaller peak density value in the African region due to the wave number-four density structure effect modulated by the same behavior of the vertical ion drifts. The suggested driver for this longitudinal wave number-four in the ion density and vertical **E**x**B** drift is the diurnal non-migrating eastward tide with zonal wave number-three (DE3) [*England et al*., 2006; *Immel et al*., *2006, Kil et al*., 2007]. Similar wave number-four patterns are detected during the solstices but are more evident during the northern summer. Observations during the equinox of the longitudinal density variations [*Kil et al*., 2007; *Oh et al*. 2008] from ROCSAT-1 show that the local maximum peak density values on the dayside from 1200 to 1400 LT are near the Indian, American and Pacific sectors. Another local density peak is observed near the African sector, but the plasma peak density values are less than at the other longitude regions. Even though a local peak is near the African sector this is smaller in comparison with the other local density peaks. We have to be wary that there are gaps

in the data we use near the African region, particularly at low latitudes, which are not significant in the results but may produce some discontinuity in the observations since the data have been interpolated.

## 4.5 Conclusions

We have examined the latitude and longitude variations in local time distribution of meridional **E**×**B** drifts for different seasons using plasma drift observations from the ROCSAT-1 satellite from November 1999 to December 2003. Three major features show significant latitude variations that are described here for the first time.

First, we observe daytime meridional drifts that are largely driven by the E-region dynamo and show significant latitude variation that we attribute to the relative importance of diurnal and semi-diurnal wind fields as a function of latitude. The second main feature observed is the latitude and longitude variation of the prereversal post-sunset enhancement. The PRE has been studied extensively and it is now generally understood in terms of a vertical polarization field that is applied across the nighttime F region by the zonal F-region neutral wind [*Farley et al*., 1986; *Eccles et al*., 1998]. The field is applied between the height above the corresponding apex height at which the flux-tube-integrated Pedersen conductivity is a maximum and the bottomside F-region. The PRE is produced by the horizontal fringing field associated with a vertical polarization of the nighttime F region produced by an eastward zonal neutral wind. This zonal fringing electric field will be most intense when both feet of the flux tube enter darkness at the same time. That is when the solar terminator and the magnetic meridian are aligned. When the magnetic meridian and the terminator are aligned the strength of the polarization field will depend upon the magnitude of the eastward zonal drift across the terminator. In this picture the

latitude or apex height extent of the PRE is determined by the location and magnitude of the peak in the flux-tube-integrated Pedersen conductivity. Above this apex height (latitude) the fringing field will reverse, thus being associated with a downward drift. The prereversal enhancement magnitude and location show strong variability in latitude and longitude particulary during the solstices. We note the strong seasonal dependence in the absolute excursion of the vertical drift. The upward morning drifts are much larger during the equinox period than during the northern winter or northern summer months. The largest upward vertical drifts occur in the local time region from 0800 to 1200, and then weaken significantly before the appearance of the PRE. The largest morning ion drifts are observed during equinox near the Indian sector, and the smallest during the northern summer near the Brazilian sector. At latitudes higher than 20º there is a reversal of the ion drift from upward (outward) to downward (inward) which is more prominent during the solstices. This feature appears generally in the local time sector after local noon, with more intensity near 1500 LT during the northern winter. During northern summer this reversal of the ion drift is more intense before local noon in the American sector but can extend to 1400 LT in the African, Indian and Pacific sectors. The presence of semidiurnal tides in the E region might be the origin of the features observed during the daytime. The other significant feature observed is the presence of a downward enhancement of the ion drift near sunrise. In this case the possible sources that produce the downward enhancements interact in a more complicated manner than during the postsunset enhancement since the action of fringing fields in the F region and currents produced in the E region and the Hall conductivity can have opposite effects that might cancel or produce the downward enhancement depending on the dominance of one of the possible sources. In most of the longitudes observed the downward enhancement

occurs before 0600 LT, but sometimes it can extend to later local times, particularly at higher latitudes.

Additionally, we observe larger daytime total ion concentration values during the equinox compared to the June and December solstices. These large density magnitudes are correlated with the presence of the largest morning upward drifts during the same period and their evolution in local time. The presence of EIA is evident when a larger PRE is observed. The effects of the annual asymmetry are also showen. Largest density values are observed during the northern winter than during the northern summer, but the largest levels of ion concentration are detected during the equinox, particularly when a larger meridional drift latitude extension is observed and the onset of the upward drift occurs earlier near the dawn terminator.

Our results are consistent with previous studies of the ionosphere at low latitudes [*Fejer et al*., 2008; *Oyekola*, 2006; 2009] and with measurements from Jicamarca at the magnetic equator.

# CHAPTER 5

# QUIET TIME ZONAL ION DRIFTS

## 5.1 Introduction

In this chapter we describe the behavior of the zonal ion drifts extracted from the ROCSAT-1 data using the same methodology outlined in chapter 2. The data are organized in the same way as those shown in chapter 4 and the connections between the two mutually perpendicular components of the **E**x**B** drifts are discussed.

## 5.2 Observations

Figure 5.1 shows the average east-west ion drifts distributed in magnetic latitude and magnetic local time for the period 1999-2003, corresponding to solar maximum. The color scale indicates the zonal drift magnitude and direction. The red and blue colors represent the eastward and westward direction, respectively, and the eastward direction is assumed to be positive. The left, middle and right columns show the drifts corresponding to the northern winter, the equinox and the northern summer respectively. Each panel of each column illustrates the zonal drift corresponding to different geographic longitude sectors that are indicated to the right of the panels. The longitude regions are representative of the Central American-Pacific, South American-Peruvian, South American-Brazilian, African, Indian and Pacific sectors corresponding to the 270º, 290º, 310º, 0º, 90º and 180º longitude regions respectively. These sectors were selected to study representative longitude sectors characterized by different offsets between the geographic and the magnetic equator, and by different magnetic declinations. They

can be compared directly with the characteristics of the meridional drifts in the same longitude sectors described in chapter 4. As before, values at the corresponding conjugate hemisphere are mirrored since the **E**x**B** ion drifts are the same at conjugate latitudes.

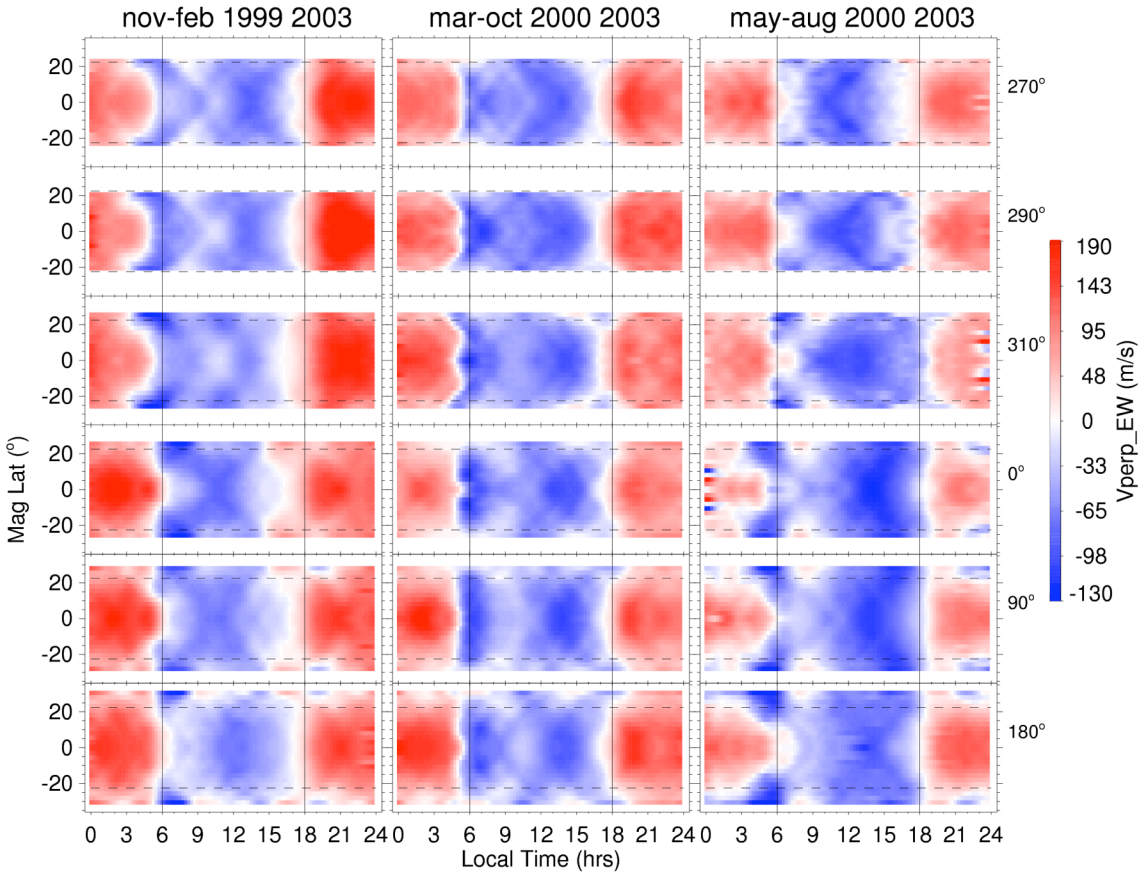


Figure 5.1. Latitudinal and local time dependence of quiet time ion drifts perpendicular to **B** in the east-west direction for the 270º, 290º, 310º, 0º, 90º and 180º longitude sectors during the years 1999-2003 (solar maximum). The average ion drift values are obtained for the northern winter solstice (left panel), the equinox (middle panel) and the northern summer solstice (right panel).

The vertical lines indicate the approximate location of the dawn and dusk terminators that will be helpful to compare the reversal times of the zonal drifts under different conditions. The horizontal dashed lines drawn at 20º magnetic latitude assist in comparing latitude variations in

different longitude sectors. As expected, the zonal drifts are generally westward by day and eastward at night. However, local time variations in the east-west drifts show significant seasonal, longitude and latitude variability.

The peak values of the daytime westward drifts and the nighttime eastward drifts are usually located at the lowest latitudes, with the magnitude decreasing with increasing latitude. However, at a given local time except near the terminators, the zonal drifts retain their same direction over the latitude range sampled by our data. At latitudes near 20º and above, a semidiurnal component in the zonal drift is apparent during the daytime. This is quite evident at most longitudes where daytime westward drifts turn eastward. It is also seen in the meridional drifts described in chapter 4.

Closer to the equator the daytime peak in the zonal drift is dependent on longitude and season. During northern winter it appears before local noon in the African and Indian sectors while in the American sectors it appears much later, near 1400 LT. In the American sectors there is a presence of a secondary westward peak located near 0830 LT. In the northern summer months the opposite behavior is seen with the peak westward flows appearing near 1400 LT in the African and Indian sectors and near 1000 LT in the American sectors. During equinox the peak appears near 1300 LT in all longitude sectors. Two local time peaks in the westward zonal drift near the equator sometimes appear when an enhancement in the westward drift appears near sunrise during equinoxial periods.

The peak values of the eastward drift in the northern summer are generally smaller than the drifts in the other seasons. The largest eastward drifts are located in the American region (270º, 290º, 310º) during the northern winter. During this season, the eastward peak appears before midnight in the American sector but after midnight in the African, Indian and Pacific

sectors. During the equinox, the magnitude of the east-west drifts also has latitude (apex-height) and longitude dependencies, but these are less significant than during the solstices. The largest eastward drifts are observed near the lowest latitudes in the 90º and 180º longitude sectors with magnitudes of about 190 m/s near 2100 LT. During the northern summer, the largest eastward drifts are observed near the lowest latitudes in the Pacific, Central America and Peruvian sectors. The peak magnitudes are about 130 m/s, and are also located near 2100 LT. The latitudinal extension of the early morning eastward drifts is the smallest near the 0º, 90º and 180º longitude regions. These drifts extend up to latitudes of about ±20º and then reverse direction to the west.

The largest latitudinal variability in the zonal drifts exists near the terminators due to a change in the local time at which the reversal from eastward to westward drift occurs. The morning reversal time tends to occur earlier at higher latitudes. During northern winter the sunrise transition from eastward to westward drift occurs at successively earlier local times with increasing latitude. At the sunset terminator the local time of the reversal from westward to eastward drift does not change significantly with latitude. In addition to the latitude variation in the local time of the drift reversal, the reversal local time is itself a function of longitude. In the African, Indian and Pacific sectors it occurs near 0600 LT in northern winter but before 0500 LT in the American sectors. The latest morning reversal time is observed near the Pacific region slightly after 0600 LT. By contrast, during northern summer the dawnside reversal occurs near 0600 LT in the American sectors, but earlier in the African, Indian and Pacific sectors. During this season, the morning reversal time shows more pronounced latitude (apex-height) variability than the evening reversal time. In the African region, the morning reversal time is the earliest for all longitude sectors and is observed in the local time interval from 0300 to 0500 LT. During equinox the morning reversal time is near 0500 LT for all longitudes. This reversal time is less

variable with increasing latitude than during the solstices but this latitude dependence is more evident in the American sector particularly near the 290º and the 310º longitude sectors. We note again that the earlier local time of the dawnside reversal is associated with an enhancement in the westward zonal drift near 0600 LT.

While the evening reversal time is a weak function of latitude below about 20º, it does change as a function of season and longitude. In northern winter it occurs earliest in the African sector between 1600 and 1700 and later, near 1800 in the Pacific and American sectors. By contrast, in the northern summer months the reversal time lies just before 1700 in the Peruvian sector and after 1800 in the Brazilian, African and Indian sectors. At equinox the reversal time lies before 1800 in the American sectors but is much closer to 1800 in the African through Pacific sectors.

An inspection of the local time variation of the zonal drifts in different latitude and longitude sectors shows immediately a difference in the peak values of the eastward and westward drifts and in the duration over which the drifts are eastward and westward. These factors lead to a net superrotation or subrotation of the ionosphere that we investigate further and illustrate in Figure 5.2.

We average the zonal ion drifts for all local times and longitude sectors every 2.5º in magnetic latitude. The top, middle and bottom panel illustrate the observations for northern winter, equinox and northern summer and for the same longitude sectors shown in Figure 5.1. Positive magnitudes indicate eastward net superrotation and negative magnitudes show evidence of subrotation. As observed in Figure 5.2, the superrotation effect is latitude (apex-height) dependent. It decreases with increasing latitude (apex-height) with a maximum near the magnetic equator. During the northern winter, superrotation is seen in all longitude sectors observed.

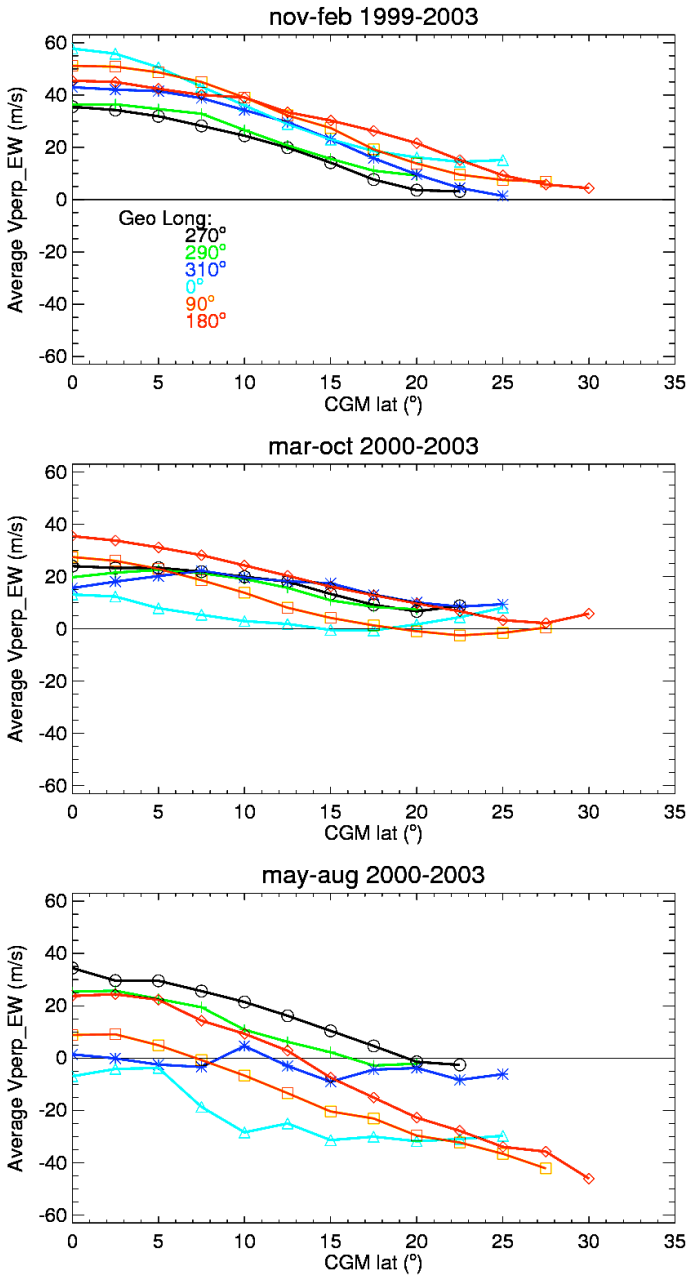


Figure 5.2. Net superrotation effect obtained from averaging the east-west drift values in local time. Results for the northern winter solstice (top), equinox (middle), and the northern summer solstice (bottom) are shown. The longitudes correspond to the longitude regions shown in Figure 5.1.

Near the equator the net superrotation has an average value of about 45 m/s and decreases to a velocity lower than 20 m/s at magnetic latitudes higher than 20º. During the equinox, the superrotation is also evident in all longitude sectors but with values almost half of those seen in northern winter**.** The superrotation generally decreases with increasing latitude. However, near the 290º and 310º longitude sectors we observe small local maxima near 5º and 7.5º latitudes. Interestingly, the minimum superrotation at equinox occurs in the African longitude sector where the maximum superrotation is seen in northern winter. During northern summer the superrotation at the equator is more variable with longitude and decreases with increasing latitude so that beyond 20º magnetic latitude the ionosphere subrotates at all longitudes. In the African longitude region the ionosphere subrotates at all latitudes, even at the magnetic equator. The longitude variation is largely produced by the dramatic seasonal variations in the African, Indian and Pacific longitude sectors.

Figure 5.3 shows the local-time average eastward and the local-time average westward drifts that contribute to the superrotation of the ionosphere. A separation in this manner allows a very rough division into the contributions made by the E-region dynamo, which largely produces the westward drifts during the daytime, and the contributions made by the F-region dynamo, which largely produces the eastward drifts during the nighttime.

During the equinox period the net westward drift, driven by the E-region dynamo, shows no variation with longitude but a significant decrease with increasing latitude. This behavior is consistent with hemispherically symmetric wind systems coupled with a conductance that decreases with increasing latitude.

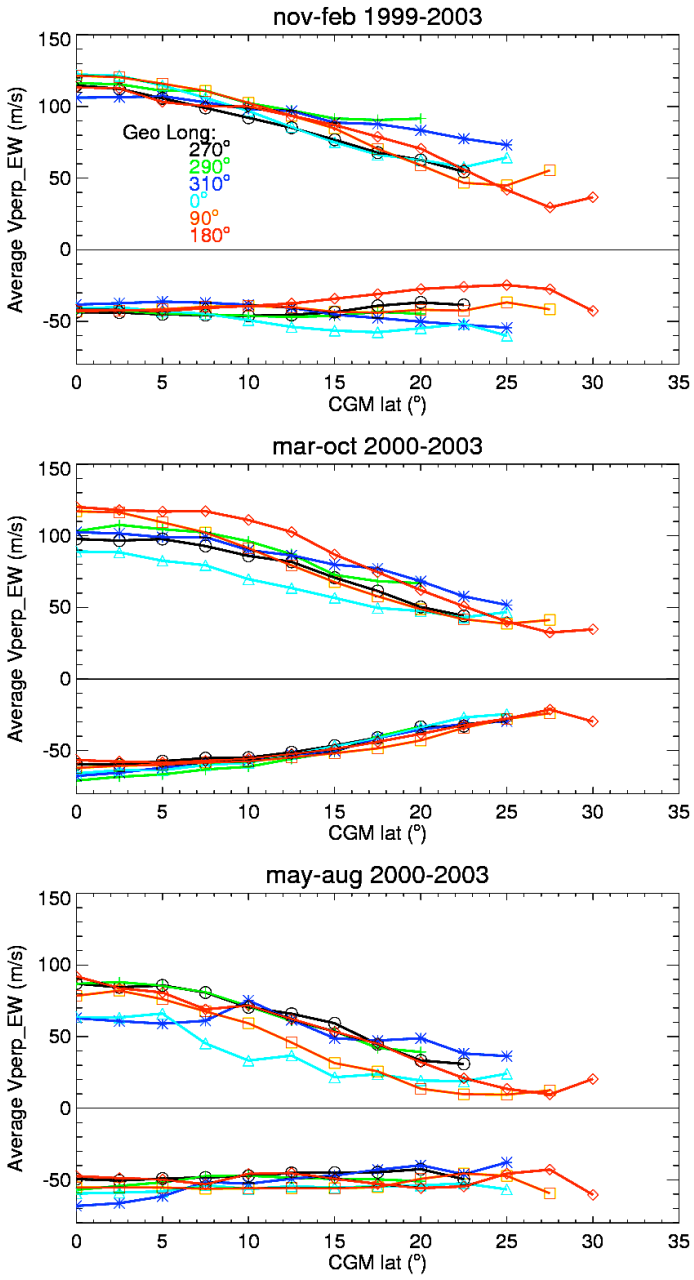


Figure 5.3. Latitudinal variation of the net eastward and westward ion drifts averaged in local time for different longitude sectors.

During the solstices however, there exist significant variations with longitude, but much less variation with latitude. This behavior appears consistent with the expected hemispheric

asymmetries in the wind system and the conductance during these periods. In the latitude region below 15 degrees the net westward drifts are smallest during the northern winter period when the net superrotation of the ionosphere is largest.

The local-time average eastward drift is driven principally by the F-region dynamo at night, and decreases with increasing latitude during all seasons. In the northern winter the longitude variations are minimal but become increasingly variable and smaller in magnitude during equinox and into the northern summer solstice. Coupled with a similar longitude variability and an increase in the local-time average westward drift from the E-region dynamo, the net superrotation decreases significantly during the equinoxes and even further in the northern summer. We note that the largest changes in the net superrotation of the ionosphere occur in the transition from northern winter to northern summer in the longitude regions where the magnetic equator is both north and south of the magnetic equator. In these regions both a decrease in the F-region-driven eastward drift and an increase in the E-region-driven westward drift combine to reduce the net superrotation and in fact produce a net subrotation of the ionosphere.

## 5.3 Discussion

Zonal drifts in the F-region are produced by meridional electric fields that are generated in the E region and the F region. These fields are the result of meridional currents driven by zonal winds in the F region and by zonal and meridional winds in the E region. During the daytime it is customary to neglect the effects of F-region currents since they can be driven in closed loops through the conducting E region with a very small electric field. E-region winds effectively create a poleward electric field that creates westward drifts during the daytime. At night the E-region conductance is quite small but the E-region wind system drives currents that

create an equatorward electric field and a corresponding eastward **E**x**B** drift in the F region. In addition, at night the eastward F-region wind drives upward and outward currents that must be largely countered by a downward/inward electric field since they cannot easily be closed in the E region. This results in an additional component to the eastward **E**x**B** drift seen in the F region.

The combined effects of the E-and F-region dynamos are responsible for both the vertical drift perturbations seen near sunrise and sunset in the previous chapter, and the net superrotation of the ionosphere described here. It is difficult to assess separately the impact of these two sources, but by considering the net westward daytime drifts and the net eastward nighttime drifts some important distinguishing features of these two drivers are revealed. We find that the observed F-region zonal ion drifts, in excess of 150 m/s, are larger than the F-region zonal neutral winds reported by *Wharton et al*. [1984]. If the E region were a perfect insulator and the F-region winds showed no dependence on latitude and altitude, we would expect the F-region zonal ion drifts to exactly reflect the zonal neutral wind. Clearly an additional contribution to the eastward ion drift is required during the nighttime, and simple models [*Crain et al*., 1993b] show that the separate contributions for the E region and the F region at night increase the net eastward drift above that produced from a single source.

The observations here show a dramatic change in the net superrotation as a function of season and latitude, driven primarily by changes in the net eastward drift across the nightside. The local time average eastward drift at the equator near 600 km altitude is above 100 m/s during the northern winter, decreases to near 100 m/s at equinox and to much lower values near 70 m/s during northern summer. The drifts decrease almost linearly with latitude at the rate of about 2.5 m/s/degree. Principally the F-region dynamo drives this change over a range of latitudes where the conductance is expected to be a weak function of latitude. We therefore suspect that the

decrease in eastward drift as a function of latitude results from a decrease in the zonal F-region wind with latitude.

Observed longitude variations in the net eastward drift can be produced by changes in both the F-region zonal wind and the F-region conductance. However, near the equator the largest and most similar longitude variations are seen in the African and Indian sectors, where the magnetic equator is north of the geographic equator, and in the Brazilian sector where the magnetic declination is negative. We therefore suggest that the longitude variations are most likely produced by changes in the F-region nighttime conductance. Changes in the conductance can be produced by different **E**x**B** drift patterns and by neutral winds in the magnetic meridian that moderate the loss rate of the plasma in the F region.

In the American sector where the magnetic declination is negative but the magnetic equator is close to the geographic equator both a zonal and meridional neutral wind can act to induce plasma motions along the magnetic field. During northern summer these winds act in concert to induce field aligned plasma motions. In one hemisphere the winds act to decrease the plasma loss rate and preserve the F-region conductivity. In the other hemisphere they act to increase the plasma loss rate and decrease the F-region conductivity. On aggregate we expect the interhemispheric winds to have little effect on the F-region conductance. During northern winter the meridional and zonal winds act in opposition to minimize the field-aligned plasma motions. Thus we do not expect the neutral winds to account for the large seasonal changes observed in this longitude region. However, we note that in the American sectors a pre-reversal enhancement in the upward drift is commonly seen during the northern winter months and is significantly diminished in the northern summer months [*Scherliess and Fejer*, 1999]. An upward drift just prior to sunset will act to preserve the F-region plasma, and therefore the conductance, for a

longer period during the night. We might thus expect the F-region zonal wind to be more effective in producing a polarization field during the northern winter period.

In the African and Indian sectors the appearance of a pre-reversal enhancement is much less dependent on season and therefore may not be a large contributor to a seasonal change in the F-region conductance. However, the displacement of the geomagnetic and geographic equators produces meridional winds that drive the plasma down in both hemispheres during northern summer, while during northern winter the induced plasma motions are upward in the summer and downward in the winter. We thus expect the F-region conductance to be larger in the winter than in the summer with a corresponding maximum in the net eastward drift in the winter as is observed. We note again that recent determination of the flux tube integrated Pedersen conductivity as a function of apex height does indeed produce northern winter peak values near 24 mhos at 1100 km and 18 mhos at 700 km.

## 5.4 Conclusions

We have examined the zonal ion drifts using satellite measurements from ROCSAT-1. The ion drifts are mainly eastward during the day and eastward during the night between ± 20º magnetic latitude. There is evidence of latitudinal (apex-height), longitudinal, local time and seasonal variability of the east-west plasma drifts. The eastward **E**x**B** drift peaks are larger than the maximum westward drifts mainly during the December solstice and the equinox period but the eastward drifts can be smaller than the westward drifts during the June solstice. The eastward drift magnitude generally decreases with increasing latitude. The superrotation effect observed has latitude (apex-height), longitude and seasonal dependences. The net superrotation effect is mainly present during the December solstice and equinox. The most prominent superrotation is

seen in the December solstice with maximum values at the equator of about 45 m/s. The magnitude of the superrotation decreases with increasing latitude. Subrotation also occurs mainly during the June solstice. This is produced by the presence of westward drifts larger than the eastward drifts at latitudes greater than 10º, or by westward drifts that extend in local time periods longer than the periods of eastward drifts. This subrotation effect is observed mainly during the northern summer above 10º CGM latitude in the 0º, 90º and 180º longitude sectors.

We find that the seasonal changes in the net superrotation of the ionosphere are induced largely by changes in the F-region Pedersen conductance that are produced by ExB drifts and neutral wind induced field-aligned plasma motions. These effects contribute differently in different longitude regions to produce large seasonal and longitude variations. The decrease in the superrotation with increasing latitude appears to be due largely to the latitude variations in the neutral wind.

# CHAPTER 6

# CONCLUSIONS AND FUTURE WORK

## 6.1. Conclusions

Electric fields and plasma drifts are important parameters for the understanding of the ionosphere. In this region the ion motions affect the ion density distribution. One evident example is how the vertical drifts near the equator affect the way the plasma is distributed in latitude and altitude. Consequently the knowledge of the ion density helps us to understand the dynamics of the ionosphere. On a global scale, the latitudinal and longitudinal dependence of the drifts require a more detailed study. Using satellites we can obtain better coverage in latitude and longitude of the ion drift motions than with ground-based radars. Since the ROCSAT-1 and DMSP satellites provide ion drift measurements at low and middle latitudes, we utilize their measurements in order to study the latitudinal apex-height variation of the ion drifts for different longitude sectors. Besides the variability due to changes in the location, the low and mid-latitude plasma drifts respond differently to geomagnetic activity. Therefore we perform an analysis of the ion drifts during storm times and quiet times in order to obtain a more accurate description of the ionosphere/thermosphere region. Ionospheric drifts are main inputs for modelling the low and mid-latitude ionosphere/thermosphere system. Therefore with this work we can improve knowledge of parameters required by models in order to get more reliable space weather predictions. After removing biases and offsets from the original ROCSAT-1 measurements we obtained an improved data set of ion drifts that is available for the scientific community. From the signatures of the ion drifts we can infer the drivers and features of the parameters involved in

the generation of the electric fields, such as winds, conductivites and magnetic fields, and describe how and why these parameters change in latitude (apex-height) and longitude.

In addition to describing the quiet time distribution of meridional and zonal drifts at the equator and middle latitudes, we also examined ion drift pertutbations at the magnetic equator near 0600, 0900, 1800, 2100 LT and near noon and midnight local times. Changes in the interplanetary magnetic field (IMF) strongly affect these drift perturbations. Upward perturbations in the vertical drifts are detected during southward turnings of the IMF and during daytime hours that extend to 1800 and 2100 LT. Downward drift perturbations are observed during nighttime when the IMF turns southward. An opposite effect is observed when the IMF turns northward, but the drift perturbations are smaller than those seen during the southward IMF turnings. The storm time perturbations in the drift are consistent with the combined effect of the penetration electric field, disturbance dynamo and overshielding.

During quiet times, the main features of the meridional drifts are revealed by describing the latitude (apex-height), longitude, seasonal, and local time variations. A prereversal enhancement in the vertical ion drift responds to the action of the F-region dynamo and the gradients in the flux tube integrated Pedersen conductivities, which determines both the latitude distribution of the PRE feature and the latitude at which the peak magnitude occurs. Longitudinal variations in the PRE are determined mainly by the change in longitude of the magnetic field declination. The daytime meridional drifts are affected mainly by the E-region dynamo winds and we can infer the presence of diurnal and semidiurnal components in the wind. A downward enhancement is also observed in the meridional drifts near sunrise, which is associated with the electric field produced across the local time region where the zonal wind changes from westward to eastward. The zonal ion drifts are mainly driven by diurnal wind components in the E region

and the F region. The net westward daytime drift driven by the E-region wind is usually less than the net eastward nighttime drift driven by the F-region wind. This leads to a net superrotation of the ionosphere which is more prominent at low latitudes. We find longitude, latitude and seasonal variations in the net superrotation of the ionosphere that can be attributed to the roles of **E**x**B** drifts and neutral winds that change the F-region Pedersen conductance.

## 6.2. Future Work

Applying the same technique we used to obtain the **E**x**B** drifts we can study the plasma velocities in the direction parallel to the magnetic field using the ROCSAT-1 data near 600 km altitude. This will complement the description of the ion motion in the upper ionosphere and will allow us to infer the behavior of F-region winds in the northern and southern hemispheres. The studies during quiet times can also be conducted for different levels of solar flux allowing the impact of this variable to be assessed.

We plan to compare the climatology of the ion drifts obtained here for solar maximum conditions with theoretical models such as TIEGCM and correlate our results during quiet and perturbed times. Additional studies of the wind systems can be conducted using empirical models such as HWM07 or numerical models such as Global Scale Wind Model (GSWM) to analyze and compare the features of the winds with the plasma motions extracted from our data. A complementary study of the variations of the conductivity may help to understand with more detail the processes involved in the E-region and F-region dynamo that produces the latitude, longitude, seasonal and local time variation of the ion drifts.

## BIBLIOGRAPHY


Basu, S., Su. Basu, K. M. Groves, E. MacKenzie, M. J. Keskinen, and F. J. Rich (2005), Near-simultaneous plasma structuring in the midlatitude and equatorial ionosphere during magnetic superstorms, *Geophys. Res. Lett.*, 32, L12S05, doi:10.1029/2004GL021678.

Blanc, M., Richmond, A.D. (1980), The ionospheric disturbance dynamo, *J. Geophys. Res.*, 85, 1669.

Chang, Y.-S., Chiang, W.-L., Ying, S.-J., Holt, B.J., Lippincott, C.R., Hsieh, K.-C. (1999), System Architecture of the IPEI Payload on ROCSAT-1. *TAO*, Supplementary Issue, 7-18, March 1999.

Coley, W. R., R. A. Heelis, and N. W. Spencer (1994), Comparison of Low-Latitude Ion and Neutral Zonal Drifts Using DE 2 Data, *J. Geophys. Res.*, 99(A1), 341–348.

Crain, D. J.; Heelis, R. A., Bailey, G. J., Richmond, A. D. (1993a), Low-latitude plasma drifts from a simulation of the global atmospheric dynamo, *J. Geophys. Res.*, 98, A4, 6039-6046.

Crain, D. J., Heelis, R. A., Bailey, G. J. (1993b), Effects of electrical coupling on equatorial ionospheric plasma motions - When is the F region a dominant driver in the low-latitude dynamo?, *J. Geophys. Res.*, 98, A4, 6033-6037.

Eccles, J. V. (1998), Modeling investigation of the evening prereversal enhancement of the zonal electric field in the equatorial ionosphere, *J. Geophys. Res.*, 103, 26709.

England, S. L., Immel, T. J., Sagawa, E., Henderson, S. B., Hagan, M. E., Mende, S. B., Frey, H. U., Swenson, C. M., Paxton, L. J. (2006), Effect of atmospheric tides on the morphology of the quiet time, postsunset equatorial ionospheric anomaly, *J. Geophys. Res.*, 111, A10, CiteID A10S19.

Farley, D. T., E. Bonelli, B. G. Fejer, and M. F. Larsen (1986), The Prereversal Enhancement of the Zonal Electric Field in the Equatorial Ionosphere, *J. Geophys. Res.*, 91(A12), 13,723–13,728.

Fejer, B. G., Kudeki, E., Farley, D. T. (1985), Equatorial F region zonal plasma drifts, *J. Geophys. Res.*, 90, 12, 249-12,255.

Fejer, B. G., E. R. de Paula, I. S. Batista, E. Bonelli, and R. F. Woodman (1989), Equatorial F Region Vertical Plasma Drifts During Solar Maxima, *J. Geophys. Res.*, 94(A9), 12,049–12,054.

Fejer B.G., (1991), Low latitude electrodynamic plasma drifts: a review, *J. Atmos. Terr. Phys*., 53, 677.

Fejer, B. G., E. R. de Paula, S. A. Gonzalez, and R. F. Woodman (1991b), Average vertical and zonal F region plasma drifts over Jicamarca, *J. Geophys. Res*., 96(A8), 13,901–13,905.

Fejer, B.G. (1993), F region plasma drifts over Arecibo - Solar cycle, seasonal, and magnetic activity effects, *J. Geophys. Res.*, 98, A8, 13,645-13,652.

Fejer, B. G., de Paula, E. R., Heelis, R. A., Hanson, W. B. (1995), Global equatorial ionospheric vertical plasma drifts measured by the AE-E satellite, *J. Geophys Res.*, 100, A4, 5769-5776.

Fejer B.G. (1997), The electrodynamics of the low-latitude ionosphere: recent results and future challenges, *J. Atmos. Solar-Terr. Phys*., 59, 1465.

Fejer B.G., Scherliess L. (1995), Time dependent response of equatorial ionospheric electric fields to magnetospheric disturbances, *Geophys. Res. Lett.*, 22, 851.

Fejer, B. G., Scherliess, L. (1997), Empirical models of storm time equatorial zonal electric fields. *J. Geophys. Res.*, 102, 24047.

Fejer, B. G., Scherliess, L., de Paula, E. R. (1999), Effects of the vertical plasma drift velocity on the generation and evolution of equatorial spread F, *J. Geophys. Res.*, 104, A9, 19859-19870.

Fejer, B. G., Jensen, J.W., Su, S. -Y. (2008), Quiet time equatorial F region vertical plasma drift model derived from ROCSAT-1 observations, *J. Geophys. Res.*, 113, A05304, doi:10.1029/2007JA012801.

Fesen, C. G., Crowley, G., Roble, R. G., Richmond, A. D., Fejer, B. G. (2000), Simulation of the pre-reversal enhancement in the low latitude vertical ion drifts, *Geophys. Res. Lett.* 27, 1851.

Fuller-Rowell, T. J., Codrescu, M. V., Risbeth, H., Moffett, R. J., Quegan, S. (1996), On the seasonal response of the thermosphere and ionosphere to geomagnetic storms, *J. Geophys. Res.*, 101, A2, 2343-2354.

Fuller-Rowell, T. J., Millward, G. H., Richmond, A. D., Codrescu, M. V. (2002), Storm-time changes in the upper atmosphere at low latitudes, *J. Atmos. Solar-Terr. Phys*., 64, 12-14, 1383-1391.

Hargreaves, J.K. (1995), The solar-terrestrial environment, Cambridge University Press, New York.

Hartman, W. A., and Heelis R. A. (2007), Longitudinal variations in the equatorial vertical drift in the topside ionosphere, *J. Geophys. Res.*, 112, A03305, doi:10.1029/2006JA011773.

Heelis, R. A. and Hanson W. B. (1998), Measurements of Thermal Ion Drift Velocity and Temperature using Planar Sensors, Measurement Techniques in Space Plasmas, Geophysical Monograph Series, 102, AGU, 61, 1998.

Heelis, R. A. (2004), Electrodynamics in the low and middle latitude ionosphere: a tutorial, *J. Atmos. Solar-Terr. Phys*., Volume 66, Issue 10, p. 825-838.

Herrero, F. A., and H. G. Mayr (1986), Tidal decomposition of zonal neutral and ion flows in the Earth's upper equatorial thermosphere, *Geophys. Res. Lett.*, 13(4), 359–362.

Holt, B. J. (1995), SSIES-3 Plasma Monitor Systems and Related GSE R & D Equipment Information Report, Volume I of II, The University of Texas at Dallas W.B. Hanson Center for Space Sciences. UTD-DIR-A04-01-25951.

Huba, J. D., G. Joyce, and J. A. Fedder (2000), Sami2 is Another Model of the Ionosphere (SAMI2): A new low-latitude ionosphere model, *J. Geophys. Res.*, 105(A10), 23,035–23,053.

Huba, J. D., Joyce, G., Sazykin, S., Wolf, R., Spiro, R. (2005), Simulation study of penetration electric field effects on the low- to mid-latitude ionosphere, *Geophys. Res. Lett*., 32, 23, CiteID L23101.

Immel, T. J., Sagawa, E., England, S. L., Henderson, S. B., Hagan, M. E., Mende, S. B., Frey, H. U., Swenson, C. M., Paxton, L. J. (2006), Control of equatorial ionospheric morphology by atmospheric tides, *Geophys. Res. Lett.*, 33, 15, CiteID L15108.

Isham, B.; Tepley, C. A., Sulzer, M. P., Zhou, Q. H., Kelley, M. C., Friedman, J. S., González, S. A. (2000), Upper atmospheric observations at the Arecibo Observatory: Examples obtained using new capabilities, *J. Geophys. Res.*, 105, A8, 18609-18638.

Kelley, M. C. (1989), *The Earth's Ionosphere: Plasma Physics and Electrodynamics*, Academic Press, Inc., San Diego, CA.

Kil, H., DeMajistre, M., Paxton, L. J., and Zhang, Y. (2006), *F*-region Pedersen conductivity deduced using the TIMED/GUVI limb retrievals, *Ann. Geophys*., 24, 1311-1316.

Kil, H., Oh, S.-J., Kelley, M. C., Paxton, L. J., England, S. L., Talaat, E., Min, K.-W., Su, S.-Y. (2007), Longitudinal structure of the vertical E × B drift and ion density seen from ROCSAT-1, *Geophys. Res. Lett.*, 34, 14, CiteID L14110.

Liu, H., H. Lühr, S. Watanabe, W. Köhler, V. Henize, and P. Visser (2006), Zonal winds in the equatorial upper thermosphere: Decomposing the solar flux, geomagnetic activity, and seasonal dependencies, *J. Geophys. Res.*, 111, A07307, doi:10.1029/2005JA011415.

Maruyama, N., Richmond, A. D., Fuller-Rowell, T. J., Codrescu, M. V., Sazykin, S., Toffoletto, F. R., Spiro, R. W., Millward, G. H. (2005), Interaction between direct penetration and disturbance dynamo electric fields in the storm-time equatorial ionosphere, *Geophys. Res. Lett*., 32, 17, CiteID L17105.

Oh, S.-J., Kil, H., Kim, W.-T., Paxton, L. J., and Kim, Y. H. (2008), The role of the vertical ***E***×***B*** drift for the formation of the longitudinal plasma density structure in the low-latitude F region, *Ann. Geophys*., 26, 2061-2067.

Oyekola, O.S. (2006), Comparison between nighttime ionosonde, incoherent scatter radar, AE-E satellite, and HF Doppler observations of *F*-region vertical electrodynamic plasma drifts in the vicinity of the magnetic equator, *J. Geophys. Res.* **111**, A11318, doi:10.1029/2006JA011844.

Oyekola, O. S. (2009), Equatorial F-region vertical ion drifts during quiet solar maximum, *Adv. Space Res*., 43, 12, 1950-1956.

Pingree, J. E., and B. G. Fejer (1987), On the Height Variation of the Equatorial *F* Region Vertical Plasma Drifts, *J. Geophys. Res.*, 92(A5), 4763–4766.

Prabhakaran Nayar, S. R., Mathew, T. J., Sreehari, C. V., Sumod, S. G., Devasia, C. V., Ravindran, S., Sreeja, V., Kumar Pant, T., and Sridharan, R. (2009), Electrodynamics of the equatorial F-region ionosphere during pre-sunrise period, *Ann. Geophys*., 27, 107-111.

Ren, Z., W. Wan, L. Liu, R. A. Heelis, B. Zhao, Y. Wei, and X. Yue (2009), Influences of geomagnetic fields on longitudinal variations of vertical plasma drifts in the presunset equatorial topside ionosphere, *J. Geophys. Res.*, 114, A03305, doi:10.1029/2008JA013675.

Richmond, A. D., Roble, R. G. (1987), Electrodynamic effects of thermospheric winds from the NCAR thermospheric general circulation, *J. Geophys. Res.*, 92, 12365-12376.

Richmond, A. D., Ridley, E. C., Roble, R. G. (1992), A thermosphere/ionosphere general circulation model with coupled electrodynamics, *Geophys. Res. Lett.*, 19, 601-604.

Richmond, A. D. (1995), Ionospheric electrodynamics using magnetic apex coordinates. *J. Geomag. Geoelectr*., 47, 191-212.

Rishbeth, H. (1971a), Rotation of the Variation of Upper Atmosphere, *Nature* **229**, 333 - 334 (1971) , doi:10.1038/229333a0.

Rishbeth, H. (1971b), Polarization fields produced by winds in the equatorial F-region, *Planet. Space Sci.*, *19*, 357-369.

Rishbeth, H. (1997), The ionospheric E-layer and F-layer dynamos - a tutorial review, *J. Atmos. Terr. Phys*., 59, 1873.

Scherliess, L., Fejer, B. G. (1997), Storm time dependence of equatorial disturbance dynamo zonal electric fields, *J. Geophys. Res.,* 102, 24037.

Scherliess, L., Fejer, B. G. (1998), Satellite studies of mid- and low-latitude ionospheric disturbance zonal plasma drifts, *Geophys. Res. Lett.,* 25, 1503.

Scherliess, L., Fejer, B. G. (1999), Radar and satellite global equatorial F region vertical drift model, *J. Geophys. Res.*, 104, A4, 6829-6842.

Spiro, R.W., Wolf, R.A., Fejer, B.G. (1988), Penetration of high-latitude-electric-field effects to low latitudes during SUNDIAL 1984, *Ann. Geophys*., 6, 39-50.

Su, S.-Y., Yeh, H.C., Heelis, R.A., Wu J.-M., Yang, S.C., Lee, L.-F., Chen, H.L. (1999), The ROCSAT-1 Preliminary Results: Low-Latitude Ionospheric Plasma and Flow Variations, *TAO*, 10, 4, 787-804.

Su, S. ‐ Y., C. K. Chao, and C. H. Liu (2009), Cause of different local time distribution in the postsunset equatorial ionospheric irregularity occurrences between June and December solstices, *J. Geophys. Res.*, 114, A04321, doi:10.1029/2008JA013858.

Tarpley J.D. (1970), The ionospheric wind dynamo-II. Solar tides, *Planet. Space Sci.*, 18 (7), 1091-1103.

Wharton, L. E., N. W. Spencer, and H. G. Mayr (1984), The Earth's thermospheric superrotation from Dynamics Explorer 2, *Geophys. Res. Lett.*, 11(5), 531–533.

Woodman, R. F. (1970), Vertical Drift Velocities and East-West Electric Fields at the Magnetic Equator, *J. Geophys. Res.*, *75*(31), 6249–6259.

Wolf, R. A. (1995), *Magnetospheric configuration, in Introduction to Space Physics*, M. G. Kilverson and C. T. Russel (Eds.), Cambridge Univ. Press, Cambridge, England, 288-239.

Yeh, H. C., Su, S.Y., Yeh, Y.C., Wu J.M., Heelis R.A., Holt, B.J. (1999a), Scientific Mission of the IPEI Payload Onboard ROCSAT-1, *TAO*, Supplementary Issue, 19-42.

Yeh, H.C., Su, S.-Y., Heelis, R.A., Wu, J.-M. (1999b), The ROCSAT-1 IPEI Preliminary Results: Vertical Ion Drift Statistics, *TAO*, 10, 4, 805-820.

Zeng, Z., A. Burns, W. Wang, J. Lei, S. Solomon, S. Syndergaard, L. Qian, and Y.-H. Kuo (2008), Ionospheric annual asymmetry observed by the COSMIC radio occultation measurements and simulated by the TIEGCM, *J. Geophys. Res.*, 113, A07305, doi:10.1029/2007JA012897.

Zhou, Q. and Sulzer, M. (1997), Incoherent scatter observation of the F region ionosphere at Arecibo during January 1993, *J. Atmos. Solar-Terr. Phys.,* **59** (17), 2213–2229.

# VITA

Edgardo Enrique Pacheco Josán was born in La Oroya, Junín, Perú, on November 24th 1974, the son of Delfin Pacheco and Carmen Josán. After graduating from Colegio Americano Miraflores School, he attended the Pontificia Universidad Católica del Perú where he received a Bachelor of Science in Electronics Engineering in 1999. He began working in the Jicamarca Radio Observatory, Geophyical Institute of Peru, in December 1999. In the summer of 2004 he enrolled in the graduate physics program at the University of Texas at Dallas where he received his Masters degree in Physics in May 2007.